International PhD Program in Neuroscience

XXXI CYCLE

Protein Misfolding and Aggregation in Neurodegeneration: *In Vitro* And *In Vivo* Study Cases

PhD Thesis

Ramona Belfiore

Coordinator and Tutor:

PROF. SALVATORE SALOMONE

Co-Tutors:

PROF. VITO DE PINTO

PROF. SALVATORE ODDO

BIOMETEC
DEPARTMENT OF BIOMEDICAL AND BIOTECHNOLOGICAL SCIENCES

DECEMBER 2018

TABLE OF CONTENTS

LIST OF ABBREVIATIONS……**4**

ABSTRACT…….....**6**

GENERAL INTRODUCTION……..**9**

PROTEIN MISFOLDING AND AGGREGATION…….**9**

NEURODEGENERATIVE DISEASES……..**10**

AMYOTROPHIC LATERAL SCLEROSIS (ALS)……**11**

PROTEIN MISFOLDING IN ALS……...**14**

SOD1…….**14**

Human SOD1……**15**

SOD1 ALS-linked mutants …….....**16**

MITOCHONDRIAL DISEASE IN ALS……...**17**

VDAC.....**19**

SOD-VDAC interaction in ALS……....**22**

ALZHEIMER'S DISEASE (AD)……**23**

PROTEIN AGGREGATION AND ACCUMULATION IN AD…… ..**24**

Amyloid protein……**24**

Aβ pathologic role……**25**

Tau protein……**26**

Interaction of Aβ and tau in AD……**27**

Mouse models of Aβ and tau…….**28**

GLIAL REACTIVITY IN AD……...…**31**

CHAPTER 1……...**33**

Hexokinase I N-Terminal Based Peptide prevents the VDAC1-SOD1 G93A interaction and re-establishes ALS cell viability

CHAPTER 2……...**86**

Temporal and Regional Progression of Alzheimer's disease-like pathology in 3xTg-AD mice

GENERAL DISCUSSION AND CONCLUSIONS…….....**140**

REFERENCES…….....……....**142**

LIST OF PUBLICATIONS AND SCIENTIFIC CONFERENCES… **153**

ACKNOWLEDGEMENTS……...……. **155**

LIST OF ABBREVIATIONS

CNS	Central nervous system
PNS	Peripheral nervous system
FTD	frontotemporal dementia
ALS	Amyotrophic Lateral Sclerosis
GWAS	Genome-wide association study
SMN1	Survival motor neuron 1
DPP6	Dipeptidyl Peptidase Like 6
VEGF	Vascular endothelial growth factor
ROS	Reactive oxygen species
SOD1	Superoxide dismutase 1
TARDBP	Transactive response DNA-binding protein
FUS	Fused in sarcoma
VCPV	**V**alosin containing protein
VAPB	VAMP-associated protein type B
WT	Wild type
ATP	Adenosine triphosphate
VDAC	Voltage-dependent Anion Channel
OMM	Outer mitochondrial membrane
ADP	Adenosine diphosphate
NADH	Nicotinamide adenine dinucleotide
G6P	Glucose-6-phosphate
AD	Alzheimer's disease
FAD	Familial form of AD

ApoE	Apolipoprotein E
Aβ	Amyloid-β
NFT	Neurofibrillary tangles
APP	Amyloid precursor protein
CTFα	C-terminal fragment
BACE	β-site APP cleaving enzyme
LTP	Long-term potentiation
LTD	Long-term depression
MAPT	Microtubule associated protein tau
PHFs	Paired helical filaments
TPK1	Thiamin pyrophosphokinase 1
GSK3-β	Glycogen synthase kinase 3- β
GFAP	Glial fibrillary acidic protein

ABSTRACT

Neurodegenerative diseases are nowadays increasing in incidence and widely distributed around the world. Many scientists are currently working on developing therapeutic tools to stop this rise and prevent the onset of disorders like Alzheimer's (AD), amyotrophic lateral sclerosis (ALS) and Parkinson's (PD). Despite those disorders show very different symptoms and morbidity, intracellular and extracellular protein misfolding and accumulation appears as a common pathological pathway. In the present thesis work I analyzed two cases of toxic protein deposition involved in ALS and AD onset using both in vitro and vivo techniques to study these toxic accumulations in cell culture, bacteria and animal models.

First, I looked at Superoxide Dismutase 1 (SOD1) mutant protein G93A (mutSOD1-G93A) whose neuronal deposit is associated to familial and sporadic Amyotrophic Lateral Sclerosis (ALS). Both ALS patients and transgenic mouse models show mitochondrial abnormalities such as swelling and vacuolization in spinal cords as pathological hallmarks. In this context, the mitochondrial porin VDAC1 (voltage dependent anion channel 1) has been proposed as a binding target of SOD1 mutant forms to mitochondria. To study how hVDAC1 interplays with mutSOD1-G93A we produced recombinants wtSOD1, mutSOD1-G93A and His-tagged recombinant VDAC1 protein. Interestingly, by affinity studies we found that VDAC1 protein specifically binds mutSOD1-G93A but not wtSOD1. Notably, it is known that the N-Terminal end of Hexokinase 1 (N-HK1) interacts with VDAC1: thus, we produced a synthetic peptide corresponding to the first 11 aa of human HK1 and tested its action as a potential interfering molecule between VDAC1-mutSOD1-G93A bond. In an electrophysiological study we observed that adding N-HK1

peptide promotes a significant instability of VDAC1 channel affecting the pore's gating. Next, in a binding assay we verified the N-HK1 peptide interference in SOD1G93A-VDAC1 interaction. Both in a protein-protein interaction and in a protein–mitochondrial interaction we obtained a decrease of SOD1-VDAC1 binding in dependence of the increased NHK1 peptide concentration (85% in mitochondria). Summarizing our overall results, they show that in ALS condition, mut-SOD1-G93A binds VDAC1 and impairs HK1 binding and our results suggest for N-HK1 peptide a neuroprotective potential in ALS patients. Starting from these experiments it is possible to select one or more HK1 peptide having the highest chance of interfering with ALS-linked VDAC1/mutSOD1 toxic aggregates in in vivo models. The NHK-1 peptide is now patented.

The second part of my thesis work was focused on the Amyloid and tau protein accumulation in 3xTg-AD mice. In order to study neuropathology and cognitive deficits in Alzheimer's disease (AD), several transgenic models of AD have been identified. Accumulation of amyloid-β and fibrillary tangles as well as impairments in working and learning memory are age-related hallmark of AD pathology. After almost 15 years from his creation, the 3xTg-AD mouse model is still one of the most reliable transgenic models. Despite the huge number of funding about this transgenic model in AD, it is still to be defined the detailed age-related progression of amyloid and tau pathology for each brain region. To produce a progressive characterization of Aβ and tau pathology in 3xTg-AD mice we aged female mice at 2, 6, 12 and 20 months of age. We tested mice in a behavioral assay named Morris Water Maze (MWM) and we used in vitro biochemical assays (ELISA, IHC, IF) to observe Aβ soluble and insoluble fraction as well as tau phosphorylation in both cortex and hippocampus of 3xTg-AD mice. Our data on MWM

demonstrate a progressive impairment in learning with a strongly significant difference between 3xTg-AD mice and controls (C57129 mice) from 6 months of age. Notably, we also found a progressive increase in both soluble and insoluble $A\beta_{40}$ and $A\beta_{42}$, an age dependent tau hyperphosphorylation at specific AD linked phospho-sites, and an intense glial reactivity. Overall, our data confirm that female 3xTg-AD mice consistently show AD-like pathology, therefore this transgenic mouse model can be used as an extremely powerful tool to investigate pathogenic mechanisms underlying Alzheimer's disease.

GENERAL INTRODUCTION

PROTEIN MISFOLDING AND AGGREGATION

Most of the process involved in biological system's activity are regulated by protein activation and protein-protein interaction (Westermarck et al., 2013). The correct functionality of these macromolecules, consisting in a linear sequence of amino acids, depends on their capacity to form three-dimensional structures and create more complexes interactions thanks to functional groups such as carboxylic acids, alcohols, thioethers etc (Belmont et al., 2001).

Inside the cells, proteins can self-assembly and, thanks to molecular chaperons, adopt the right folding (Ellis and Hartl, 1999). It is known that an incorrect protein folding can indeed lead to protein disfunction (gain or loss of function) and aggregation (Dobson, 2003). In many cases of conformational disorders, the pathological effect of protein misfolding is the gain of ability to alternatively interact under oligomeric forms, amorphous aggregates and fibrillar structures.

Those mis-functional aggregates can eventually create toxic intracellular and extracellular deposits that interfere with cell's survival (Dobson, 2004). Causes and mechanisms responsible of protein's misfolding can act at several levels of proteins synthesis: somatic mutations, epigenetic changes, transcriptional/translational mistakes (Bucciantini et al., 2002), unfunctional chaperon systems (ubiquitin–proteasome pathway, autophagy–lysosome pathway etc.) post transcriptional and trafficking errors are some of the most

represented events in misfolded protein-dependent diseases (Barral et al., 2004; Shinde and Inouye, 1993).

NEURODEGENERATIVE DISEASES

Neurodegeneration is a major cause of disease and source of an increasing worldwide morbidity and mortality (Erkkinen et al., 2018; Kompoliti et al., 2017). World impact, epidemiology and treatment of neurodegenerative diseases are extremely variegated although some of them such as Alzheimer's disease, Amyotrophic Lateral Sclerosis and Parkinson's disease do share key pathological events (Spires-Jones et al., 2017).

Notably, neurodegenerative diseases show synaptic dysfunction, neuroinflammation and sever neuronal loss (Kempuraj et al., 2016; Lepeta et al., 2016) which can involve selective regions of the central nervous system (CNS) and peripheral nervous system (PNS).

Interesting evidences specifically underline the existence of an overlap of clinical and pathological manifestation among different neurodegenerative disease: for instance, ALS patient sometimes show also frontotemporal dementia (FTD) and patients with FTD frequently show parkinsonian-like extrapyramidal symptoms (Rebekah M Ahmed et al 2016). Moreover, cognitive, behavioral, metabolic and primary motor's changes have been observed to appear similar in many neurodegenerative disorders.(Camandola and Mattson; Levenson et al., 2014)

AMYOTROPHIC LATERAL SCLEROSIS (ALS)

Amyotrophic Lateral Sclerosis (ALS) is a neurodegenerative disease that selectively affects motoneurons of specific regions of the central nervous system (CNS) and leads to the death of patients in a few years from the onset (Grad et al., 2017; Wijesekera and Leigh, 2009). ALS was first described in 1869 by the French neurologist Jean-Martin Charcot, who first linked the progressive paralytic syndrome to the presence of lesions of the white and gray matter of the affected tissues (Goetz, 2000)

Today, this pathology has become the most common disorder of motor neurons with onset in adulthood: It shows an incidence equal to about 1 out of 100,000 individuals in the world, which decreases in some ethnic groups, such as the American Indians (Alonso et al., 2009; Grad et al., 2017; Ringholz et al., 2005), and increases dramatically in specific geographical regions such as Guam, Kii Peninsula in Japan and western New Guinea. In addition, incidence rates seem to increase with age, peaking between 70 and 80 years, and are higher in men than in women (Alonso et al., 2009). ALS is classified into two distinct forms: a sporadic form (sALS), the most widespread and without an apparent cause, and a hereditary-familial form (fALS), with autosomal dominant genetic transmission in most of the cases (Rowland and Shneider, 2001). Although today enormous progresses have been made in research, the onset of ALS, especially in sporadic forms, remains mysterious. Many advances, however, have been made on the understanding of familiar forms, many of which are today associated with known mutations. However, the lethal prognosis and the absence of treatments for ALS, suggest that much still needs to be done in the field of applied research.(Chiò et al., 2009; Gordon et al., 2013)

More than a century after Charcot's description, despite ALS etiology in most of the patients is still unknown, the genetic discoveries made on the familial form have greatly improved the understanding of the pathology. In fact, fALS concerns about 10-20% of cases and involves specific mutations in over 60% of cases.

Even in the sporadic form, association studies in genomics (GWAS) have been used to look for susceptibility factors that promote the death of motor neurons, without obtaining similar results.

For example, the abnormal number of copies of SMN1 appears to be a genetic risk factor (Corcia et al., 2002), as well as the DPP6 and VEGF genes, could be susceptible only in some geographical areas (Diekstra et al., 2012). Also, some environmental factors have been correlated with the onset of this pathology and among them the advancing age or exposure to tobacco smoke, although there is not enough evidence, as well as athleticism competitive sport or exposure to pesticides (Nelson et al., 2000; Scarmeas et al., 2002; Sutedja et al., 2007).

Specifically, a study conducted in Italy between 1970 and 2001 showed a risk equal to 6.5 times higher in professional soccer players than non-players (Chiò et al., 2005) and that repeated traumas can contribute to the onset of all neurodegenerative diseases (Beghi et al., 2010).

Not less important in the pathogenesis or the course of ALS appears to be the damage due to oxidative stress caused by the accumulation of reactive oxygen species (ROS); such damage, which may be a prelude to cell apoptosis and death of motor neurons (Bhat et al., 2015; Martin, 1999), would be due to different mechanisms including damage to crucial

molecules, the intracellular increase of free Ca^{2+} and the release of excitatory amino acids. Indeed, some researchers have reported in patients with sporadic and familial ALS, a high presence of typical oxidation products, such as malondialdehyde or oxidized membrane proteins, DNA and phospholipids.

Even if less widespread, familial forms of ALS are the most studied: it is not excluded, indeed, that the effects of specific mutations can promote mechanisms that are completely analogous to those that occur in sporadic forms. Over the years, the analysis of the mutations involved, showed a clear pathogenetic role of genes coding for proteins of fundamental importance for the cell.

Among these, the most common mutations involve the gene coding for SOD1 (Cu / Zn superoxide dismutase 1), TARDBP (transactive response DNA-binding protein of 43 kD), and FUS (fused in sarcoma) (Millecamps et al., 2010); although in a minor way, the genes encoding angiogenin, ataxin-2, ubiquilin-2, VCP (valosin containing protein) and VAPB (VAMP-associated protein type B) also seem to be associated with the disease; however, in many cases, the fALS phenotype is extremely similar. This suggests that the pathology may be due to different causes that converge in a single pathophysiological path (Ravits et al., 2013).

Despite the mechanisms that contribute to the death of motor neurons are not entirely clear, it is possible to state that, as in other neurodegenerative diseases, an important event may concern the aggregation of misfolded mutant proteins.

The incorrect protein folding, even partial, associated with these mutant proteins, can lead to the formation of toxic aggregates, which can influence the functioning of other cellular

organelles; moreover, it seems that the presence of misfolded proteins can cause a conformational change in wild type proteins in the vicinity: this could explain how a disease that starts at a focal point is then transmitted widely to all the affected tissue (Kanouchi et al., 2012)

PROTEIN MISFOLDING IN ALS:

SOD1

Superoxide dismutase (SOD) is a family of ubiquitous enzymes, which play a key role in the cell's defense mechanism against ROS. SOD proteins catalyze the dismutation of superoxide anion to hydrogen peroxide and molecular oxygen, thanks to the presence of one or more metal ions that play the role of cofactors.

The appearance of SOD in cells can be considered an evolutionary response to the presence of an oxidizing atmosphere, and therefore rich in ROS. Its mechanism has in fact originated in the first photosynthetic organisms and has evolved in the most complex organisms. Studies on his structural homologies and amino acid sequences permitted to determine the existence of two main SOD families: SOD containing Fe, Mn or Ni, and those containing Cu / Zn. (Youn et al., 1996).

In mammals, three distinct isoforms of SOD have been identified and characterized: SOD Cu / Zn, (isoforms 1 and 3), and MnSOD, (isoform 2). Although these isoforms perform similar functions, they show structural characteristics, chromosomal localization, metal cofactors and distinctly different cellular distribution (Parge et al., 1992). Researches on SOD gene sequences revealed that all three of the above genes consist of

five exons interrupted by 4 introns and that the promoters in SOD1 and SOD2 have a very rich region in GC, a TATA box and a CCAAT box. In the promoter region of SOD3, regions rich in GC were found both with two CCAAT boxes but not the classic TATA box (Folz and Crapo, 1994).

The most important isoform is undoubtedly the SOD1: indeed, it catalyzes about 95% of all the dismutation reactions that occur in the cell as it is present mainly in the cytosol; however, less abundant SOD1 has also been found in many organelles, such as lysosomes, peroxisomes, nucleus, and intermembrane space of mitochondria. Contrarily, SOD2 is kept strictly within the mitochondrial matrix, while the isoform 3 is present on the cell surface and in extracellular fluids such as lymph, synovial fluid and plasma.

Human SOD1

Human SOD isoform 1 is a homodimer enzyme, consisting of two identical subunits of 32 KDa. Each subunit is organized in a flattened barrel structure made by eight antiparallel β sheets and seven loops (Bordo et al., 1994). Furthermore, each subunit contains a Cu and a Zn ion joined by weak, non-covalent interactions. The secondary structure of Cu, Zn-SOD1 is made up of β antiparallel sheets and has two loops that make up the zinc binding site and the electrostatic channel through which superoxide is guided towards the active site. The Zn atom seems to exclusively have a structural role as it is needed to stabilize the active site: although it has been shown that its removal decreases the redox potential of Cu^{2+} and the catalytic property of the whole enzyme. The Zn ion is bound to the barrel structure thanks to three histidine (in positions 64, 72, 81) and to an aspartic

acid residue (84). The Cu ion, which represents the true catalytic site, is linked to four histidine imidazole (46, 48, 63, 120) to form a tetrahedral structure.

Inside the protein a positively charged channel is formed thanks to the presence of charged amino acid residues, which thanks to their arrangement allow the formation of an electrostatic field that facilitates the approach and the subsequent association of the superoxide radical with the metal. The reaction in which superoxide dismutase participates is the following (Santovito et al., 2006):

$$SOD\text{-}Cu^{2+} + O^{2-} \rightarrow SOD\text{-}Cu^{+} + O^{2}$$

$$SOD\text{-}Cu^{+} + O2^{-} + 2H^{+} \rightarrow SOD\text{-}Cu^{2+} + H_2O_2$$

SOD1 ALS-linked mutants

The involvement of SOD1 in ALS was discovered in 1991, when mutations on chromosome 21q22.1, the gene locus of SOD1, were associated with some forms of ALS; two years later, in 1993, Rosen described eleven mutations in the SOD1 gene. Today, mutations have become more than 150 (http://alsod.iop.kcl.ac.uk) and the SOD1-mediated pathology, referred to as ALS1 or type1, represents the first cause of fALS, thus covering about 25- 25% of cases (Santovito et al., 2006).

Nowadays, most of the characterized ALS-linked mutations on SOD1 gene are missense substitutions, distributed in all five exons. Furthermore, it has been shown that eight frameshift deletions and five insertions, all placed in exons 4 and 5, lead to an early truncation of the protein (Cudkowicz et al., 1997) and could be involved in the pathology. Every single mutation can be associated with specific characteristics and course. For example, one of the most frequent mutations, A4V (substitution of alanine in position 4

with valine), although it shows minor signs in the motor neuron, characterized an onset of the disease at a young age and a very rapid course, usually lasting less than 12 months (Juneja et al., 1997); the same aggressive phenotype is shared by other less common and completely different mutations, such as C6F, C6G, and G10V (Aksoy et al., 2003; Kim et al., 2003; Morita et al., 1996).

Despite over 20 years of research, the SOD1-mediated toxicity mechanism has not been clarified. Firstly, it was thought that the disease was caused by the loss of the antioxidant activity of SOD1 following mutation, with enormous consequences for the oxidation-reduction stress of the motoneuron. However, experimental evidence indicates that most of the SOD1 ALS-linked mutants are active and exhibit partial or total WT-like folding. Therefore, the toxicity mediated by SOD1 mutants must be ascribed to other unknown characteristics. One of the most studied hypotheses concerns, once again, the possibility that the misfolded proteins (even only partially, as in the case of the WT-like mutants) can form toxic aggregates for the cell. Furthermore, the aggregates of SOD1 can directly or indirectly promote a degeneration of cell organelles.

MITOCHONDRIAL DISEASE IN ALS

Mitochondria are cellular organelles that play a key role in bioenergetic metabolism as they are involved in the synthesis of ATP, regulation of the redox state of the cell, osmotic regulation, pH control, cytosolic calcium homeostasis and cellular signaling (Rutter and Rizzuto, 2000). Mitochondria form watertight compartments in two lipid membranes: the inner membrane and the outer membrane. The inner membrane houses the mitochondrial

respiratory chain and provides a very effective barrier to ionic flow. It also looks towards the mitochondrial matrix, which contains the components of the tricarboxylic acid and beta oxidation cycle (Reddy, 2007). The highly porous outer membrane allows substances with a low molecular weight to move between the cytosol and the intermembrane space.

Mitochondrial dysfunction has been observed in the spinal cord of patients with ALS and transgenic mouse models of ALS, and seems to be due to morphologic anomalies of the organelle as swelling and vacuolization. These characteristics have undoubtedly shown the involvement of the mitochondrion in the ALS and they appear as events following molecular interactions.

Furthermore, some studies have highlighted the relationship between mitochondrial dysfunction and accumulation of SOD1 mutants. These studies were performed in transgenic mice harboring SOD1 G93A point mutation. The G93A mutant represents one of the most prevalent mutations in patients with familial ALS; it is defined WT-like because of his property to act like the wild protein and has also been indicated as an excellent representative model for the study of SOD1 ALS-linked mutants (Higgins et al., 2002). In these works, it has been shown that G93A-SOD1 co-localizes with the outer membrane of mitochondria (Kawamata and Manfredi, 2008) and this could cause a perturbation of the physiological regulation of communication and exchange between mitochondria and cytosol, also explaining the reason for this altered morphology mitochondrial. However, it is not entirely clear why the G93A mutant is selectively recruited into the mitochondria of affected tissues (Liu et al., 2004). In summary, this study allowed to hypothesize that the association of SOD1 mutant aggregates may be an early event in the pathogenesis of ALS, causing damage to the mitochondrial membrane with

consequent loss of mitochondrial membrane potential, swelling and vacuolation of the organelle (Wong et al., 1995). Besides alteration of mitochondrial morphology, the damage caused by accumulation of SOD1 mutant, can produce interruption of the mitochondrial respiratory chain activity (Jung et al., 2002), reduction of mitochondrial Ca^{2+} and buffering capacity of the mitochondria (Carrì et al., 1997). In support of this, it has been observed that the dysregulation of the electron transport chain complexes is present both in SOD1-G93A transgenic mice and in human patients with ALS. SOD1 mutations also appear to influence not only the mitochondria function, morphology and bioenergetics, but also the axonal transport of mitochondria is interrupted by SOD1 mutants in ALS (Bowling et al., 1993).

Further confirmation is given by the study by Israelson et al, who discovered that SOD1 G93A mutants, but also other forms such as G85R, accumulate on the cytoplasmic face of the outer mitochondrial membrane by binding the voltage-dependent anionic channel (VDAC) (Israelson et al., 2010)

VDAC

The family of mitochondrial pores VDAC (Voltage-dependent Anion Channel) represents the most abundant protein class of outer mitochondrial membrane (OMM) among all the eukaryotes. The VDAC have a molecular weight of about 32 kDa and form aqueous pores that can work as a molecular filter for solutes from 3000 up to 5000 (Sampson et al., 1997; Schein et al., 1976); The VDAC was first studied around 40 years ago, when Schein et al detected the pore-forming activity in an extract of Paramecium tetraurelia mitochondria

(Sampson et al., 1998). Mammalians have three different isoforms known as VDAC1, 2 and 3. Although the structure of the genes is widely preserved the expression of the three isoforms varies depending on the tissue: for instance, isoforms VDAC1 and 2 are expressed mainly in heart, skeletal muscle, liver and brain whereas VDAC3 is expressed in testicles, liver, ovary, adrenal, lung, spleen and renal muscles. Over all, out of the three isoforms, VDAC1 is the most expressed and the most studied isoform, followed by VDAC2 and VDAC3 (Craigen and Graham, 2008; Yamamoto et al., 2006).

VDAC1 is composed by 19 β-strands, arranged to form a barrel, and by an α-helix at the N-terminal end facing the inside of the channel. The N-terminal is thought to be involved in maintaining the correct pore conformation and for the voltage dependent gating, which turns out to be the main characteristic of the VDAC.

Electrophysiological studies have shown that, VDAC1 can vary its conductance according to the applied voltage. At low voltage values, ranging from + 10 to -10 mV, VDAC1 shows a high conductance, and is in an open state; when the voltage reaches values higher than ± 30 mV, it adopts a closed conformation with inferior conductance (Mannella, 1997). Therefore, it is believed that the voltage of the mitochondrial membrane can influence the state of opening of the channel and thus the function of the mitochondria.

In line with his role in bidirectional traffic, VDAC1 allows the passage through the OMM of substrates such as pyruvate, malate, succinate, ions, ATP/ADP And NADH (Shoshan-Barmatz et al., 2010). Consequently, VDAC1 down-regulation results in the reduction of the exchange of metabolites between mitochondria and cytosol, which makes VDAC1 essential to produce energy and to the cell growth. Similarly, alterations of the mitochondrial function are related to the closure of the VDAC1, which limits the normal

flow of metabolites from inside and outside the mitochondria (Holmuhamedov and Lemasters, 2009; Vander Heiden et al., 2000). Due to its location, VDAC1 can interact with the proteins that mediate and regulate the integration of mitochondrial functions with other cellular activities: for instance, VDAC1 interacts with Hexokinase and Creatine kinase to convert ATP just generated into high energy reserve forms such as glucose-6-phosphate (G6P) and creatine phosphate, respectively in brain and muscles. The over-expression of VDAC1 in some cancer cells may be correlated to its multifunctional activities, as required by the demanding cells raised amount of energy (Shoshan-Barmatz et al., 2017). The set of functions of VDAC1 in the mitochondria are summarized in the figure 1.

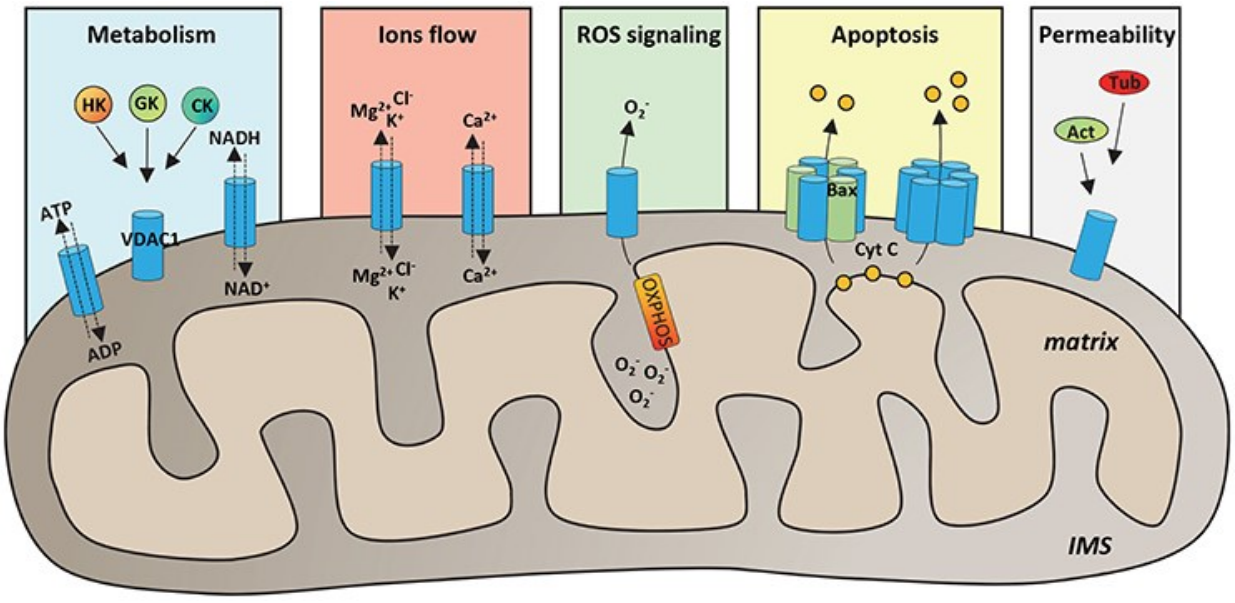

Figure 1: Functional roles of VDAC1 in physiological conditions (A. Magrì et al. 2018)

SOD-VDAC interaction in ALS

In their work, Israelson et al. show a series of experimental evidence to indicate the link between SOD1 and VDAC1 's ALS-linked mutants as the main cause of mitochondrial dysfunction (Le Verche and Przedborski, 2010). In this study, in fact, it was seen that VDAC1, but not VDAC2, coimmuno-precipitates with the catalytically active mutants SOD1 G93A, and with those inactive, H46R and G85R in affected tissues and extracted from the transgenic mice; Conversely, the wild-type protein is not able to aggregate and adhere to the mitochondria. In addition, despite the brain tissue not showing pathology, contains abundant amounts of VDAC1 and SOD1 mutant, no evidence of an interaction between the two proteins was found, demonstrating that the interaction is tissue-specific. The authors suggest that this regional specificity could be related to the higher content in the brain of protein interacting with VDAC1, principally Hexokinase, which is less expressed in the spinal cord (Le Verche and Przedborski, 2010). Hexokinase can next compete with mutant SOD1 and drastically reduce the bond to VDAC1. Furthermore, electrophysiological studies have shown that mutants SOD1 proteins G93A e G85R, differently from the WT SOD1, reduce the ionic conductance of VDAC1. These functional data suggest that, in the presence of mutant SOD1, VDAC1 can be partially closed, and that this conformational state has a negative impact on normal mitochondrial functions.

From this study, it emerged an exciting new hypothesis: a mitochondrial channelopathy as basis of neurodegeneration that occurs in motor neurons affected by ALS. Since mutants of SOD1 ALS-linked do accumulate on the OMM, as a cause of alteration of mitochondrial functions this event could contributing to motor neuron’s degeneration in familial form of ALS.

ALZHEIMER' S DISEASE

Alzheimer's disease (AD) is the most common neurodegenerative disorder worldwide. Estimates indicate that more than 26 million people are living with AD and by 2050 the number of people with this disorder may reach 100 million (2016). Nowadays no effective cures have been found for AD patients that generally dye in 3 to 10 years after diagnosis. Aging is the major risk factor for the development of Alzheimer's disease especially in the 95% of cases that are classified as sporadic and of unknown causes (Bekris et al., 2010). Sporadic form of AD normally occurs late in life and has it been shown that 33-50% of people older than 85 have AD (Bekris et al., 2010). Thought the years the average age of population is becoming higher and consequently the number of new AD cases is estimated to increase very quickly (Bird, 2008).

The remaining 5% of AD cases are familial form of AD (FAD) and are commonly triggered by mutations in one of three genes, presenilin 1 and 2 and amyloid precursor protein (APP, Querfurth and LaFerla, 2010). The presence of one of those mutation generally unsure the future insurgence of AD although several other mutations can be responsible of FAD. Notably, the presence of a specific form of ApoE gene (ApoE4) represent a major risk factor of AD and in many cases anticipate the age of onset in patents that have predisposition to the disease: this often leads to an earlier and higher severity of the pathology and so of the prognosis. Moreover, it's possible to distinguish early onset and late onset AD cases and both can occur in a familial or sporadic form of the disease.

Clinically, one of the first symptoms of AD is the deficits in episodic memory (Welsh et al., 1992). As the disease progresses, other cognitive domains are involved and deficits in

language, executive functions, and learning tasks appear evident. Finally, patients become bedridden and perish due to other comorbidities. Two hallmarks of neuropathology in AD are plaques, mainly composed of amyloid-β (Aβ) peptide, and neurofibrillary tangles (NFT), mainly formed by hyperphosphorylated tau (Selkoe, 2001). The events triggering AD pathology and the molecular mechanisms linking aging to AD are not known.

PROTEIN AGGREGATION AND ACCUMULATION IN AD

Amyloid protein

Aβ is as small peptide generated by proteolytic reaction from an integral membrane glycoprotein, the amyloid precursor protein (APP). In a physiological scenario, APP protein can be processed by two different pathways: non-amyloidogenic and amyloidogenic pathway (O'Brien and Wong, 2011). The non-amyloidogenic pathway requires a cleavage from α-secretase, which produce a soluble N-terminal fragment (sAPPα) -released in the extracellular space- and a C-terminal fragment (CTFα) -cleaved to a membrane-bound C-terminal fragment and a soluble N-terminal fragment (p3) by a γ-secretase (Branca et al., 2014). Differently, the amyloidogenic pathway starts with the cleavage of APP at residue 99 by the β-site APP cleaving enzyme (BACE, Vassar et al., 1999) and the release of sAPPβ to the extramembrane space.

Next, a γ-secretase cleaves the intramembrane C99-terminal predominantly generating extracellular Aβ peptides and intracellular C-terminal domain. The γ-secretase cleavage most frequently happens at two different positions, generating either $A\beta_{40}$ or $A\beta_{42}$. The former is more common while the latter is more toxic (Chow et al., 2010).

In normal condition, at the extracellular space, Aβ binds to different isoforms ApoE protein: ApoE 2 and 3 leads more likely to his transportation to degradation pathways, whereas the bond to ApoE 4 seems to favorite the accumulation and aggregation of Aβ peptides (Kanekiyo et al., 2014).

Mutations in the APP gene and presenilins gene have been identified and several of these mutations lead to early-onset autosomal-dominant familial Alzheimer's disease (eFAD), likely by increasing total Aβ production or by selectively increasing of the longer more amyloidogenic $A\beta_{42}$ species (Ryan and Rossor, 2010). Unbalance on BACE1 expression, Aβ-EpoE interaction and neprilysin levels have been shown to be positively correlated with plaques deposition and severity of the disease (Tarasoff-Conway et al., 2015).

Aβ pathological role

It has been shown as Aβ peptide is able to create different conformational states with different fibrillary structures in in vitro experiments (Cheon et al., 2016). This capacity in vitro is confirmed also on experiments with Aβ purified from human brains: the structure of Aβ fibrils was different according to the AD phenotype of different patients (Condello et al., 2018).

When Aβ conformers of sporadic and familial AD and brain-derived plaques were inoculated in transgenic mice, AD pathology on those mice changed in speed, propagation, and plaque phenotype: this yield to suppose that Aβ conformation is responsible of different state of propagation and correlates with the cognitive impairment (Sengupta et al., 2016). These observations also correlate with the data suggesting that Aβ role in

synaptic toxicity: Aβ peptides are able to inhibit long-term potentiation (LTP) and reduce synaptic plasticity (Li et al., 2011) possibly causing the reduction of cognitive ability in AD. Moreover, the inhibition of LTP by Aβ produce the induction of hippocampal long-term depression (LTD) causing changes in changes in postsynaptic responsiveness or excitability (Bliss and Cooke, 2011).

Tau protein

The MAPT (microtubule associated protein tau) is a phosphoprotein mostly present in axons to stabilize the microtubule structure (Drubin and Kirschner, 1986) . Tau is a major component of NFTs characterizing AD brains and their accumulation is related to neuronal loss and cognitive deficits (Mandelkow and Mandelkow, 2012).

In human, tau gene is located on chromosome 17 and is composed by 15 exons: his alternative splicing at exons 2, 3 and 10 in the human brain leads to existence of six isoforms (Liu and Gong, 2008). According to both the number of imperfect tandem repeated sequences and number of inserts at N-terminal we distinguish zero, one, or two inserts of 29 amino acids at the N-terminal part (exon 2 and 3 - 0N, 1N and 2N), and three or four repeat-regions at the C-terminal part (exon 10-3R, 4R) (Kadavath et al., 2015).

No mutations of tau gene have been found in AD although mutant tau protein is present in several disease such as FTD and Pick's disease as prove that changes in tau protein are linked to neurodegeneration and cognitive impairment (Iqbal et al., 2010). In AD brains, tau is phosphorylated to a higher degree at physiological sites and is also phosphorylated in additional sites that are defined specific of AD pathology.

Pathologically phosphorylated and hyperphosphorylated tau detach from microtubules and accumulates as paired helical filaments (PHFs) and NFTs (Alonso et al., 2006). Those pathological sites include pSer422, pThr212/pSer214 (AT100), and pThr231/pSer235 (AT180, Xia et al., 2015).

Thus, despite there is not genetic association between tau and AD onset, extracellular accumulation of tau surrounded by reactive microglial does significantly drive AD pathology especially in early states of the disease.

Interaction of Aβ and tau in AD

As the amyloid cascade hypothesis says, Aβ deposit may be the first responsible of triggering AD contributing to tau accumulation as NFT and causing neuronal death (Rajmohan and Reddy, 2017)). Despite many evidences support this hypothesis, the molecular mechanisms linking the two pathological accumulation is still unknown.

When Lewis et al. (2001) crossed two independent transgenic lines, one overexpressing mutant APP and the other overexpressing mutant tau, the double transgenic mice developed Aβ pathology at the same age as the single APP transgenic mice but showed enhanced tau pathology. This led the authors to conclude that either APP or Aβ influences tau pathology in vivo. Many in vitro studies have proposed tau as downstream mediator of Aβ toxicity in primary neuronal cultures: for instance, Takashima and colleagues reported a role for a GSK3β homologous as TPK1 since treatment of primary hippocampal cultures with Aβ causes an increase of his activity and correlates with the Aβ-induced neurotoxicity (Takashima, 2006).

As Aβ-treated neurons were also positive for Alz50, a conformational specific tau antibody, (Yankner et al., 1989) and TPK1 is linked to phosphorylation of tau (TAKASHIMA et al.), this observation suggests that Aβ can induce tau pathology via TPK1. The involvement of GSK3β in Aβ-induced toxicity has been confirmed by other studies (Hooper et al., 2008; Llorens-Marítin et al., 2014; Takashima, 2006) that show that Aβ can enhance the activity of different kinases that phosphorylate tau.

By use of tau knock-out mice it has been proved that Aβ toxicity needs the presence of tau protein: when treated with Aβ, hippocampal neurons from wild-type mice or from mice expressing human tau showed neuronal degeneration in 96h while neurons lacking tau did not showed degenerations (Rapoport et al., 2002).

It was also observed that Aβ can induce tau formation of filaments via activation of caspase 3 protein: the latter is able to cleave tau at his C-terminal, producing a more toxic form of tau (delta-tau) which is also found in NFT (Gamblin et al., 2003; Noble et al., 2013) and is increased in as the cognitive impairment in AD.

Finally, some observations have been done on the role of both calcium and mitochondria on Aβ-tau-mediated spine-loss and cognitive deficits: Aβ induced-dendritic spine loss correlates positively with presence of missorted tau, increased calcium levels and impaired mitochondrial distribution(Spires-Jones and Hyman, 2014; Zempel et al., 2010).

Mouse models of Aβ and tau

The use of mouse model represents one of the best tools of research in AD despite none of them recapitulate the full scenario of the disease. After the APP gene was isolated,

several groups have attempted to generate transgenic models of AD (Higgins et al., 2002; Mucke et al., 1994; Quon et al., 1991).

The first successful model of Aβ pathology was the PDAPP mice where levels of the human APP were more than 10-fold over endogenous mouse APP levels (Elder et al., 2010). At mid-age these mice develop Aβ deposits which increase as the mice age and are distributed among hippocampus, corpus callosum and cerebral cortex. The PDAPP mice also develop behavioral deficit, neuritic plaques, synaptic loss and gliosis (Jacobsen et al., 2006; Schaeffer et al., 2011).

Another widely used mouse-model, the Tg2576 mice overexpressing APP, develop Aβ deposits by 9-10 months as well memory impairments in an age-related manner (Dineley et al., 2002; Westerman et al., 2002). Most of the APP animal models develop Aβ pathology especially represented by accumulation of the longer and toxic form ($A\beta_{42}$): the presence of the $A\beta_{42}$ is indeed negatively correlated with cognition levels much more than $A\beta_{40}$ peptide (Murphy and LeVine, 2010).

Differently of what happen in human brain though mice model exclusively expressing mutant APP don't show NFT deposition. The double transgenic APP/PS1 mice show an earlier onset of Aβ pathology which indicate the importance of mutations at PS genes which is still is not sufficient to generate NFT in those mice (Hall and Roberson, 2012). AD pathology is not genetically referred to tau mutations, although other disease like FTDP-17 are characterized by NFT deposition due to a mutation known as tauP301L (Ramsden et al., 2005).

Many groups of researchers have been working on generating mice overexpressing the human mutant tau gene to better study NFT formation and their involvement in AD (Lewis et al., 2001). Gotz and collaborators in 2001 overexpressed the human tau P301L using the Thy1.2 promoter successfully observing the formation of NFT in hippocampus and neocortex. However, those mice don't show changes in cognition indicating that tau mutation and NTF accumulation is not sufficient to generate cognitive neither Aβ pathology: at that point was clear that both tau and Aβ pathology are needed to recreate AD-like pathology.

To this end, both groups Gotz et al and Lewis et al., with different approaches, generated transgenic mice with APP ant tau mutations: although as these mice show intense motor deficits and die prematurely was not possible to use them in behavioral tasks. To obtain a model with both plaques and tangles Oddo and colleagues generated the 3xTg-AD mice: these transgenic mice harbor three mutant human genes, APPSwe, Tau P301L, and PSN1 M146V. Extracellular plaques and NFT tangles deposition appear in early stages and increase as the mice age: by 12 months of age those mice show a full- AD like pathology comprehensive of synaptic dysfunction, LTP deficits and cognitive impairments. These changes are associated with selective neuroinflammation and progressive cognitive impairments have also been widely reported. These mice are being used by over 100 investigators throughout the world, which has led to the generation of multiple independent colonies.

Converging evidence indicates that the phenotype of 3xTg-AD mice has shifter over the years and contradicting reports about onset of pathology or cognitive deficits are apparent in the literature (Hebda-Bauer et al., 2013; Montacute et al., 2017; Oh et al., 2010).

Here I sought to stage the current progression of AD-like pathology in 3xTg-AD mice. The data obtained will facilitate the design of preclinical studies in which these are used to test new therapeutic approaches.

GLIAL REACTIVITY IN AD

One of the hallmark of AD pathology is represented by astrogliosis and microgliosis (Serrano-Pozo et al., 2011). The CNS is indeed involved in a series of inflammatory events that in a normal scenario are physiologically balanced to protect the neuronal component from external or internal pathological stimuli (Kyritsis et al., 2014).

Astrocytes in AD brains show a wide reactivity which manifests as increased expression of glial fibrillary acidic protein (GFAP) protein and are mostly distributed around amyloid plaques as their main role is neuroprotection and delimitation of damaging deposits(Sofroniew and Vinters, 2010). They also contribute to ATP, glutamate and GABA trafficking, calcium homeostasis, regulation and release of inflammatory cytokines and grow factors (Verkhratsky et al., 2016). Indeed, elevated levels of proinflammatory cytokines as TNFα, LPS, IFNγ and IL-1β appear in human brains and several mice models of Alzheimer's disease (Rubio-Perez and Morillas-Ruiz, 2012).

In the same way of the astrocytes, microglial cells in CNS are activated by toxic triggers and have been shown to surround both amyloid plaques and NFT in AD brains (Solito and Sastre, 2012). Intrigant questions regard the function of gliosis in neurodegeneration and point the attention to a very delicate balance between protective and toxic roles of astrocytes and microglia activation.

Specific founding show that an initial reactivity is necessary for protection against amyloid deposits and in a pathological scenario, as the brain age, an insufficient response from glial cells leads to an overload of amyloid triggers (Grolla et al., 2013; Liddelow and Barres, 2017; Sokolowski and Mandell, 2011).

On the other side, an excessive inflammatory response can be itself the cause of acceleration of the progression of neuronal loss in AD pathology (Clayton et al., 2017). For instance, studies have shown that microglia and astroglia activate each other in a continuous loop that bring to increased APP and BACE1 expression and Aβ production in astrocytes (Heneka et al., 2005; Zhao et al., 2011).

This suggest that the balance between proinflammatory and anti-inflammatory response plays a main role in aging related disease like AD to avoid neuronal death and behavioral deficits (Sochocka et al., 2017).

CHAPTER 1

Scientific Reports | 6:34802 | DOI: 10.1038/srep34802

Hexokinase I N-terminal based peptide prevents the VDAC1-SOD1 G93A interaction and re-establishes ALS cell viability

Andrea Magrì[1,2,3], **Ramona Belfiore[2,3]**, Simona Reina[1,2,3], Marianna Flora Tomasello[4], Maria Carmela Di Rosa[1,2], Francesca Guarino[2,3], Loredana Leggio[1,2], Vito De Pinto[2,3] & Angela Messina[1,2]

1 Department of Biological, Geological and Environmental Sciences, Section of Biochemistry and Molecular Biology, University of Catania, Italy**.**
2 National Institute of Biostructures and Biosystems (INBB), Italy.
3 Department of Biomedical and Biotechnological Sciences, University of Catania, Italy.
4 CNR Institute of Biostructures and Bioimaging, Catania, Italy.

Abstract

Superoxide Dismutase 1 mutants associate with 20–25% of familial Amyotrophic Lateral Sclerosis (ALS) cases, producing toxic aggregates in mitochondria, notably in spinal cord. The Voltage Dependent Anion Channel isoform 1 (VDAC1), in the outer mitochondrial membrane, is a docking site for SOD1 G93A mutant in ALS mice and the physiological receptor of Hexokinase I (HK1), which is poorly expressed in mouse spinal cord. Our results demonstrate that HK1 competes with SOD1 G93A for binding VDAC1, suggesting that in ALS spinal cord the available HK1-binding sites could be used by SOD1 mutants for docking mitochondria, producing thus organelle dysfunction. We tested this model by studying the action of a HK1-N-terminal based peptide (NHK1). This NHK1 peptide specifically interacts with VDAC1, inhibits the SOD1 G93A binding to mitochondria and restores the viability of ALS model NSC34 cells. Overall, our results suggest that NHK1 peptide could be developed as a therapeutic tool in ALS, predicting an effective role also in other proteinopathies.

Introduction

Amyotrophic Lateral Sclerosis (ALS) is a fatal neurodegenerative disease characterized by the progressive degeneration of both upper and lower motor neurons [1] (MNs). Over 160 missense mutations in the Superoxide Dismutase 1 (SOD1) gene account for 20–25% of familial ALS cases [2], causing MNs death by accumulation of mutant SOD1 (mutSOD1) insoluble toxic aggregates [3]. Interestingly, mutSOD1 aggregates associate with the mitochondrial cytoplasmic side, especially in spinal cord MNs, producing mitochondrial failure [4,5]. Despite it is well known that mitochondria play a central role in bioenergetics metabolism, oxidative stress, apoptosis and axonal transport, the intimate underlying mechanism linking mitochondrial dysfunction in MNs of ALS patients or mice to mutSOD1 still remains elusive. Moreover, it is not yet well understood why MNs are more susceptible to the disease in comparison to other tissues. A previous report showed that, only in the ALS rat spinal cord, mutSOD1 bind directly to the Voltage Dependent Anion Channel isoform 1 (VDAC1), reducing its channel activity [6]. VDAC1 is considered the master regulator of the mitochondria thanks to its crucial action of gate for metabolic and energetic substrates of the organelle [7,8]. Moreover, VDAC1 is the physiological receptor of Hexokinases [9] (HKs). HKs catalyze the glucose phosphorylation and, by binding to VDAC1, they gain a preferential access to newly synthesized ATP. Furthermore, mitochondrial-bound HKs protect the cell from apoptosis, since they diminish VDAC1 propensity to interact with pro-apoptotic protein Bax [10,11]. Interestingly, reduced levels of HK1 were detected in spinal cord, compared to the brain or to other tissues [12]. Therefore, high levels of mutSOD1 binding to VDAC1 correlate with low levels of HK1 in spinal cord. Based on these evidences, we have hypothesized

that in ALS a reduction of HK1 concentration increases VDAC1 propensity to interact with mutSOD1, producing thus mitochondrial dysfunction and cell death.

In this work, we demonstrate the intrinsic ability of SOD1 G93A, but not SOD1 wild type (SOD1 WT), to interact with VDAC1 and to compete with HK1 for binding VDAC1. We also show that a synthetic peptide, corresponding to the HK1 N-terminal region (NHK1 peptide) is able to interact with VDAC1, in *in vitro* and *in cellulo*, modifying its channel conductance. In addition, the NHK1 peptide inhibits the VDAC1-SOD1 G93A interaction in mitochondria purified from NSC34, a mouse motor neuron-like hybrid cell line. Moreover, the expression of the NHK1 peptide in NSC34 cell stably expressing SOD1 G93A, a recognized ALS cell model, recovers the mitochondrial malfunctioning linked to mutSOD1, and largely contrasts the cell death. Overall, our data suggest that VDAC1 and HK1 play a key role in the bioenergetics metabolism of the MNs and could be considered as a promising therapeutic target in ALS.

Results

SOD1 G93A, at variance with SOD1 WT, binds VDAC1 with high affinity. The interaction between VDAC1 and SOD1 G93A in ALS model rat was reported [6] and later questioned [13]. To validate our experimental plan, recombinant human VDAC1, SOD1 WT and SOD1 G93A were expressed, purified and refolded (Fig. S1), and the affinity of SOD1 proteins for mitochondria or VDAC1 was checked by means of several approaches. Intact isolated mitochondria from the motor neuron-like NSC34 cells were incubated with SOD1 WT or G93A, and mitochondrial membranes were precipitated by centrifugation. Then, the SOD1 concentration was revealed by western blot in mitochondrial membranes

or in the supernatant fraction, using VDAC1 as a loading control. Results in Fig.1A show that, while SOD1 WT was found exclusively in the supernatant, a fraction of SOD1 G93A co-precipitated in the mitochondrial pellet. According to the literature [3,6], this data indicates that the recombinant SOD1 G93A, but not SOD1 WT, binds the mitochondria surface. The affinity of SOD1 proteins for VDAC1 was then studied by using an in vitro binding assay. Purified and refolded VDAC1 was immobilized on Ni-NTA magnetic beads and incubated with SOD1 proteins. Then, VDAC1-binding complexes were isolated by the application of a magnetic field. Figure 1B shows that SOD1 G93A was found distributed between VDAC1-bound and -unbound fraction, while SOD1 WT was almost exclusively in the unbound fraction. The VDAC1-SOD1 interaction was quantitatively assayed by Microscale Thermophoresis (MST) analysis. MST measures any variation in the thermal migration of a fluorescently labeled binding partner; changes of fluorescence in a heated spot of the protein solution is a function of increasing interacting protein concentration and can be exploited to calculate the binding affinity coefficient (K_d). The fluorescent-labeled VDAC1 was incubated with increasing concentrations of SOD1 proteins and the changes in fluorescence monitored. Again, as shown in Fig.1C, while no fluorescence change was visible in the presence of SOD1 WT, the incubation with growing concentrations of SOD1 G93A produced fluorescence decrease, indicating that SOD1 G93A specifically interacts with VDAC1. Depletion curve was used to calculate the K_d, which was estimated 4,81 μM.

Overall, the results showed here indicate that the mutant SOD1 G93A specifically interacts with the cytosolic surface of purified mitochondria and with the purified VDAC1

with high affinity. The SOD1 WT is instead unable to bind mitochondria and VDAC1, confirming the data in the literature [6].

SOD1 G93A modulates VDAC1 channel activity. A most relevant VDAC feature is the voltage dependence [14]. VDAC1 is characterized by a typical conductance of 4 nS in 1 M KCl, at low positive or negative voltages (± 10 mV). In these conditions, the channel stays stably in an open and high-conducting state. However, raising the voltage, already at ± 20–30 mV, VDAC1 switches rapidly to a closed and low-conducting state, where it can remain for quite a long time [14–16]. The ability of SOD1 proteins to interfere with VDAC1 activity was analyzed in terms of conductance perturbation. Purified VDAC1 was reconstituted into a planar phospholipid bilayer (PLB) and its channel conductance was monitored before and after addition of SOD1 proteins, on cis or trans side of the membrane. Fig. 2A shows a typical record of ion current through a single VDAC1 channel, in 1 M KCl and an applied potential of + 25 mV. In these experimental conditions, the addition of SOD1 WT did not modify the VDAC1 closed state. Conversely, the addition of SOD1 G93A, on the cis side of the membrane, promoted VDAC1 channel instability: the conductance switched from the stable low-conductance state to several high-conducting states, indicating a specific interaction between the two proteins. Moreover, the effect of SOD1 proteins on the voltage-dependence of VDAC1 was monitored by triangular voltage ramps from 0 to ± 50 mV. The upper curve in Fig.2C shows the typical VDAC1 voltage response. The current linearly follows the voltage applied up to about ± 25 mV, where VDAC1 decreases its channel conductance through step-like transitions, remaining in low-conducting states. A perturbation of voltage-dependence is exclusively visible when SOD1 G93A interacted with VDAC1 (lower

curve, Fig.2C), while no modification in the usual VDAC1 pattern was noticeable upon addition of SOD1 WT (middle curve, Fig.2C). In conclusion, VDAC1 loses its ability to linearly respond to the voltages applied in the presence of the mutant SOD1 G93A.

SOD1 G93A competes with Hexokinase I (HK1) towards binding-site(s) on VDAC1. It is well known that HKs bind to VDAC1 in physiological conditions [9]. We hypothesized that the available area for interaction with soluble proteins is a limited, exposed portion of the transmembrane pore VDAC1. This hypothesis suggests that there could be a competition between different proteins towards the same, or close, site(s) of the VDAC1. For this reason, we repeated the VDAC1-SOD1 G93A binding assay, adding increasing concentrations of HK1. We found that SOD1 G93A binds VDAC1 (Fig.3A): the addition of HK1 strongly decreased (about 40%, Fig.3B) the SOD1 G93A bound to immobilized-VDAC1 (Fig.3A), despite the concentration of SOD1 G93A was overwhelming the stoichiometry of VDAC1 binding site(s). The reduction corresponds to the increase of HK1 in VDAC1-bound fraction, and it is proportional to the HK1 concentrations added in the assay (Fig.3A). Therefore, in such experimental conditions, HK1 is able to impair the VDAC1-SOD1 G93A interaction, suggesting a competition of the two proteins for the same binding site(s). The interference of HK1 in the VDAC1-SOD1 G93A interaction was further investigated in NSC34 cells stably transfected with inducible human SOD1 G93A (NSC34-SOD1G93A), a recognized ALS cell model, and compared with SOD1 WT (NSC34-SOD1WT) expressing cells [17]. We previously controlled that the motor-neuron NSC34 cell line contain a low level of total HK1 in comparison to other cells, as shown in Fig. S2. HK1 mostly localizes to mitochondria (Fig. S2). NSC34-SOD1G93A or NSC34-SOD1WT cells were then transiently

transfected with increasing concentrations of constructs encoding HK1-GFP and the measured fluorescence was related to the mitochondria-bound HK1-GFP. The expression of HK1-GFP was also controlled in NSC34 cells (see Fig.S3), where HK1-GFP localization was also analyzed by fluorescence microscopy. As expected, in NSC34-SOD1WT cells, most of HK1-GFP localized to mitochondria, as demonstrated by the typical punctuated staining (Fig.3C). However, in NSC34-SOD1G93A cells the HK1-GFP signal became diffused, indicating a partial shift towards the cytosol (Fig.3C). A quantification of the mitochondria-related fluorescent signal was obtained after a limited permeabilization with digitonin18 of NSC34 cells expressing SOD1 WT or G93A. In this experiment, the cytosolic GFP fluorescence was allowed to leave the cell and the fluorescence retained inside the cell was assumed to be due to the mitochondria-associated HK1-GFP. Indeed, the permeabilization of NSC34-SOD1WT or G93A stable cell lines, transfected also with GFP, promoted the loss of the signal, in any tested condition. Conversely, the signal was strongly retained (60–70%) in NSC34-SOD1WT expressing also HK1-GFP (Fig.3D), indicating that HK1-GFP binds to mitochondria, in proportion to the added concentration. Interestingly, in NSC34-SOD1G93A, HK1-GFP in the cell was reduced (30–40% of the control). Therefore, the HK1-GFP ability to bind mitochondria was clearly reduced in the presence of SOD1 G93A, but not of SOD1 WT (Fig.3D). Considering that HK1 binds mitochondria exclusively docking VDAC1, this result supports our hypothesis that HK1 and SOD1 G93A compete for the same VDAC1 binding site/s.

A N-terminal HK1-based peptide interacts with VDAC1 and modulates its channel conductance. It is well known that the N-terminal end of HK1 is responsible of the

enzyme interaction with VDAC1 and modulates its channel activity [19–21]. To evaluate the ability of HK1 N-terminus to interfere with the binding between VDAC1-SOD1 G93A, we produced a synthetic NHK1 peptide, corresponding to the first 11 amino acids of human HK1. The electrophysiological behavior of human VDAC1, reconstituted into a PLB, was monitored before and after addition of NHK1 on the cis or trans side of the membrane. Under standard experimental condition (1 M KCl and an applied potential of + 25 mV) the VDAC1 channel was mainly in low-conducting closed states. The addition of NHK1 on one side of the membrane induced several fast and reversible events of VDAC1 low-conducting closed states (reported in Fig.4A). The effect of NHK1 on the channel conductance is even more evident by plotting the amplitude values obtained in the current traces as a function of the number of events. While for VDAC1 alone the amplitude values appear as a main peak corresponding to the closed states (Fig.4B), the presence of NHK1 caused a different distribution of events: an additional, different peak corresponding to the open state was visible, together with the closed states peak (Fig.4C). No influence on the electrophysiological activity was instead detected upon addition of a scramble peptide (ScNHK1) used as control (data not shown). The effect of NHK1 on the voltage-dependence of VDAC1 was monitored by triangular voltage ramps. Again, while no difference was found in presence of ScNHK1 (upper curve, Fig.4D), the presence of NHK1 strongly affected the channel voltage-dependence of VDAC1 (lower curve, Fig.4D). In this experiment, indeed, VDAC1 completely loose, very precociously (already at ± 15 mV applied), its ability to linearly respond to the applied voltage: a continuous switch from open to closed states was observed, especially at positive potentials. Similarly, the current vs. voltage (I–V) plot shows that in the presence of only VDAC1,

I–V plot is linear in the voltage range ± 10–25 mV, and the current transitions (slope), corresponding to decreased conductance states, appeared outside this range (Fig.4E). Upon NHK1 incubation, VDAC1 current transitions at positive voltages are very noisy and pass through different sub-conductance states (Fig.4F). Notably, at negative membrane potentials, regions of decreased slope appeared already at −10 mV, suggesting that NHK1 peptide raises VDAC1 sensitivity to negative voltage applied. No similar result, instead, was observed in the presence of ScNHK1 (data not shown). The electrophysiological analysis strongly indicates the ability of NHK1 peptide to interact specifically with VDAC1 and to modulate its channel conductance and voltage-dependence.

NHKI peptide highly impairs the interaction between SOD1 G93A and VDAC1. To evaluate the NHK1 ability to interfere with VDAC1-SOD1 G93A interaction, a binding assay was performed. Increasing concentrations of NHK1 were added to immobilized-VDAC1, before SOD1 G93A addition. Results in Fig.5A clearly show that, in the presence of 10 and 25 μ M of NHK1 peptide, the amount of SOD1 G93A in VDAC1-bound fraction was reduced by the 40% and 80%, respectively (Fig.5B). No similar effect was observed by repeating the assay in presence of ScNHK1. This result indicates that, in vitro, NHK1 strongly impairs the interaction between VDAC1 and SOD1 G93A in a more effective way than the whole HK1 protein. In fact, a 20-fold smaller concentration of peptide was used to obtain a result similar to that obtained by using the whole HK1 in the previous experiment (see Fig.3A). The ability of NHK1 to inhibit SOD1 G93A from binding the mitochondrial surface was investigated using intact mitochondria purified from NSC34 cells. Mitochondria were incubated with SOD1 G93A, in the presence or absence of 60

μM NHK1 peptide. Figure 5C shows that SOD1 G93A was distributed between the supernatant and mitochondrial fractions, in the absence of peptide. Following incubation with NHK1, a dramatic decrease of 85% SOD1 G93A bound to mitochondria was seen (Fig.5D). Again, no effect was found by incubating mitochondria with the ScNHK1 peptide. These results prove that NHK1 peptide strongly hinders the SOD1 G93A binding to purified VDAC1 or mitochondria.

NHK1 peptide restores the NSC34-SOD1G93A cells viability counteracting the mitochondrial dysfunction. In order to analyze the effect of NHK1 peptide in our ALS-like *in cellulo* system, the subcellular distribution of NHK1 peptide was investigated. NSC34 cells were transiently transfected with a plasmid encoding for a HA-tagged NHK1 peptide and for a mitochondrial-targeted Red Fluorescent Protein (mtDsRED) [18]. Immunofluorescence assays in Fig.6A revealed that NHK1 peptide mainly co-localized with mtDsRED signal, indicating its ability to bind mitochondria in NSC34 cells. Then, the NHK1 peptide, as well as the whole HK1 as control, was expressed in NSC34-SOD1G93A or SOD1WT to evaluate its ability to counteract the toxicity mediated by mutSOD1. Literature reports indicate that SOD1 mutant expression in NSC34 cell promote a significative loss of cell viability, accordingly with the specific mutation [22]. Our results show that, upon expression of SOD1 G93A, NSC34 cells loose about 20% of cell survival (Fig.6B). However, this toxic effect was counteracted by the NHK1 expression: an improvement of cell viability, (about 50% of the control, Fig.6B) was observed; furthermore, a similar but lower effect was also found upon overexpression of the whole HK1 (Fig.6C). Therefore, supplementation of NHK1 peptide (or HK1) to NSC34-SOD1G93A cells promotes a recovery of the cell viability. To evaluate the NHK1

influence on mitochondrial functionality, mitochondrial membrane potential variation (ΔΨ m) was assayed in the presence of NHK1 peptide or HK1. ΔΨ m is related to the ATP production by oxidative phosphorylation; therefore, it is considered an indication of good mitochondrial and cellular health [23,24]. Using mitochondria-targeted fluorescent probes, we estimated in flow cytometry the rate of mitochondrial depolarization. NSC34-SOD1G93A cells shown a high level of depolarized mitochondria compared to NSC34-SOD1WT. Indeed, as showed in Fig.7A, the emission peak of fluorescence for NSC34-SOD1G93A cells was significantly lower compared to the NSC34-SOD1WT peak. The uptake of the probe into mitochondria is ΔΨ m-dependent: thus, this result means that SOD1 G93A expression strongly affects the cell energetic metabolism. A quantification of fluorescent-negative NSC34-SOD1G93A cells, corresponding to the depolarized mitochondria rate, was performed as previously reported [24], and resulted in a dramatic increase of about 60%, compared to NSC34-SOD1WT (Fig.7B). In this dramatic situation, the NHK1 expression, but not ScNHK1, resulted in a partial recovery of the physiological ΔΨ m, since depolarized mitochondria were reduced by 20% in NSC34-SOD1G93A cells (Fig.7B, S4).

Similarly to NHK1 peptide, the expression of the whole HK1 reduced the depolarized mitochondria of about 15% (Fig.7C). In conclusion, the NHK1 peptide, and minimally the whole HK1, is able to partially recover the mitochondrial functionality and, consequently, the cell vitality in the ALS model NSC34 cells.

Discussion

A previous report showed that mutSOD1 interact with VDAC1 in spinal cord mitochondria from ALS model rat6. In our work we preliminary confirmed that the mutant SOD1 G93A, but not the SOD1 WT, is able to interact with VDAC1 immobilized on magnetic beads. Furthermore, we determined, by MST analysis, the binding affinity of SOD1 G93A with VDAC1 and the effect of SOD1 G93A on VDAC1 conductance. Our electrophysiological data showed that, at the voltages applied which stably close VDAC1, SOD1 G93A, but not the SOD1 WT, promotes a prolonged instability of VDAC1 conductance. On the other side, Israelson and coworkers demonstrated that addition of SOD1 G93A to PLB-reconstituted VDAC1, at the voltages applied which stably maintain VDAC1 in an open state, promotes a partial closure of VDAC1 channels [6]. Therefore, both results strongly support a direct effect of mutated SOD1 G93A on VDAC1 conductance. From the literature and from these convincing results we hypothesized that VDAC1 could be the specific docking site on the OMM for the SOD1 G93A, and possibly for all SOD1 mutants. The influence of the interaction in the gating features of VDAC1 could indeed explain the mechanism of impairment of the bioenergetics metabolism and the oxidative stress of the ALS MNs [6]. In this perspective, the physiological interactions involving VDAC1 in spinal cord MNs could be altered in ALS, giving thus an explanation for the specific susceptibility to the disease showed by this tissue. Another recent report showed that SOD1 G93A, but unexpectedly also SOD1 WT, preferentially bound to Bcl2, rather than VDAC1, in ALS mitochondria [13]. The binding promoted a conformational change of Bcl2 that, in turn, altered its physiological interaction with VDAC1, producing mitochondrial dysfunction [13]. This means that SOD1 G93A might bind VDAC1 or

alternatively Bcl2. However, a detailed analysis of gene expression in mouse spinal cords reveals that Bcl2 level is extremely low and further decreases with the aging of mice [25]. In the same database, it is shown that VDAC1 is highly expressed in brain and spinal cord with no special age difference [25]. Therefore, the VDAC1-SOD1 G93A interaction should be predominant in ALS spinal cord MNs, in comparison to VDAC1-Bcl2 interaction. This is further strengthened by the ability of specific antibodies against misfolded SOD1 proteins (e.g. against DES2-3H1 SOD1 domain) to recognize SOD1 mutant deposits interacting with VDAC1 on the cytosolic surface of mitochondria [26]. Moreover, it has also been clearly reported that mitochondria from brain or spinal cord differentially respond to injury, with an imbalance in oxidative stress that may contribute to the susceptibility of spinal cord MNs in neuropathologies [27]. Considering these evidences, we have addressed our work towards the characterization of the binding site of mutSOD1 on the surface of ALS MNs mitochondria. VDAC1, the main pore and the most abundant protein of the OMM, is also known as the receptor of HK1, an important enzyme for the energy production [11]. HK1 exploits the VDAC1 as a channel bringing the newly synthesized ATP to glucose phosphorylation. HK1, as HK2, utilizing the N-terminal domain, binds to VDAC1. The interaction with HK1 has also another important consequence: it can modulate the VDAC1 activity [20] and the Bcl2-VDAC1 interaction, which in turn, regulates the apoptotic intrinsic pathway [10]. Intriguingly, brain is very rich of HK1 and HK2, while spinal cord shows a peculiarly low HK1 concentration and no HK2 expression [6,25,28]. It is known that, in affected tissues of ALS rat, VDAC1-linked mutSOD1 level is inversely correlated to the HK1 concentration6. We thus hypothesize that in spinal cord mitochondria from ALS MNs, a competition for the

VDAC1 binding site might happen between mutSOD1 and HK1, the physiological interactor. When the mutSOD1 affinity, or concentration, is higher than HK1, mitochondria can be subject to a double effect: to become more susceptible to the mutSOD1-mediated toxicity and to lose the anti-apoptotic protection exerted by HK1 when bound to the organelle. In this work, by using in vitro and *in cellulo* approaches, we proved that HK1 and specifically its N-terminal domain, competes with SOD1 G93A for binding to common site/s on VDAC1. The in vitro results show that the increase of HK1 concentration promotes a decrease of SOD1 G93A affinity for the immobilized VDAC1. In addition, we demonstrate that HK1-GFP in NSC34 cells highly competes with SOD1 G93A for binding VDAC1. Conversely, SOD1 WT expression does not compete with HK1 for the organelle's binding site. We also demonstrated that HK1-GFP counteracts the mitochondria toxicity found in NSC34-SOD1G93A. Increasing evidences indicate that HKs play a decisive role not only in glycolysis but also in cell survival, carrying out a defense action on many cell types or contrasting disease pathways [29–32]. Not coincidentally, VDAC1-HKs complexes allow the cancer cells to grow faster (Warburg effect) and, to date, destroying these complexes has been considered a putative therapy [33,34]. In order to develop our findings towards a perspective therapy for ALS, we produced a synthetic NHK1 peptide corresponding to the N-terminal domain of human HK1, and tested it in our experimental models. Our interest in this domain comes from the consideration that it is sufficient to specifically target the enzyme to VDAC1, as demonstrated when it is deleted from the protein [19,21,35]. Moreover, the moiety corresponding to the first 11 residues of HK1 represents the most hydrophobic part of N-terminus, forming a "tail" structured in α -helix, which is believed responsible to take

contact with the OMM and, thus, with VDAC1 [36,37]. We have found that the NHK1 peptide specifically interacts with VDAC1, destabilizing its gating properties and considerably modifying its conductance at any voltage applied. Moreover, NHK1 peptide highly counteracts the SOD1 G93A binding to beads-immobilized VDAC1, about 20 times more efficiently than the whole HK1. Similar results were found also in isolated mitochondria and in the chosen ALS cell model (NSC34-SOD1G93A). Interestingly, the expression of NHK1 peptide in NSC34-SOD1G93A produced an important decrease in the toxicity mediated by mutSOD1, and promoted the recovery of mitochondrial depolarization. In conclusion, the NHK1 peptide in our hands contrasts the VDAC1 interaction with SOD1 G93A. As a consequence, the measured life parameters remarkably improved. Although in this work we support the VDAC1 involvement in ALS mitochondrial dysfunction, we are well aware that many other aspects remain to be clarified. To give just an example, the amino acid sequence of the three VDAC isoforms [38] is conserved, thus it is possible that the commercially available antibodies against VDAC do not perfectly match the VDAC1 isoform. While VDAC2 does not seem to interact with mutSOD1 [6], no information about VDAC3 involvement is available, even if this isoform is expressed in the spinal cord as much as VDAC1 and it was shown that it is able to interact with a number of cytosolic proteins [39]. Therefore, it will also be interesting to examine the possible involvement of VDAC3 in ALS, especially in light of its ability to function as a buffer for mitochondrial ROS [40]. Furthermore, mitochondrial dysfunction and aggregation of toxic peptides/proteins correlate not only to ALS, but also to other neurodegenerative diseases, like Alzheimer's [41] or Parkinson's [42]. Interestingly, amyloid beta peptide, such as alpha-synuclein, bind VDAC1 [43,44].

Consequently, we suppose that NHK1 peptide could contrast also these specific interactions, producing a healthy effect in Alzheimer or Parkinson disease. In conclusion, our results provide new insight into the mechanism underlying the benefits of mutSOD1/ VDAC1 inhibition against neurodegeneration and give details to explain the etiology of ALS. In addition, we propose that NHK1 peptide, possibly mimicking the contact surfaces between SOD1 G93A and VDAC1, can be used to interfere with this interaction and relieve the ALS mitochondrial dysfunction recovering cell viability (Fig.8). Our work suggests for NHK1 peptide a powerful neuroprotective potential which needs to be especially assessed for its therapeutic relevance in ALS.

Methods

Preparation of recombinant proteins and peptide. The N-terminal 6xHis-tagged VDAC1, the Strep-tagged SOD1 WT and the ALS-linked SOD1 G93A mutant were expressed in E. coli and purified as detailed explained in Supplementary Information. The recombinant human HK1 was purchased by Sigma. A peptide corresponding to residues 2–12 (N-terminal region) of human HK1 protein (IAAQLLAYYFT) was produced by GenScript Inc. (Piscataway, USA) and is called in the text: NHK1 peptide. A scramble peptide, ScNHK1 (FAQLTIALAYY), was synthetized and used as control.

Mitochondrial binding assay. Intact mitochondria were purified from NSC34 cells by Mitochondrial isolation kit (Miltenyi Biotech), according with manufacturer's instructions. Isolated, intact mitochondria, in the storage buffer provided, were quantified by Lowry method. Mitochondria were incubated with 2 μg of purified SOD1 WT or G93A for 1 h at RT, under constant shaking in storage buffer. Alternatively, a pre-incubation with

60 μNHK1 peptide for 1 h, in the same condition, was performed. Mitochondrial pellet was collected by centrifugation for 2 min at 13000×g. Supernatants were collected, and mitochondrial pellets were lysed using 3% Triton X-100. Proteins in mitochondrial or supernatant fraction were detected by western blot and quantified as explained in Supplementary Information. At least, three independent experiments were performed.

In vitro VDAC1-SOD1 binding assays. Recombinant VDAC1 was immobilized onto Ni-NTA Magnetic Agarose Beads (Qiagen) by exploiting its 6xHis-tag, according with manufacture's protocol. For each experiment, a large excess of VDAC1 (30 μM) were incubated with 50 μ L of beads suspension in Interaction Buffer (IB) (300 mM NaCl, 50 mM NaH_2PO_4, 20 mM imidazole, pH 8.0) to saturate all sites. Beads were collected using the magnet-based system DynaMag-2 (Life Technologies) and washed twice in Wash Buffer (300 mM NaCl, 50 mM NaH_2PO_4, 20 mM imidazole, 0.05% Tween-20, pH 6.3) to remove any excess of VDAC1. Beads-immobilized VDAC1 were incubated with 6.25 μ M SOD1 WT or G93A, for 1 h at RT, under constant shaking, in 100 μ L of IB. The assay was also performed by pre-incubating immobilized-VDAC1 for an extra 1 h with increasing concentration of purified human HK1 (0, 100, 200 μM) or NHK1 peptide (0, 5, 10, 25 μM), before SOD1 G93A addition. Beads were recovered using Dyna-Mag2 system and VDAC1-complexes were eluted from beads using 50 μL of Elution Buffer (300 mM NaCl, 50 mM NaH_2PO_4, 300 mM imidazole, pH 3.5). Any protein in VDAC1-bound and -unbound fractions was evaluated by western blot. Three independent experiments were performed for each condition tested.

Microscale Thermophoresis. Microscale Thermophoresis (MST) analysis was performed using the NanoTemper Monolith NT.115 apparatus (NanoTemper

Technologies, Munich, Germany) as described [45]. VDAC1 was fluorescently-labeled using the NanoTemper protein-labeling kit Green/Blue. 100 nM labeled-VDAC1 were incubated, for 5 min at RT in the dark, with serial dilutions of SOD1 WT or G93A (from 1.22 nM to 20 μ M), in PBS with 0.05% Tween 20. Afterwards, the samples were loaded into a glass capillary (Monolith NT Capillaries) and thermophoresis analysis was performed (light-emitting diode 20%, IR laser 20 to 80%). In every determination at least three independent experiments were performed.

VDAC1 channel reconstitution, recording and analysis. Purified VDAC1 was reconstituted into a Planar Lipid Bilayer (PLB) apparatus (Warner Instruments, Hamden, CT, USA), previously described [46]. Bilayers were prepared using asolectin (Sigma) dissolved in decane (Sigma) containing 1% chloroform (Sigma) across a 200 μm hole in a derlin cuvette (Warner Instruments). Experiments were performed in 1 M KCl, 10 mM Hepes, pH 7.040,46. Control experiments using empty membrane and/or detergents were performed to avoid activity in any of the above solutions. Data were acquired using a Bilayer Clamp amplifier (Warner Instruments) at 100 μs/point, filtered at 200 Hz and analyzed offline using Clampfit 10.4 program set (Axon Instruments, Union City, CA, USA). Single channel analysis of VDAC1 was performed in presence or not of 0.2 μM of SOD1 WT or G93A, 15 μM NHK1 or ScNHK1 peptide.

Motor neuron cell lines. The mouse motor neuron-like NSC34 cell line (CELLutions Biosystem Inc.), and/or the NSC34 cells stably transfected with pTet-ON plasmid (Clontech) harboring sequences encoding for SOD1 WT (NSC34-SOD1WT) or G93A (NSC34-SOD1G93A) [17] were used as ALS model cell line. Cell maintenance,

induction, plasmids and transfection condition are explained in detail in Supplementary Information.

Analysis of HK1-GFP mitochondrial retention signal. NSC34-SOD1WT and NSC34-SOD1G93A cells were seeded on 24-well plates and transfected after 24 h from induction using 0,25 (low), 0,5 (medium) or 1 (high) μg of pEGFP-N1-HK1 or empty pEGFP-N1. Cells were harvested after additional 24 h by trypsinization and split into two separate tubes. One series was resuspended in Krebs Ringer Buffered Saline (130 mM NaCl, 3.6 mM KCl, 10 mM HEPES, 2 mM $NaHCO_3$, 0.5 mM NaH_2PO_4, 0.5 mM $MgCl_2$, 1.5 mM $CaCl_2$, 4.5 g/l glucose, pH 7.4) to obtain the not-permeabilized sample. The other series was subject to selective permeabilization of plasma membrane by incubation for 2 mins with 25 μ g/mL digitonin (Sigma) in Intracellular Buffer (130 mM KCl, 10 mM NaCl, 20 mM HEPES, 1 mM $MgSO_4$, 5 mM succinate pH 7.2) supplemented with 50 μ M EGTA to avoid Ca^{2+} induction of the permeability transition in the mitochondria of permeabilized cells. Cells were then analyzed by flow cytometry on FL1 log mode. The retention of HK1-GFP signal was calculated considering the residual GFP signal in the permeabilized sample compared to the respective non permeabilized one. The loss of the GFP signal in cells expressing a cytosolic GFP was used as control. Data reported are representative for three sets of independent experiments, each performed in triplicate and based on 100.000 events for each group. Data were statistical analyzed by chi-square test. A $p < 0,001$ was taken as significant.

Cell viability assay. 24 h-induced NSC34-SOD1WT and NSC34-SOD1G93A cells seeded on 24-well plates were transfected using 0,25 μg of pEGFP-N1-HK1 or empty pEGFP-N1 or 0,5 μg of pMCS-mtDsRED-NHK1 or scramble or empty pCMS-mtDsRED.

Cell viability was analyzed using 3-(4,5-dimethylthiazol-2-yl)-2,5- diphenyltetrazolium bromide (MTT) [47] (Sigma). A colorimetric assay was performed using the microplate reader Varioskan (Thermo Scientific). Reported data are representative for three sets of independent experiments, each performed in triplicate. Data were statistically analyzed using one-way ANOVA followed by Bonferroni post hoc test. The values $p < 0.05$ and $p < 0.01$ were taken as significant.

Measurements of mitochondrial membrane potential (ΔΨm). ΔΨ m was measured using tetramethyl-rhodamine methyl ester (TMRM) or Rhodamine 123 (RH123) (Molecular Probes) according to the excitation/emission wavelength of the transfection reporter or of the transfected fluorescent protein used. Both probes accumulate in active mitochondria due to their positive charge, whereby the reduction of ΔΨ m leads to the release of fluorescent probes. Transfected NSC34-SOD1WT and NSC34-SOD1G93A cells were washed with PBS and incubated for 30 min at 37 °C with Krebs Ringer Buffered Saline supplemented with either 200 nM TMRM or 0.1 μ g/mL RH123 and 20 μM Verapamil (as a multi drug-resistant pump inhibitor) (Sigma). Cells were then harvested and immediately analyzed by flow cytometry. Cells were excited by an air-cooled argon 488 nm laser, reading the GFP fluorescence of HK1-GFP or RH123 fluorescence in FL1 log mode; TMRM and mtDsRED used as transfection reporter of NHK1 peptide were read on FL3 log mode. Only viable cells detected by reading the scattering indicated as FSC and SSC, were considered for our analysis. The threshold physiological value of ΔΨ m was estimated by using cells exposed to 1 μM of the uncoupling agent FCCP as a negative control. Data reported are representative for three sets of independent experiments, each performed at least in triplicate and based on 20.000 events for each

group. Data were statistical analyzed by chi-square test. A $p < 0,001$ was taken as significant.

Flow cytometry. A CyFlow® ML flow cytometer (Partec) system was used. The system is equipped with three laser sources and 10 optical parameters with dedicated filter setting and a high numerical aperture microscope objective (50 NA 0.82) for the detection of different scatter and fluorescence signals. Data obtained were acquired and gated by using the FCS Express 4 software (DeNovo).

Statistical analysis. Significance was determined as reported and indicated as $*p < 0.05$, $**p < 0.01$ and $***p < 0.001$.

Figures

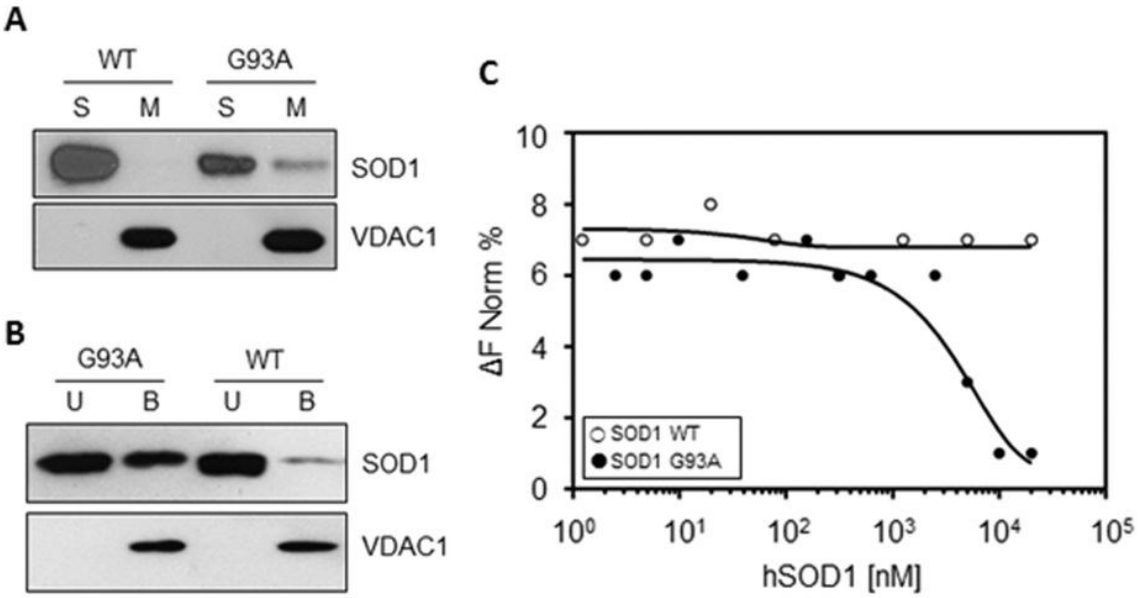

Figure 1. SOD1 G93A interacts with the cytosolic surface of mitochondria and VDAC1. (A) Representative western blot analysis (n = 3 independent experiments) of in vitro mitochondria-SOD1 proteins binding assay. Intact purified mitochondria were incubated with SOD1 WT or G93A and precipitated by centrifugation. VDAC1 was used as loading control. An aliquot of SOD1 G93A was found in mitochondrial pellet (M); on the contrary, SOD1 WT was exclusively present in the supernatant fraction (S). (B) Representative western blot analysis (n = 3 independent experiments) of in vitro binding assay between VDAC1 and SOD1 proteins. SOD1 G93A was found distributed between VDAC1-bound (B) or -unbound (U) fraction, while SOD1 WT was found almost exclusively in U fraction. (C) MST analysis of VDAC1-SOD1 interaction. Variation in normalized fluorescence (ΔFNorm %) was found exclusively for SOD1 G93A, indicating a specific interaction with VDAC1

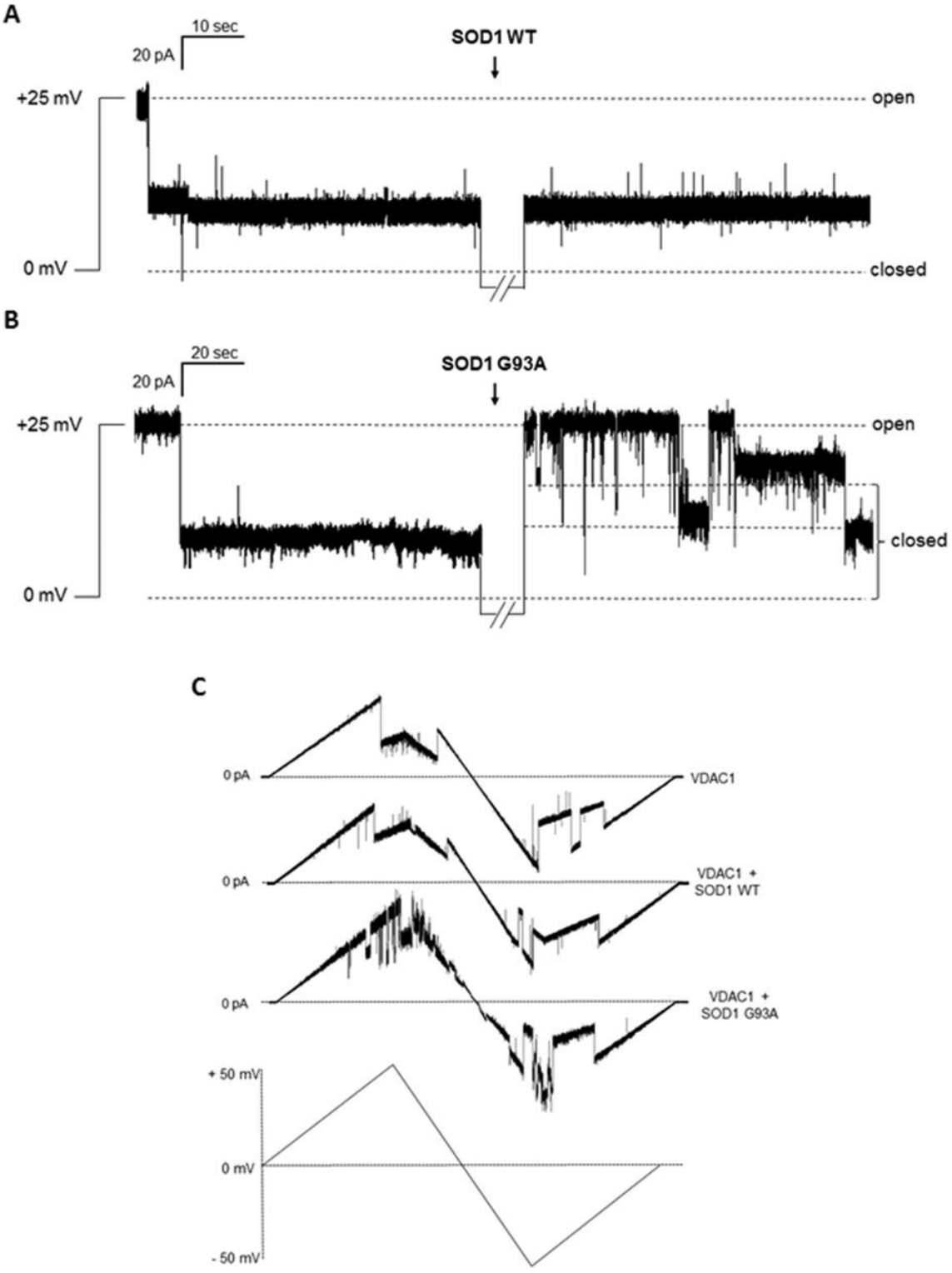
A
10 sec
20 pA
SOD1 WT
+25 mV
open
0 mV
closed
B
20 sec
20 pA
SOD1 G93A
+25 mV
open
closed
0 mV
C
0 pA
VDAC1
0 pA
VDAC1 +
SOD1 WT
0 pA
VDAC1 +
SOD1 G93A
+ 50 mV
0 mV
- 50 mV

Figure 2. Electrophysiological characterization of VDAC1-SOD1 interaction at the PLB. (A) A representative trace of single channel analysis of VDAC1 conductance at + 25 mV in 1 M KCl before and after the addition of SOD1 WT (n = 4). VDAC1 stably switched to the closed state depending on the applied voltage. Presence of SOD1 WT did not affect the channel conductance, since VDAC1 remained stable in its typical closed state. (B) A representative trace of single channel analysis of VDAC1 recorded using same condition in (A) before and after the addition of SOD1 G93A (n = 4). Presence of SOD1 G93A promoted instability of VDAC1 conductance. (C) Triangular curve of different experiments performed in a symmetric 1 M KCl solution with VDAC1 inserted in the membrane (n = 15) (upper curve) or upon addition of SOD1 WT (n = 5) (middle curve) or SOD1 G93A (n = 6) (lower curve). The addition of SOD1 G93A promoted instability of channel conductance at several voltages applied. At the bottom of the figure, the applied voltage curve.

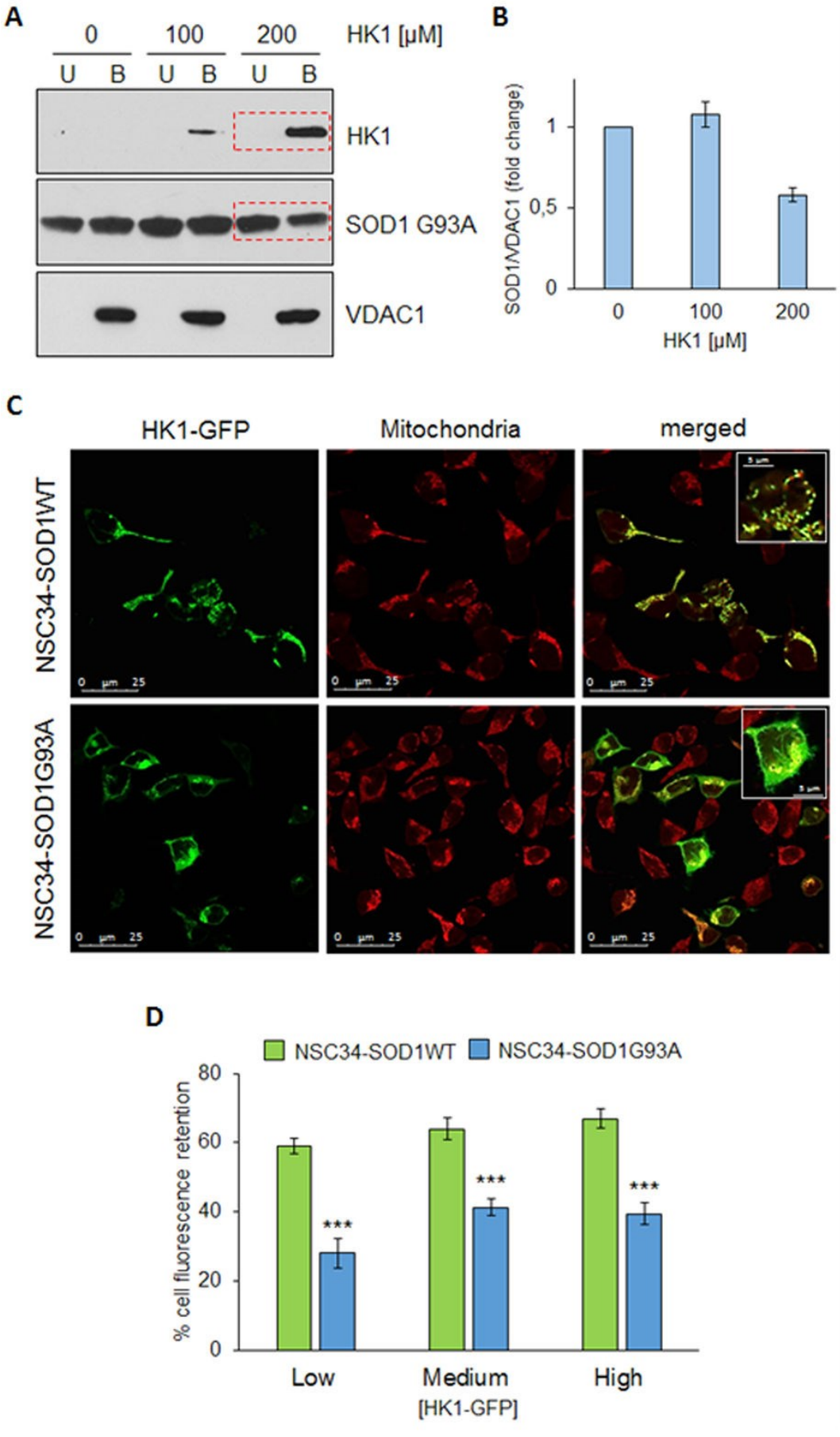
A
0
100
200
HK1 [µM]
U B U B U B
HK1
SOD1 G93A
VDAC1
B
SOD1/VDAC1 (fold change)
1
0,5
0
0
100
200
HK1 [µM]
C
HK1-GFP
Mitochondria
merged
NSC34-SOD1WT
NSC34-SOD1G93A
D
NSC34-SOD1WT
NSC34-SOD1G93A
% cell fluorescence retention
80
60
40
20
0
***
***
***
Low
Medium
High
[HK1-GFP]

Figure 3. HK1 competes with SOD1 G93A in VDAC1 binding. (A) Western blot analysis of the binding between VDAC1 and SOD1 G93A in the presence of increasing concentration of recombinant HK1 (0–200 μM). Affinity of SOD1 G93A for VDAC1 was reduced of about 40% with respect to the control in the presence of 200 μM HK1 (a representative blot from three independent experiments). (B) Relative quantification of SOD1 G93A in VDAC1-bound fraction obtained by densitometry. Data are showed as means ± SEM of n = 3. (C) Subcellular distribution of HK1-GFP detected by fluorescence microscopy in NSC34-SOD1WT or NSC34-SOD1G93A cells. In presence of SOD1 WT, HK1-GFP almost completely binds mitochondria, as showed by its co-localization with Mito-Tracker; conversely, in the presence of SOD1 G93A, HK1-GFP signal is more diffused. (D) HK1-GFP in NSC34 cells is bound to mitochondria and competes with SOD1 G93A. The fluorescent signal of the HK1-GFP was measured after plasma membrane permeabilization by digitonin. The retention of fluorescence indicates that HK1-GFP is associated to intact mitochondria. The fluorescent signal retained in NSC34-SOD1WT or G93A cell was estimated with regard to the increasing amount of HK1-GFP transfected into the cells. Data were normalized to the corresponding controls expressing the same amount of the plasmid carrying the GFP only. The amount of HK1-GFP retention grows as the amount of HK1-GFP plasmid is increased. Lower levels of HK1-GFP retention were found in NSC34-SOD1G93A compared to the SOD1WT. Data are shown as means ± SEM of n = 3; *** < 0,001 compared to NSC34-SOD1WT.

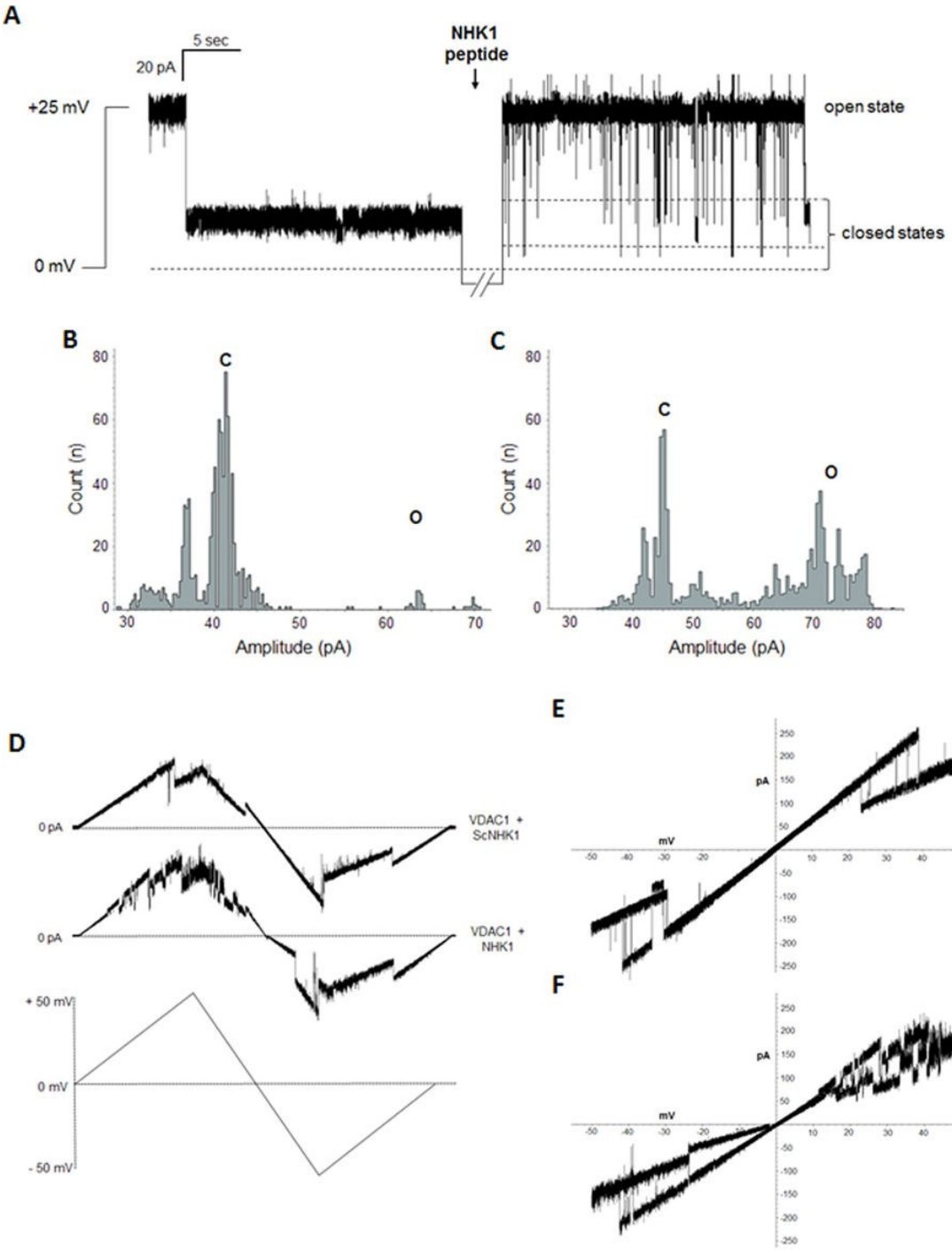

Figure 4. Electrophysiological characterization of the interaction between the NHK1 peptide and VDAC1. (A) Single channel analysis showing a representative trace of VDAC1 conductance (n = 5) at +25 mV in 1 M KCl before and after the addition of NHK1 peptide. VDAC1 stably switched to the closed state depending on the applied voltage.

Conversely, the addition of NHK1 peptide promoted the instability of the channel, affecting the pore's gating. (B, C) Plots of the distribution of channel amplitude events calculated in the absence (B) or in the presence of NHK1 peptide (C). Amplitude values for VDAC1 alone appeared as a main peak corresponding to the closed state. On the contrary, the presence of NHK1 changed the amplitude values distribution, yielding two distinct peaks, the former corresponding to the closed state and the latter to the open state. (D) Triangular curve of different experiments performed in a symmetric 1 M KCl solution with VDAC1 inserted in the membrane upon addition of a scramble peptide (n = 5) (upper curve) or NHK1 peptide (n = 8) (lower curve). The addition of NHK1 peptide promoted the instability of channel conductance at several voltages applied. At the bottom of the figure, the applied voltage curve. (E, F) Current-voltage (I–V) curves obtained from the experiments in (D). (E) I–V plot of VDAC1 alone is a linear trace at low applied voltages (from ± 10 to ± 25 mV) and show characteristic current transitions at high voltages. (F) Conversely, upon NHK1 incubation, VDAC1 I–V trace is extremely noisy (especially at positive voltages), and shows different sub-conductance states

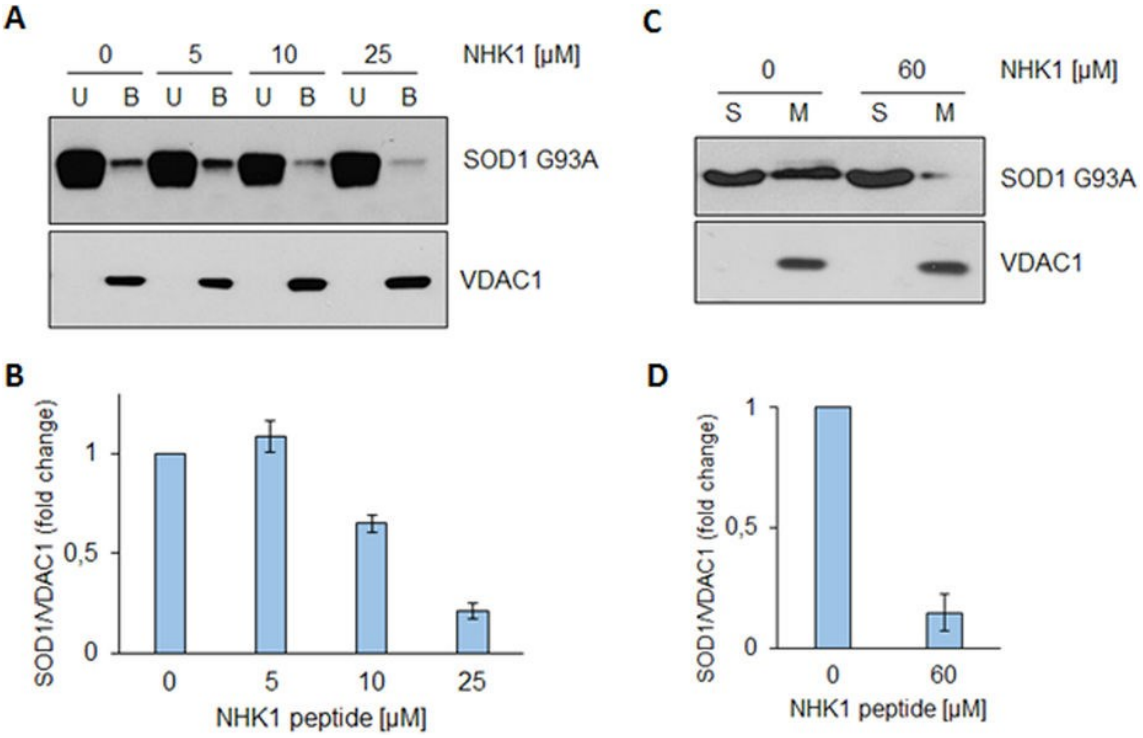

Figure 5. NHK1 peptide impairs VDAC1-SOD1 G93A interaction. (A) Representative western blot analysis of three independent experiments of the binding assay between VDAC1 and SOD1 G93A in the presence of increasing concentrations of NHK1 peptide (0–25 μ M). NHK1 reduce the binding of SOD1 G93A to VDAC1 in vitro. (B) Relative quantification of SOD1 G93A in VDAC1-bound fraction obtained by densitometry. Data are showed as means ± SEM of n = 3. (C) Representative western blot analysis of three independent experiments of the binding assay between mitochondria and SOD1 G93A in the presence of NHK1 peptide (60 μM). NHK1 dramatically reduces SOD1 G93A in mitochondrial pellet (M) to about 80% of control. S indicates supernatant fraction containing exceeding SOD1. (D) Relative quantification of SOD1 G93A in mitochondrial pellet. Data in D are means ± SEM of n = 3.

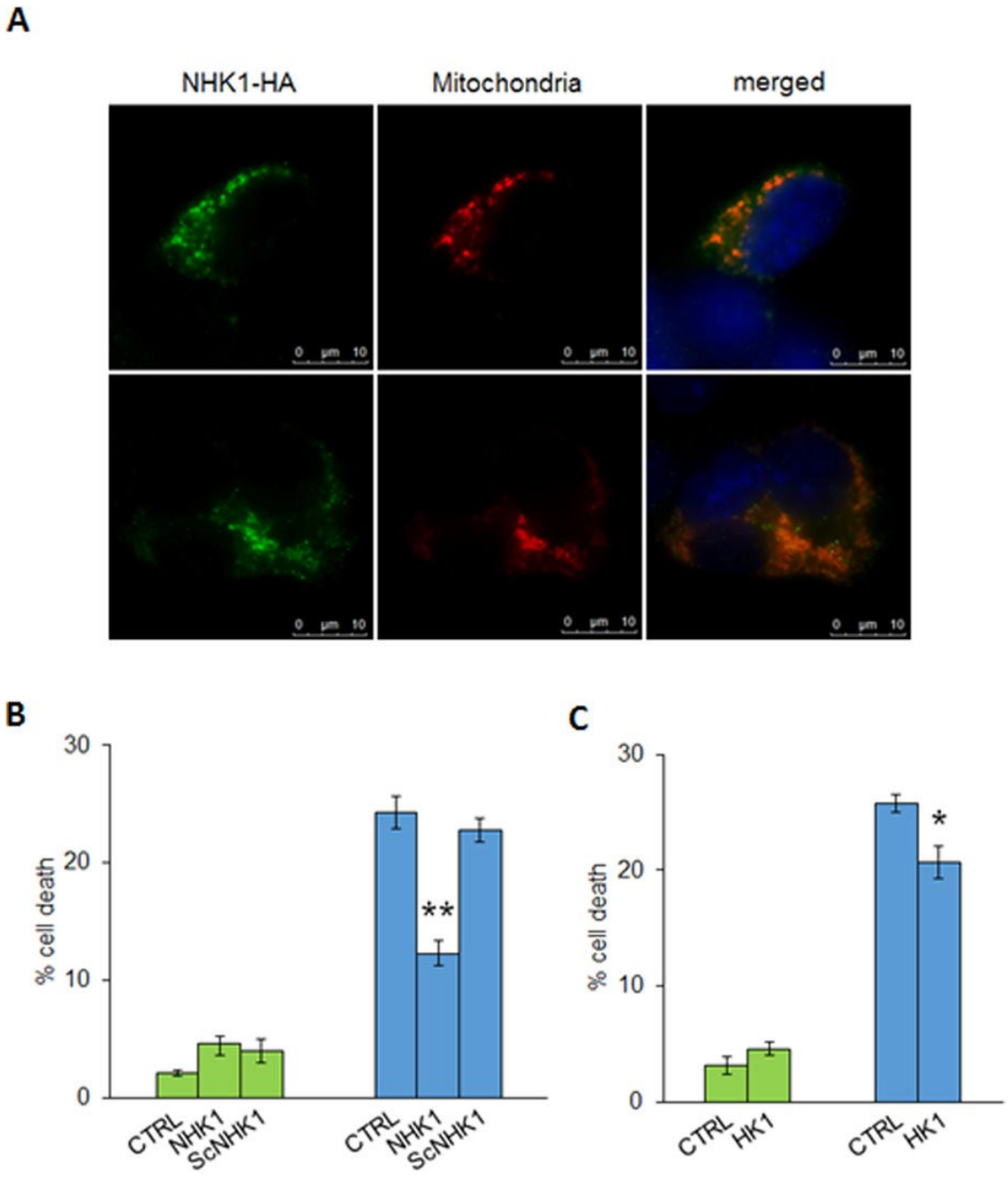

Figure 6. NHK1 peptide localize to mitochondria and improves the cell viability of NSC34 cells. (A) Fluorescence microscopy analysis of subcellular distribution of NHK1-HA peptide in NSC34 cells by indirect immunofluorescence targeting the HA tag. Mitochondria were visualized by expressing the mitochondrial-targeted mtDsRED protein. NHK1-HA peptide co-localized with mitochondria. (B) Analysis of cell death in

NSC34-SOD1WT and G93A analyzed upon transfection with an empty vector (CTRL) or a plasmid encoding either for the NHK1 peptide (NHK1) or the scramble peptide (ScNHK1). Expression of SOD1 G93A produced 20% of NSC34 cell death compared with the same cells expressing SOD1 WT. Conversely, an improvement of cell viability in NSC34-SOD1G93A was observed upon expression of NHK1 peptide. The scramble peptide does not change the cell viability, indicating a specific effect of NHK1 peptide. Data were normalized with the not induced transfected cell. Data are expressed as means ± SEM (n = 3), **p < 0.01 compared to NSC34-SOD1G93A. (C) Analysis of NSC34-SOD1WT and G93A cell death upon transfection with empty plasmid (CTRL) or plasmid encoding for HK1. The expression of HK1-GFP in combination to the SOD1 G93A promoted a slight but significant improvement of cell viability. Data were normalized for the correspondent, not induced transfected cell. Data are expressed as means ± SEM (n = 4), *p < 0.05 compared to NSC-34-SOD1G93A CTRL.

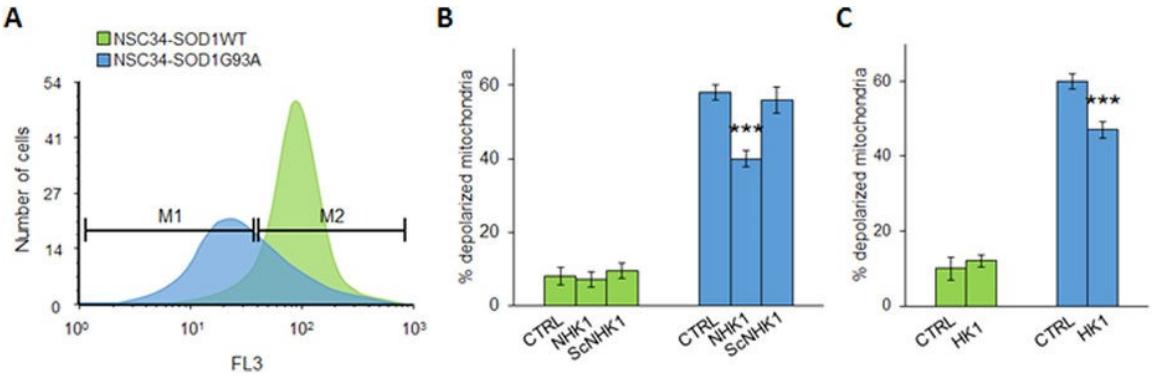

Figure 7. NHK1 peptide recovers the mitochondrial functionality of NSC34 cells. (A) Representative Flow cytometry 1D plots of induced NSC34-SOD1WT or G93A clones stained with TMRM. The fluorescence was read on FL3 channel (λ ex 550 nm/λ em 590

nm). Peak corresponding to NSC34-SOD1G93A is shifted toward lower values of fluorescence. M1 indicates cells with low $\Delta\Psi$ m values, M2 indicates cells with high $\Delta\Psi$ m. (B) Mitochondrial depolarization rate of NSC34 cells is affected by the presence of NHK1 peptide. Mitochondria depolarization was estimated by TMRM fluorescence in NSC34-SOD1WT or G93A expressing NHK1 or ScNHK1 peptide. A high rate of mitochondrial depolarization was found for NSC34-SOD1G93A, while only few depolarized mitochondria were observed in NSC34-SOD1WT. However, reduction of depolarization was observed upon expression of NHK1 peptide, but not ScNHK1. Data were normalized with the correspondent, not induced cells. Gates reported in (A) were used for quantification. Data are expressed as means ± SEM (n = 3), ***$p < 0.001$ compared to NSC34-SOD1G93A CTRL. (C) Mitochondrial depolarization of NSC34 cells in the presence of HK1. Mitochondria depolarization was estimated by RH123 fluorescence in NSC34-SOD1WT or G93A expressing HK1. Depolarization was reduced by HK1 expression in NSC34SOD1G93A. Data were normalized with correspondent not induced cells and are expressed as means ± SEM (n = 3). ***$p < 0.001$ compared to NSC34-SOD1 G93A CTRL.

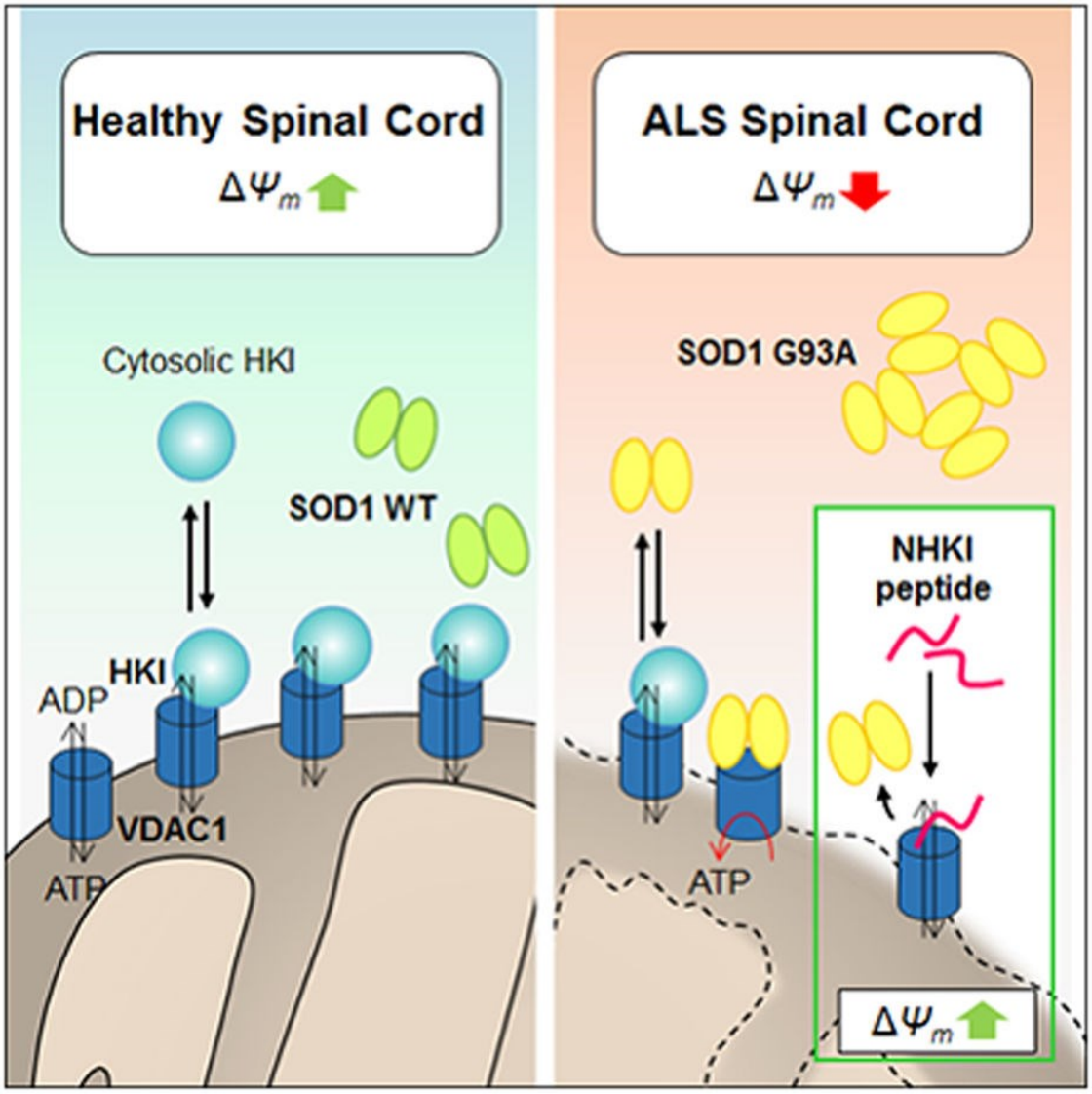

Figure 8. A proposed mechanism of action of NHK1 peptide. In physiological conditions, VDAC1 is the receptor of HK1, but not of SOD1 WT. Conversely, in ALS, SOD1 G93A binds VDAC1 and impairs HK1 binding. As a consequence, VDAC1 channel conductance and metabolic exchanges through VDAC1 are strongly impaired, thus promoting mitochondrial dysfunction. NHK1 peptide inhibits SOD1 G93A binding to VDAC1 and ameliorates mitochondrial dysfunction and, in general, the cell viability.

References

1. Pasinelli, P. & Brown, R. H. Molecular biology of amyotrophic lateral sclerosis: insights from genetics. Nat. Rev. Neurosci. 7, 710–723 (2006).

2. Rosen, D. R. et al. Mutations in Cu/Zn superoxide dismutase gene are associated with familial Amyotrophic Lateral Sclerosis. Nature 362, 59–62 (1993).

3. Vande Velde, C., Miller, T. M., Cashman, N. R. & Cleveland, D. W. Selective association of misfolded ALS-linked mutant SOD1 with the cytoplasmic face of mitochondria. Proc. Natl. Acad. Sci. USA 105, 4022–4027 (2008).

4. Liu, J. et al. Toxicity of familial ALS-linked SOD1 mutants from selective recruitment to spinal mitochondria. Neuron 43, 5–17 (2004).

5. Li, Q. et al. ALS-linked mutant superoxide dismutase 1 (SOD1) alters mitochondrial protein composition and decreases protein import. Proc. Natl. Acad. Sci. USA 107, 21146–21151 (2010).

6. Israelson, A. et al. Misfolded mutant SOD1 directly inhibits VDAC1 conductance in a mouse model of inherited ALS. Neuron 67, 575–587 (2010).

7. Shoshan-Barmatz, V. et al. VDAC, a multifunctional mitochondrial protein regulating cell life and death. Mol. Aspects Med. 31, 227–285 (2013).

8. Tomasello, M. F. et al. Outer membrane VDAC1 controls permeability transition of the inner mitochondrial membrane in cellulo during stress-induced apoptosis. Cell Res. 19, 1363–1376 (2009).

9. Fiek, C., Benz, R., Roos, N. & Brdiczka, D. Evidence for identity between the hexokinase-binding protein and the mitochondrial porin in the outer membrane of rat liver mitochondria. Biochim. Biophys. Acta 688, 429–440 (1982).

10. Abu-Hamad, S., Zaid, H., Israelson, A., Nahon, E. & Shoshan-Barmatz, V. Hexokinase-I protection against apoptotic cell death is mediated via interaction with the voltage-dependent anion channel-1: mapping the site of binding. J. Biol. Chem. 283, 13482–13490 (2008).

11. Pastorino, J. G. & Hoek, J. B. Regulation of hexokinase binding to VDAC. J. Bioenerg. Biomembr. 40, 171–182 (2008).

12. Allen Institute for Brain Science. Allen Brain Atlas Website. Available at: http://www.brain-map.org (2015).

13. Tan, W. et al. Small peptides against the mutant SOD1/Bcl-2 toxic mitochondrial complex restore mitochondrial function and cell viability in mutant SOD1-mediated ALS. J. Neurosci. 33, 11588–11598 (2013).

14. Colombini, M. Voltage gating in the mitochondrial channel VDAC. J. Membr. Biol. 111, 103–111 (1989).

15. Benz, R. Permeation of hydrophilic solutes through mitochondrial outer membranes: review on mitochondrial porins. Biochim. Biophys. Acta 1197, 167–196 (1994).

16. Reina, S. et al. Deletion of β -strands 9 and 10 converts VDAC1 voltage-dependence in an asymmetrical process. Biochim. Biophys. Acta 1827, 793–805 (2013).

17. Ferri, A. et al. Familial ALS-superoxide dismutases associate with mitochondria and shift their redox potentials. Proc. Natl. Acad. Sci. USA 103, 13860–13865 (2006).

18. Tomasello, M. F., Guarino, F., Reina, S., Messina, A. & De Pinto, V. The voltage-dependent anion selective channel 1 (VDAC1) topography in the mitochondrial outer membrane as detected in intact cell. PLoS One 8, e81522 (2013).

19. Gelb, B. D. et al. Targeting of hexokinase 1 to liver and hepatoma mitochondria. Proc. Natl. Acad. Sci. USA 89, 202–206 (1992).

20. Azoulay-Zohar, H., Israelson, A., Abu-Hamad, S. & Shoshan-Barmatz, V. In self-defense: Hexokinase promotes VDAC closure and prevents mitochondria-mediated apoptotic cell death. Biochem. J. 377, 347–355 (2004).

21. Arzoine, L., Zilberberg, N., Ben-Romano, R. & Shoshan-Barmatz, V. Voltage-dependent anion channel 1-based peptides interact with hexokinase to prevent its anti-apoptotic activity. J. Biol. Chem. 284, 3946–3955 (2009).

22. Turner, B. J., Atkin, J. D., Farg, M. A., Zang, D. W. & Rembach, A. Impaired extracellular secretion of mutant Superoxide Dismutase 1 associates with neurotoxicity in familial Amyotrophic Lateral Sclerosis. J. Neurosci. 25, 108–117 (2005).

23. Perry, S. W., Norman, J. P., Barbieri, J., Brown, E. B. & Gelbard, H. A. Mitochondrial membrane potential probes and the proton gradient: a practical usage guide. BioTechniques 50, 98–115 (2011).

24. Magrì, A. et al. Overexpression of human SOD1 in VDAC1-less yeast restores mitochondrial functionality modulating beta-barrel outer membrane protein genes. Biochim. Biophys. Acta 1857, 789–798 (2016).

25. Allen Institute for Brain Science. Allen Spinal Cord Atlas Website. Available at: http://mousespinal.brain-map.org (2015).

26. Pickles, S. et al. ALS-linked misfolded SOD1 species have divergent impacts on mitochondria. Acta Neuropathol. Commun. 4, 43 (2016).

27. Sullivan, P. G. et al. Intrinsic differences in brain and spinal cord mitochondria: implication for therapeutic interventions. J. Comp. Neurol. 474, 524–534 (2004).

28. van Raamsdonk, W., Smit-Onel, M. J. & Diegenbach, P. C. Quantitative enzyme- and immunohistochemistry of hexokinase and cytochrome c oxidase of spinal neurons in the zebrafish. Acta Histochem. 98, 143–155 (1996).

29. Roberts, D. J. & Miyamoto, S. Hexokinase II integrates energy metabolism and cellular protection: acting on mitochondria and TORCing to autophagy. Cell Death Differ. 22, 248–257 (2015).

30. Calmettes, G. et al. Hexokinases and cardioprotection. J. Mol. Cell Cardiol. 78, 107–115 (2015).

31. Corona, J. C., Gimenez-Cassina, A., Lim, F. & Diaz-Nido, J. Hexokinase II gene transfer protects against neurodegeneration in the rotenone and MPTP mouse models of Parkinson's Disease. J. Neurosci. Res. 88, 1943–1950 (2010).

32. Regenold, W. T. et al. Mitochondrial detachment of hexokinase 1 in mood and psychotic disorders: Implications for brain energy metabolism and neurotrophic signaling. J. Psychiatr. Res. 46, 95–104 (2012).

33. Mathupala, S. P., Ko, Y. H. & Pedersen, P. L. Hexokinase-2 bound to mitochondria: cancer's stygian link to the "Warburg Effect" and a pivotal target for effective therapy. Semin. Cancer Biol. 19, 17–24 (2009).

34. Shoshan-Barmatz, V., Zakar, M., Rosenthal, K. & Abu-Hamad, S. Key regions of VDAC1 functioning in apoptosis induction and regulation by hexokinase. Biochim. Biophys. Acta 1787, 421–430 (2009)

35. Wilson, J. E. Hexokinases. Rev. Physiol. Biochem. Pharmacol. 126, 65–198 (1995).

36. Xie, G. C. & Wilson, J. E. Rat brain hexokinase: the hydrophobic N-terminus of the mitochondrially bound enzyme is inserted in the lipid bilayer. Arch. Biochem. Biophys. 267, 803–810 (1988).

37. Rosano, C. et al. Binding of non-catalytic ATP to human hexokinase I highlights the structural components for enzyme–membrane association control. Structure 7, 1427–1437 (1999).

38. Messina, A., Reina, S., Guarino, F. & De Pinto, V. VDAC isoforms in mammals. Biochim. Biophys. Acta 1818, 1466–1476 (2012).

39. Messina, A. et al. Live cell interactome of the human Voltage Dependent Anion Channel 3 (VDAC3) revealed in HeLa cells by Affinity Purification Tag Technique. Mol. BioSyst. 10, 2134–2145 (2014).

40. Reina, S. et al. VDAC3 as a sensor of oxidative state of the intermembrane space of mitochondria: the putative role of cysteine residue modifications. Oncotarget 7, 2249–2268 (2016).

41. Moreira, P. I., Carvalho, C., Zhuc, X., Smith, M. A. & Perry, G. Mitochondrial dysfunction is a trigger of Alzheimer's disease pathophysiology. Biochim. Biophys. Acta 1802, 2–10 (2010).

42. Winklhofer, K. F. & Haass, C. Mitochondrial dysfunction in Parkinson's disease. Biochim. Biophys. Acta 1802, 29–44 (2010).

43. Manczak, M. & Reddy, P. H. Abnormal interaction of VDAC1 with amyloid beta and phosphorylated tau causes mitochondrial dysfunction in Alzheimer's disease. Hum. Mol. Genet. 21, 5131–5146 (2012).

44. Rostovtseva, T. K. et al. α -Synuclein shows high affinity interaction with Voltage-dependent Anion Channel, suggesting mechanisms of mitochondrial regulation and toxicity in Parkinson Disease. J. Biol. Chem. 290, 18467–18477 (2015).

45. Wienken, C. J., Baaske, P., Rothbauer, U., Braun, D. & Duhr, S. Protein-binding assays in biological liquids using microscale thermophoresis. Nat. Commun. 1, 100 (2010).

46. Checchetto, V., Reina, S., Magrì, A., Szabo, I. & De Pinto, V. Recombinant human Voltage Dependent Anion selective Channel isoform 3 (hVDAC3) forms pores with a very small conductance. Cell Physiol. Biochem. 34, 842–853 (2014).

47. Mosmann, T. Rapid colorimetric assay for cellular growth and survival: Application to proliferation and cytotoxicity assays. J. Immunol. Methods 65, 55–63 (1983).

Acknowledgements

This work was supported by ARISLA grant to A. Messina (codex: ALSINTERACTORS), by PRIN project 2010CSJX4F to V.D.P., by FIR-UNICT project 2014 to A. Messina. The authors acknowledge prof. Maria Teresa Carrì (Rome University of Tor Vergata) for providing all NSC34 cells used in the work.

Supplementary Information

Supplementary Methods

Cloning of recombinant proteins The sequence encoding the human VDAC1 was inserted into the pET-21a expression vector (Novagen) in frame with 6xHis tag at C-terminal domain, as previously reported [1]. The sequence encoding the human SOD1 wild type (SOD1 WT) was amplified by in stock plasmid using a specific couple of primers (SOD1 fw and rev) and cloned into the pET-52b expression vector (Novagen) in frame with Strep-tag at its N-terminal domain using SanDI/SacI sites. To generate the construct for the ALS-linked SOD1 G93A, the Quik Change II site-direct mutagenesis kit (Agilent) was used in combination with a specific couple of mutagenic primers (SOD1 mutG93A fw and rev). Primer sequences are listed in Supplementary Table 1. All sequences were verified by sequencing.

Expression, purification and refolding of VDAC1 proteins. E. coli BL21 (DE3) cells were transformed with the pET constructs harboring VDAC1 sequences. The 6xHis-tagged VDAC1 proteins were induced, purified and refolded as previously reported [1]. The protein purity was verified in 12% SDS-PAGE followed by Comassie staining. Purified samples were stored at - 20°C until further use.

Expression, purification and activity assay of SOD1 proteins. The pET vectors containing SOD1 constructs were used for E. coli BL21 (DE3) transformation. Protein expression was achieved by 1 mM isopropyl-β-D-thiogalactopyranoside (IPTG) (Sigma) induction at 18°C over night. Cell lysis and purification of Strep-tagged proteins by affinity chromatography using Strep-Tactin Superflow Plus Resin (Qiagen) were

performed under native conditions, according to manufacturer's protocol. Metal loading and storage was performed as reported [2]. The protein purity was verified by 12% SDS-PAGE and Comassie staining. Activity of SOD1 proteins was assayed in gel with the Riboflavin/NitroBlue Tetrazolium (RF/NBT) assay as reported [3].

Western blot analysis. Protein fractions were separated by SDS-PAGE using 4-12% Bis-Tris NuPage gel (Invitrogen) and electro-transferred to nitrocellulose membrane for Western blot analysis. The following antibodies were used for immunoblotting: SOD1 (C-17) antibody (1:1000) (Santa Cruz Biotechnology, Inc), VDAC1/porin antibody (1:1000) (Abcam), HKI antibody (1:500) (Abcam), Actin antibody (1:1000) (Sigma). A relative quantification was performed by densitometry analysis using Image Studio Lite software (LI-COR Biosciences), using VDAC1 or actin as loading control.

Motor neuron cell lines maintenance. NSC-34 cells were cultured in 5% CO2 in DMEM (Gibco) supplemented with 10% fetal bovine serum (FBS) (Gibco) and 1% penicillin/streptomycin (P/S). NSC-34-SOD1WT and NSC-34-SOD1G93A cells were cultured in 5% CO2 in DMEM F12 (Euro Clone), 10% of tetracycline-free FBS (Euro Clone), 1% P/S, in the presence of 200 µg/mL G418 (Carlo Erba) for selection maintenance. Induction of SOD1 proteins was obtained by addition of 2 µg/mL tetracycline to the medium, as described [4]. Analysis were performed after 48h from induction.

Plasmids and cell transfection. Sequence encoding for human HK1 was amplified from in stock plasmid using a specific couple of primers (HK1 fw and rev, see Supporting Table 1 for sequence) and cloned into mammalian expression vector pEGFP-N1 in frame with

eGFP sequence at C-terminal domain. The sequence encoding for 2-12 amino acid sequence of HK1 were cloned by NheI/SalI digestion into the modified mammalian expression vector pCMS-mtDsRED. pCMS-mtDsRED encodes for the Red Fluorescent Protein of Discosoma sp. targeted to mitochondria, used also as transfection marker. Oligonucleotides encoding for NHK1 peptide (NHK1 oligo fw and rev) or for scramble ScNHK1 peptide (ScNHK1 oligo fw and rev) were subject to annealing in order to obtain double strand DNA. Additional couples of oligonucleotides lacking stop codon were cloned in pCMS-mtDsRED with the HA-tag at the C-terminal domain. Oligonulceotides sequences are listed in Supplementary Table 2. All sequences were verified by sequencing. Cells were transiently transfected using Lipofectamine 3000 (Invitrogen) according with the manufacturer's instructions.

Indirect immunofluorescence of adherent cells. NSC34 cells not transfected or transfected with 0,5 µg of pCMS-mtDsRED-NHK1-HA were fixed in 3.7% formaldehyde and permeabilized using 0.3% Triton X-100. Unspecific binding was blocked by 30 min of incubation in 0,2 % gelatin in PBS. Endogenous HK1 was detected in not transfected cells by incubating over-night cells with rabbit anti-HK1 antibody (1:100) (Abcam). NHK1-HA was detected in transfected cells by incubating over-night cells with rabbit anti-HA antibody (1:100) (Santa Cruz Biotechnology, Inc.). After PBS washing, cells were exposed for 1h at RT to the secondary anti-rabbit antibody AlexaFluor 488. Coverslips were mounted with the ProLong Gold antifade mounting medium (Invitrogen) and examined by fluorescence microscopy. Co-localization with mitochondria was obtained by merging the signal HK1 or HA respectively with the signal from Mito-Traker Red (Molecular Probes) or the fluorescent reporter mtDsRED.

Fluorescence microscopy. A Leica DMI 6000B epifluorescence inverted microscope with Adaptive Focus Control was used. This system is outfitted with a controllable X-cite mercury lamp and an extensive collection of filter cubes (360, 488, 560, 604 nm excitation) for fluorescent microscopy, and a halogen lamp for bright field and DIC. It is equipped with 4 bright lenses (10, 20, 40, 63x), a high-resolution Hamamatsu Orca R2 CCD camera (1344x1024 pixels), and motorized stage (XY only). Images were obtained by using the Leica LAS Extended Annotation software.

Supplementary Tables

SOD1 fw	5'TTTGGGACCCATGGCCACGAAGGCCGTGTGCGTG3'
SOD1 rev	5TTTGAGCTCTTATTGGGCGATCCCAATTACACC3'
SOD1 mutG93A fw	5ACTGCTGACAAAGATGCTGTGGCCGATGTGTCT3'
SOD1 mutG93A rev	5AGACACATCGGCCACAGCATCTTTGTCAGCAGT3'
HK1 fw	5'TTTTGCTAGCATGATCGCCGCGCAGCTCCT 3'
HK1 rev	5'TTTTGTCGACTTAGCTGCTTGCCTCTGTGCGTAA3'

Table S1. List of the primer sequences used in this work.

NHK1 oligo fw	5'CTAGCATGATCGCCGCGCAGCTCCTGGCCTATTACTTCACGTGAG3'
NHK1 oligo rev	5'TCGACTCACGTGAAGTAATAGGCCAGGAGCTGCGCGGCGATCATG3'
ScNHK1 oligo fw	5'CTAGCATGTTCGCCCAGCTCACGATCGCCCTGGCGTATTACTAAG3'
ScNHK1 oligo rev	5TCGACTTAGTAATACGCCAGGGCGATCGTGAGCTGGGCGAACATG3'

Table S2. List of oligonucleotides sequences used in this work.'

Supplementary Figures

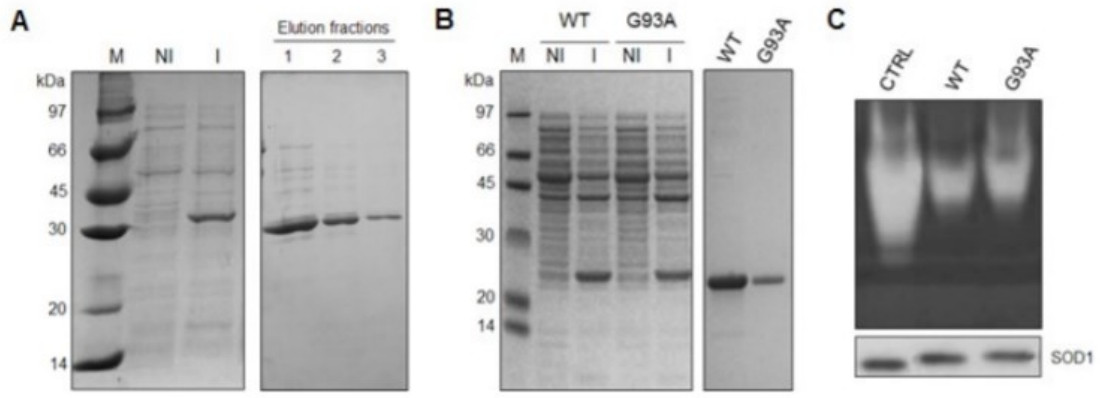

Figure S1. Production of recombinant proteins used in this work. (A) Electrophoretic analysis of total lysate of E. coli BL21 strain transformed with pET construct encoding for the 6xHis-tagged VDAC1 and electrophoretic analysis of eluted fractions after purification. As shown, a clear band of around 32 kDa is visible in IPTG-induced (I), but not in not induced (NI) sample. M: molecular weight marker. (B) Electrophoretic analysis of total lysate of E. coli BL21 strain transformed with pET construct encoding for the Strep-tagged SOD1wt and G93A and electrophoretic analysis of eluted fractions after purification. As shown, a clear band appeared at the expected molecular weight in IPTG-induced (I), but not in not induced (NI) sample. M: molecular weight markers. (C) In-gel SOD1 activity assay and relative Western blot analysis. Recombinant SOD1wt and G93A were active. As a control, a SOD1 purchased from Sigma was used (CTRL).

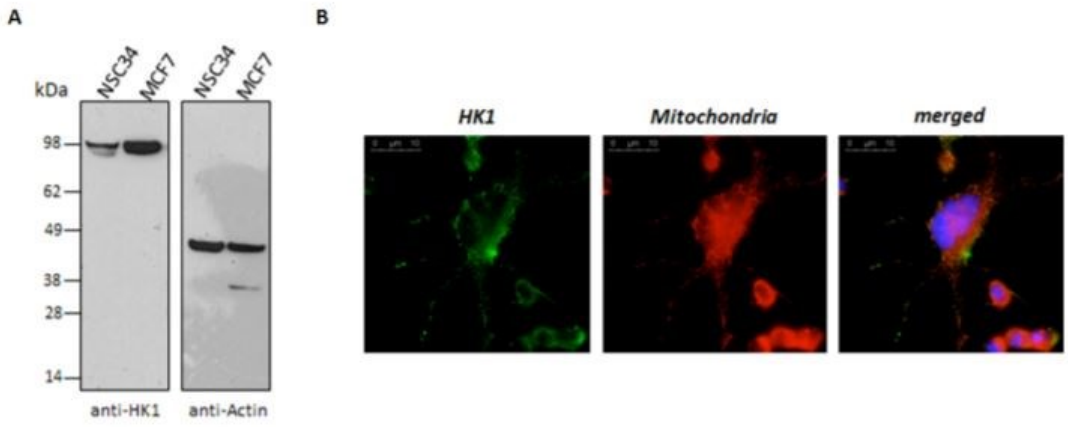

Figure S2. Analysis of endogenous HK1 expression in NSC34 cells. (A) Western blot analysis of HK1 expression in total lysate of NSC34 or MCF7 cells. MCF7 cells were used here as control, since HK1 is abundant in this cell line. As reported, total level of HK1 is significantly lower in NSC34 cells compared to that of control. Actin was used as loading control. (B) Indirect immunofluorescence of adherent NSC34 cells with anti-HK1 antibody shows the subcellular distribution of endogenous HK1. As showed by the typical punctuated deposit and by the co-localization with Mito-Tracker, most of HK1 localized to mitochondria.

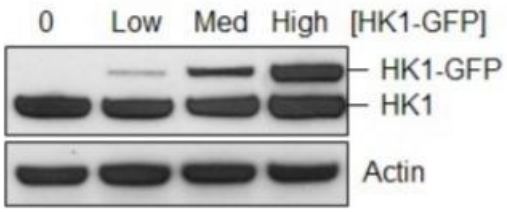

Figure S3. Expression of HK1-GFP in NSC34 cells. Western blot analysis of total lysate of NSC34 cells transfected with increasing concentration of pEGFPN1-HK1. As the plasmid in the transfection experiment is raised from low to medium to high

concentrations, a protein band corresponding to the HK1-GFP appears. The level of endogenous HK1 (lower band recognized by the Ab) was not affected.

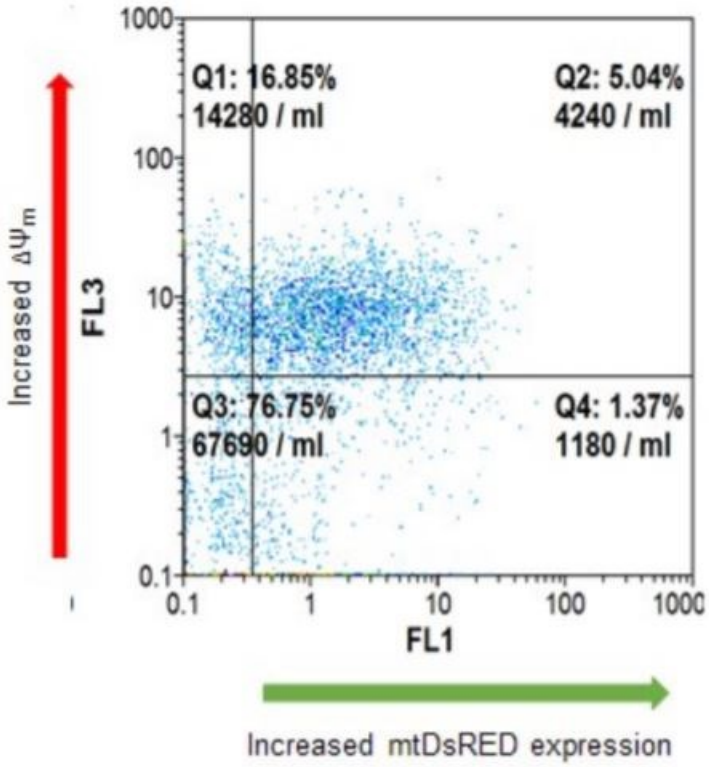

Figure S4. ΔΨm analysis in presence of NHK1 peptide. Representative flow cytometry dot plot of NSC34-SOD1G93A cells transfected with NHK1 peptide and stained with TMRM. Q2 and Q4 indicate cells expressing NHK1 peptide, while Q1 and Q3 are not transfected cells (control) form the same population. The transfected cells are mainly placed in the region Q2 corresponding to the highest ΔΨm values, while non-transfected cells are equally distributed in Q1 and Q3.

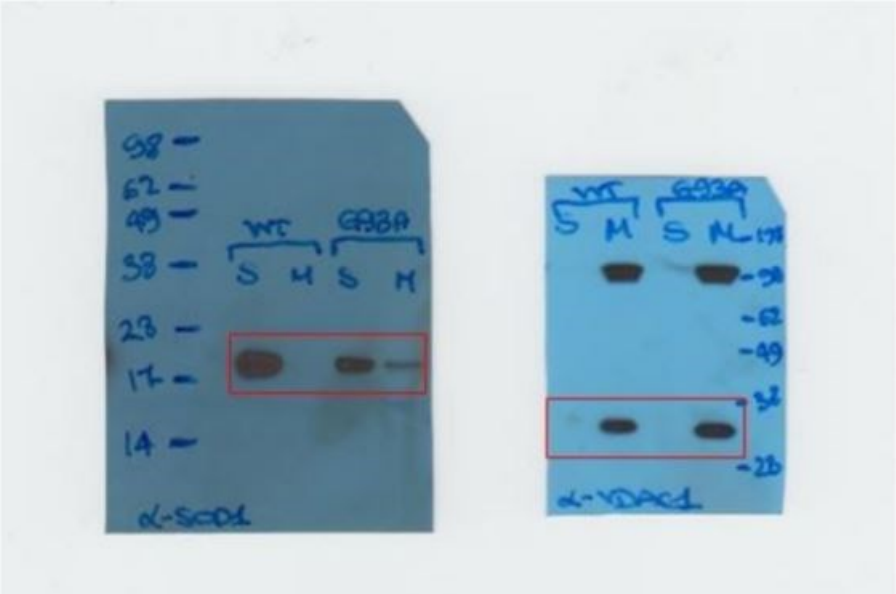

Figure S5. Full scans of original western blots showed in Fig. 1A. In red, the cropped area corresponding to that showed in the main figure. Proteins fractions were loaded in duplicate onto 4-12% NuPage polyacrylamide gel and electro-transferred onto nitrocellulose. Proteins were revealed by using SOD1 antibody (left) or VDAC1 antibody (right).

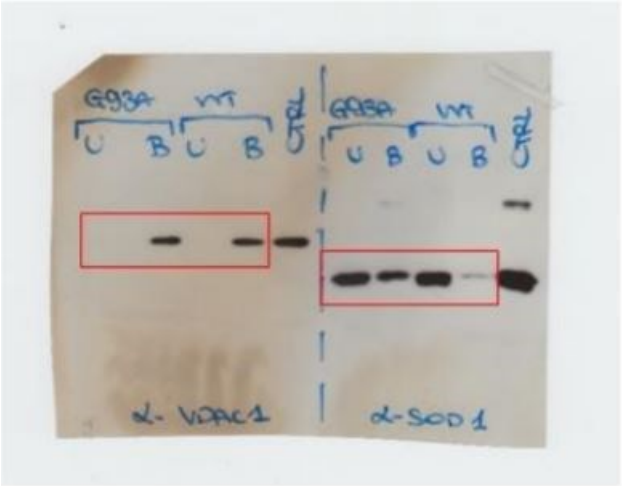

Figure S6. Full scans of original western blots showed in Fig. 1B. In red, the cropped area corresponding to that showed in the main figure. Proteins fractions were loaded in

duplicate onto 4-12% NuPage polyacrylamide gel and electro-transferred onto nitrocellulose. Proteins were revealed by using VDAC1 antibody (left) or SOD1 antibody (right). CTRL referred to the purified proteins VDAC1 or SOD1 WT loaded as a control.\

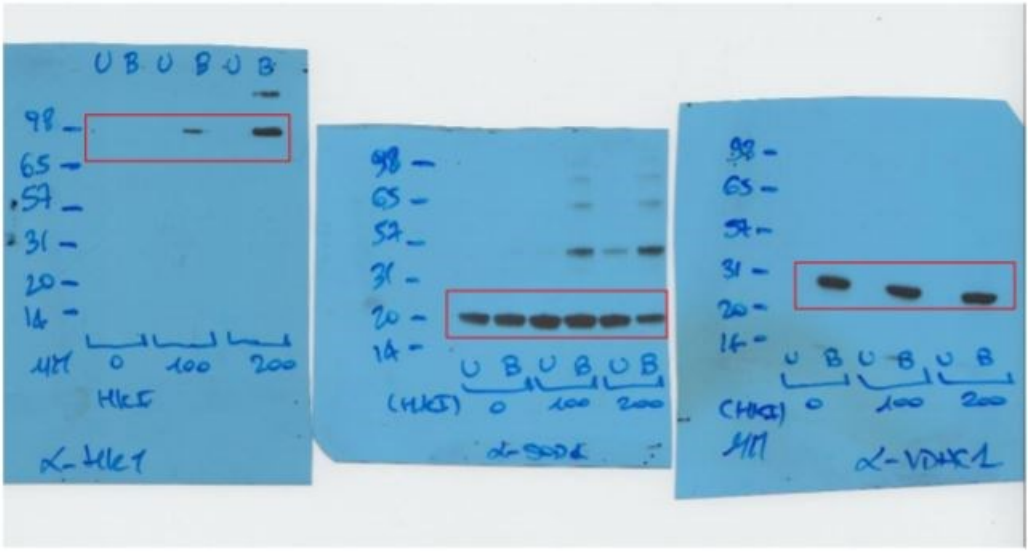

Figure S7. Full scans of original western blots showed in Fig. 3A, in red, the cropped area corresponding to that showed in the main figure. Proteins fractions were loaded in duplicate onto 4-12% NuPage polyacrylamide gel and electro-transferred onto nitrocellulose. Proteins were revealed by using HK1 antibody (left), SOD1 antibody (middle) or VDAC1 antibody (right).

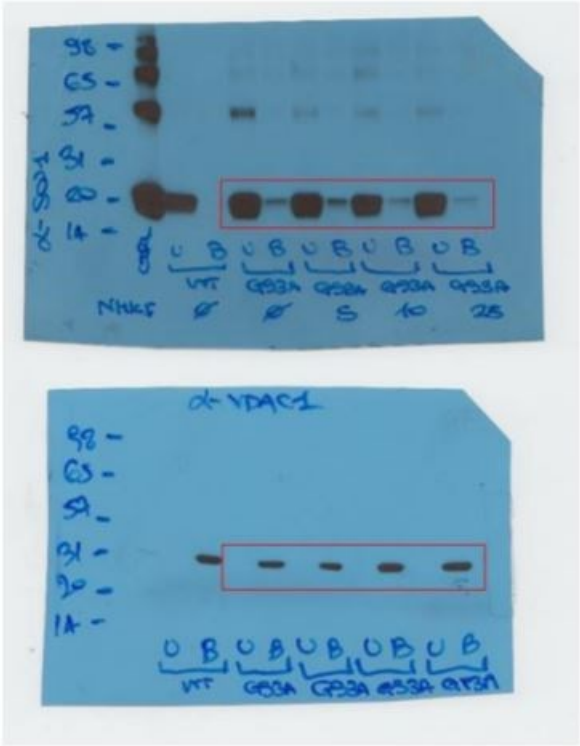

Figure S8. Full scans of original western blots showed in Fig. 5A In red, the cropped area corresponding to that showed in the main figure. Proteins fractions were loaded in duplicate onto 4-12% NuPage polyacrylamide gel and electro-transferred onto nitrocellulose. Proteins were revealed by using SOD1 antibody (upper) or VDAC1 antibody (lower). CTRL referred to SOD1 WT loaded as a control.

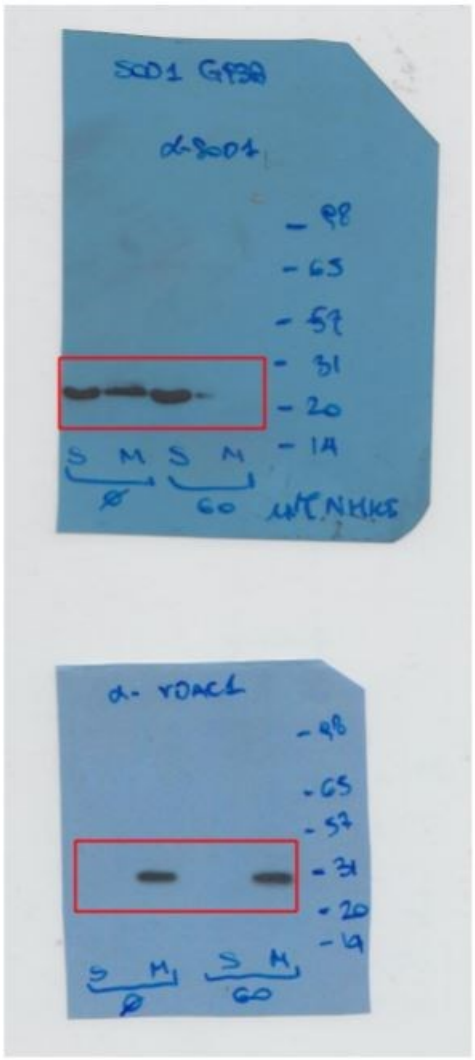

Figure S9. Full scans of original western blots showed in Fig. 5B. In red, the cropped area corresponding to that showed in the main figure. Proteins fractions were loaded in duplicate onto 4-12% NuPage polyacrylamide gel and electro-transferred onto nitrocellulose. Proteins were revealed by using SOD1 antibody (upper) or VDAC1 antibody (lower).

Supplementary References

1. Checchetto, V., Reina, S., Magrì, A., Szabo, I. & De Pinto, V. Recombinant human Voltage Dependent Anion Selective Channel isoform 3 (hVDAC3) forms pores with a very small conductance. Cell Physiol. Biochem. 34, 842-853 (2014).

2. Stevens, J. C. et al. Modification of Superoxide Dismutase 1 (SOD1) properties by a GFP tag. Implications for research into Amyotrophic Lateral Sclerosis (ALS). PLoS One 5, e9541 (2010).

3. Beauchamp, C. & Fridovich, I. Superoxide dismutase: improved assays and an assay applicable to acrylamide gels. Anal. Biochem. 44, 276-287 (1971).

4. Ferri, A. et al. Familial ALS-superoxide dismutases associate with mitochondria and shift their redox potentials. Proc. Natl. Acad. Sci. U.S.A. 103, 13860-13865 (2006).

5. Tomasello, M. F., Guarino, F., Reina, S., Messina, A. & De Pinto, V. The voltage-dependent anion selective channel 1 (VDAC1) topography in the mitochondrial outer membrane as detected in intact cell. PLoS One 8, e81522 (2013).

CHAPTER 2

Aging Cell, October 2018

Temporal and Regional Progression of Alzheimer's disease-like pathology in 3xTg-AD mice

Ramona Belfiore[1,2], Alexis Rodin[1], Eric Ferreira[1], Ramon Velasquez[1], Caterina Branca[1], Antonella Caccamo[1], and Salvatore Oddo[1, 3, #]

1 The Arizona State University-Banner Neurodegenerative Disease Research Center at the Biodesign Institute, Arizona State University, Tempe, Arizona, 85287.
2 Department of Biomedical and Biotechnological Sciences, University of Catania, Catania, Italy, 95125
3 School of Life Sciences, Arizona State University, Tempe, Arizona, 85287

ABSTRACT

Animal models of Alzheimer's disease (AD) are widely used to obtain insights into the pathogenesis of the disease, and as tools to evaluate potential therapeutic compounds. Accumulation of amyloid-β (Aβ) and fibrillary tangles, as well as neuroinflammation and memory loss are hallmarks of AD. After almost 15 years from its generation, 3xTg-AD mice are still one of the most used transgenic models of AD. Converging evidence indicates that the phenotype of 3xTg-AD mice has shifted over the years and contradicting reports about onset of pathology or cognitive deficits are apparent in the literature. Here, we sought to stage the progression of AD-like pathology in 3xTg-AD mice. We assessed Aβ and tau load, and neuroinflammation in 2-, 6-, 12-, and 20-month-old female 3xTg-AD and non-transgenic (NonTg) mice, using histological and biochemical means. We also evaluated cognitive changes using the Morris water maze. We found that ~80% of the mice analyzed had Aβ plaques in the caudal hippocampus at 6 months of age, while 100% of them had Aβ plaques in the hippocampus at 12 months of age. Cortical Aβ plaques were first detected at 12 months of age, including in the entorhinal cortex. Phosphorylated Tau at Ser202/Thr205 and Ser422 was apparent in the hippocampus of 100% of 6-month-old

mice, while only 50% of mice showed tau phosphorylation at Thr212/Ser214 at this age. Neuroinflammation was first evident in 6-month-old mice and increased as a function of age. These neuropathological changes were clearly associated with progressive cognitive decline, which was first apparent at 6 months of age and became significantly worse as the mice aged. Overall, these data indicate a consistent and predictable progression of the AD-like pathology in female 3xTg-AD mice. These data will facilitate the design of future studies using 3xTg-AD mice.

KEYWORDS: Aβ, tau, plaques, tangles, transgenic mice, cognitive deficits, microglia, inflammation, neuroinflammation, APP.

INTRODUCTION

Alzheimer's disease (AD) is the most common neurodegenerative disease [1]. It is characterized by the accumulation of extracellular amyloid plaques and intracellular neurofibrillary tangles [2, 3]. The former are primarily made of a small peptide called amyloid-β (Aβ), while the latter are made of the hyperphosphorylated protein tau [4]. Another hallmark of AD is brain inflammation, which manifests as intense reactivity of astrocytes and microglia, and increased levels of proinflammatory cytokines such as interleukin-1β (IL1β), interleukin-6 (IL6) and tumor necrosis factor-α [TNFα; 5];. Clinically, AD is first associated with episodic amnesia followed by significant deficits on semantic memory and procedural memory [4, 6]. Additional clinical manifestations such as loss of judgment, problem-solving impairment, depression and sleep disorders are also frequently associated with early stages of the disease [7].

Familial AD, which represents a minority of AD cases, is due to mutations in one of three genes, presenilin (PS) 1 and 2 and the amyloid precursor protein [APP; 8, 9]. In contrast, sporadic AD, which represents the vast majority of AD cases is of unknown etiology [10, 11]. For both familial and sporadic AD, aging is the major risk factor [12]. Genetically, tau is not linked to AD, even though neurofibrillary tangles are a primary hallmark of AD. Mutations in the tau gene cause familial tauopathies such as frontotemporal dementia, corticobasal degeneration, progressive supranuclear palsy, Pick's disease [13].

Several animal models of AD have been generated and these include transgenic mice overexpressing different AD-associated proteins [14, 15]. Overall, mouse models of AD have represented unique tools to understand underlying mechanisms of pathogenesis and have served to conduct numerous pre-clinical studies. In 2003, we generated a mouse model harboring three human mutant genes, APP, tau, and PS1 [16]. These mice recapitulate specific aspects of AD including age-dependent cognitive decline, accumulation of plaques and tangle, and age-dependent inflammation [17, 18]. Over the last 15 years these mice have been widely used by investigators throughout the world. This widespread use of the mice has led to the generation of sublines, which present different onset and progression of AD-like pathology, creating controversy and confusion in the field. Here we staged the AD-like pathology in female 3xTg-AD mice, to elucidate the spatial and temporal progression of soluble and insoluble Aβ, tau hyperphosphorylation, glial reactivity and cognitive function.

METHODS

Animals: 3xTg-AD mice used in this manuscript were previously described [16]. In this study, only female mice were analyzed since in our colony male 3xTg-AD mice show a sizeable neuropathological variability, even between littermates. Mice were housed 4-5 per cage, kept on 12-hour light/dark cycle, and were given *ad libitum* access to food and water. All animal procedures were approved by The Institutional Animal Care and Use Committee of Arizona State University.

Protein extraction: Brains from NonTg and 3xTg-AD mice were processed for biochemical analyses as described previously [19]. Briefly, mice were sacrificed by CO_2 asphyxiation, their brain removed and sagittally bisected. The left hemispheres were used for immunohistochemical analysis; the right hemispheres were dissected to separate hippocampus, cortex and cerebellum and frozen in dry ice. The hippocampal tissue was homogenized in T-PER protein extraction buffer (Thermo Fisher, Waltham, MA), containing complete protease inhibitor (Roche, Indianapolis, IN) and phosphatase inhibitor (Thermo Fisher, Waltham, MA). The homogenates were centrifuged at 4 °C for 30 minutes at 15000 rpm. The supernatant containing the soluble protein fraction was stored at -80 °C and used for ELISA and western blots. The insoluble fraction was obtained re-suspending the pellet in 70% formic acid and used to measure insoluble Aβ by ELISA.

ELISA: To detect soluble and insoluble $A\beta_{40}$ and $A\beta_{42}$, we used a commercially available sandwich ELISA kit from Thermo Fisher Scientific [20]. Briefly, soluble or insoluble fractions of brain tissue homogenates were processed in a precoated, flat bottom 96-well

plates according to the kit's instructions and read in a BioTek plate reader at 450 nm. The range of Aβ detection was between 10 and 1000 pg/ml. For each assay kit, cross-reactivity with other Aβ species was negligible when concentrations were <10 ng/ml. The concentration of Aβ (picograms per milliliter of sample) present in the homogenate was the dependent variable used for statistical analysis.

Morris Water Maze: Morris water maze tests were conducted as previously described [21]. Briefly, mice were tested in a circular tank of 1.5 meters in diameter located in a room with extra-maze cues. The platform (14 cm in diameter) location was maintained constant for each mouse during training and was submerged 1.5 cm beneath the surface of the water, which was maintained at 23 °C throughout the testing. During 5 days of training, the mice underwent 4 trials a day, alternating among 4 pseudorandom starting points. If a mouse failed to find the platform within 60 s, it was guided to the platform by the researcher and kept there for 10 s. The inter-trial interval was 25 s, during which time each mouse was returned to its home cage. Probe trials were conducted 24 hours after the last training trial. During the probe trials, the platform was removed and mice were free to swim in the tank for a single 60-second trial. The training and probe trials were recorded by a video camera mounted on the ceiling, and data were analyzed using the EthoVisio XT tracking system (Noldus Information Technology, Leesburg, VA).

Antibodies: The following antibodies were used for immunohistochemistry and immunofluorescence: from Millipore, Aβ42 (catalog number AB5078P, 1: 200). From ThermoFisher Scientific, p-Tau Thr212/Ser214 (AT100; catalog number MN1060, 1:1000); p-Tau Ser202/Thr205 (AT8; catalog number MN1020, 1:1000); Goat anti-Rabbit IgG (H+L) highly cross-adsorbed secondary antibody; Alexa Fluor Plus 555 and 488

(catalog number A32732 and A-11034, respectively; 1:200); Goat anti-Mouse IgG (H+L) highly cross-adsorbed secondary antibody; and Alexa Fluor Plus 488 (catalog number A32723; 1:200). From Vector Labs, biotinylated goat anti-rabbit and mouse IgG antibody (catalog number BA-1000 and BA-2001; 1:200). From Wako, Iba1 (catalog number 09-19741, 1:500). From Cell Signaling, GFAP (catalog number 3670S, 1:500). From GenTex, Tau pSer422 (catalog number GTX86147, 1:200). From Abcam, CD68 (catalog number ab955, 1:500). From Cell Signaling, β-actin (catalog number 3700, 1:10,000). **Immunohistochemistry and immunofluorescence**: Brains were processed as previously described [21]. Briefly, hemibrains were drop fixed in 4% parafrmaldehyde for 48 h and then transferred into 0.02% sodium azide in phosphate-buffered saline until slicing; 50 μm-thick free-floating sections were subsequently obtained using a vibratome. For immunohistochemistry, sections were washed twice with TBS (100 mm Tris pH 7.4, 150 mm NaCl) and incubated for 30 min in 3% H_2O_2, to quench endogenous peroxidase activity. Next, sections were transferred into TBS-A (100 mm Tris pH 7.4, 150 mm NaCl, 0.1% Triton X-100) and TBS-B (100 mm Tris pH 7.4, 150 mm NaCl, 0.1% Triton X-100, 2% bovine serum albumin) for 15 and 30 min, respectively. Finally, the proper primary antibody was applied overnight at 4°C. Sections were washed to remove excess antibody and incubated in the suitable secondary antibody for one h at room temperature. Signal was enhanced by incubating sections in the avidin-biotin complex (Vector Labs) for one h. Sections were then washed and developed with diaminobenzidine substrate using the avidin-biotin horseradish peroxidase system (Vector Labs, Burlingame, CA, USA). Images were obtained with a digital Zeiss camera and analyzed using ImageJ. For immunofluorescence staining, the quenching step was skipped, and after the secondary

antibody (AlexaFluor; ThermoFisher Scientific), the slices were mounted and coverslip with Prolong® diamond mounting (ThermoFisher Scientific). Images were obtained with a Leica Confocal microscope and analyzed using ImageJ. For all colocalization measurements, lasers 561 nm and 488 nm were used for excitation of secondary antibody fluorophores Alexa 555 and Alexa 488, respectively (Thermo Fisher Scientific). To obtain a Pearson correlation coefficient (PCC), we used ImageJ plugin 'Coloc2'. To quantify Aβ and Tau immunoreactivity, images from six mice/group were taken with a Zeiss AxioImager A1 using a 40X objective. To quantify colocalization in confocal imaging, we quantified and averaged 10 pictures per mouse, 6 mice per genotype. Images were analyzed using ImageJ.

Statistical analysis: Data were analyzed by Student's t-test, one-way and two-way ANOVAs using GraphPad Prism. *Post hoc* with Bonferroni's correction was used when appropriate.

RESULTS

3xTg-AD mice show an age-dependent accumulation of plaques

To assess the age-dependent progression of Aβ pathology in female 3xTg-AD mice, we immunostained sections from 2-, 6-, 12-, and 20-month-old mice with an $A\beta_{42}$-specific antibody (n = 6/age group). We selected hippocampal sections from left hemibrains that were -3.80 mm, -3.08 mm, and -2.18 mm posterior to bregma, representing the caudal, medial, and rostral hippocampus, respectively. We found that extracellular Aβ plaques were absent in 2-month-old mice (Fig. 1a-c) and first detected in the CA1/subiculum of

6-month-old mice (Fig. 1d-f). At this age, 5 out of 6 mice analyzed had plaques in the caudal hippocampus, 3 out of 6 in the medial hippocampus and none in the rostral-hippocampus. In contrast, 100% of the 12-month-old mice had plaques in all three hippocampal regions (Fig. 1g-i). By 20 months of age, $A\beta_{42}$ immunoreactivity was present throughout the hippocampus (Fig. 1j-l). Quantitative analyses of the sections confirmed the age-dependent progression of Aβ immunoreactivity in the caudal, medial, and rostral hippocampus (Fig. 1m-o, respectively; $p < 0.0001$). To further assess the progression of Aβ pathology, we measured the amount of soluble and insoluble Aβ in the hippocampus of 3xTg-AD mice by sandwich ELISA. One-way ANOVA analysis showed that soluble $A\beta_{40}$ levels were not statistically different among the four age groups (Fig. 1p; $p = 0.0685$). In contrast, we found a statistically significant age-dependent increase in insoluble $A\beta_{40}$ (Fig. 1r; $p = 0.0081$), and soluble and insoluble $A\beta_{42}$ (Fig. 1q-s; $p < 0.0001$).

To evaluate the cortical amyloid pathology, we measured Aβ load in the lateral entorhinal cortex (l-ENT), temporal association area (TEa), ectorhinal cortex (ECT), and ventral retrosplenial cortex (v-RSC). Aβ immunoreactivity was first apparent in the cortex of 12-month-old mice. Specifically, using one-way ANOVA analysis, we found that at 12 months of age the number of Aβ plaques was higher in the caudal l-ENT compared to both medial ($p = 0.0013$) and rostral l-ENT ($p < 0.0001$; Fig. 2a-d). We also observed this caudal-rostral pattern for the TEa ($p < 0.0001$), and the ECT ($p = 0.0004$; Fig. 2e-h and 2i-l, respectively). In contrast, we found that in the v-RSC, $A\beta_{42}$ immunoreactivity was significantly increased in the medial and rostral cortex compared to the caudal cortex ($p < 0.0001$ and $p = 0.0006$, respectively; Fig. 2m-p). At 20 months of age, Aβ plaques were

present throughout the cortex: a one-way ANOVA analysis showed that the number of Aβ plaques was higher in the caudal compared to both medial and rostral l-ENT ($p = 0.0002$ and $p < 0.0001$, respectively; Fig. 3a-d), TEa ($p = 0.009$ and $p = 0.001$, respectively; Fig. 3e-h), and ECT ($p = 0.09$ and $p = 0.03$, respectively; Fig. 3i-l). In contrast, we found a higher number of Aβ plaques in the medial and rostral v-RSC compared to the caudal v-RSC ($p = 0.04$ and $p = 0.03$, respectively; Fig. 3m-p). Together, these results indicate that in female 3xTg-AD mice, Aβ plaques develop first in the caudal hippocampus and as the mice age, they are present in the rostral hippocampus and several cortical regions.

3xTg-AD mice show age-dependent tau pathology

To characterize the age-related Tau phosphorylation in female 3xTg-AD mice, we immuno-stained sections from 2-, 6-, 12-, and 20-month-old mice ($n = 6$/age group) with antibodies that recognizes Tau phosphorylated at Ser422 (pS422), Ser202/Thr205 (AT8), and Thr212/Ser214 (AT100). We found that tau pS422 immunoreactivity, an early marker in the progression of tau pathology in AD [22, 23], was practically absent in 2-month-old mice (Fig. 4a-c). In contrast, 100% of the 6-month-old mice analyzed showed pS422 immunoreactivity in the caudal and medial hippocampus but not in the rostral hippocampus (Fig. 4d-f and Table 1). Finally, 100% of the 12- and 20-month-old mice had extensive pS422-positive neurons in all three brain regions (Fig. 4g-l and Table 1). Overall, one-way ANOVA indicated that in all three brain regions there was a significant age-dependent increase in pS422 immunoreactivity ($p < 0.0001$; Fig. 4m-o). A similar pattern in tau phosphorylation was detected with AT8 and AT100. To this end, we found quite not AT8 and AT100 immunoreactivity in 2-month-old mice (Additional file 1, Figure S1 and S2). In contrast, AT8 immunoreactivity was present in 100% of the 6-month-old

mice analyzed, while AT100 immunoreactivity was present in 50% of 6-month-old mice (Additional file 1, Fig. S2; Table 1). 100% of 12- and 20-month-old mice had extensive AT8 and AT100 immunoreactivity throughout the hippocampus (Figure. S1j-l and S2j-l, respectively). One-way ANOVA indicated that in all three hippocampal regions, AT8 and AT100 immunoreactivity significantly increased as a function of age ($p < 0.0001$ for both markers in all three hippocampal regions; Additional file 1, Figure S1m-o and S2m-o).

To evaluate cortical Tau phosphorylation, we measured pS422, AT8 and AT100 immunoreactivity in the lateral entorhinal cortex (l-ENT), temporal association area (TEa), ectorhinal cortex (ECT), and ventral retrosplenial cortex (v-RSC). We first detected cortical Tau pS422 immunoreactivity in 12-month-old mice. At this age, 100% of mice had a few pS422-positive neurons in the medial l-ENT cortex and 67% of mice in caudal and rostral l-ENT cortex (Additional file 1, Figure S3a-c). Indeed, using one-way ANOVA analysis with Bonferroni's correction we found that at 12 months of age pS422 immunoreactivity was higher in the medial l-ENT compared to both caudal and rostral l-ENT (Additional file 1, Figure S3d; $p < 0.0001$ and $p = 0.0261$, respectively). In contrast, pS422 immunoreactivity was not detected in the TEa, ECT, and v-RSC of 12-month-old mice (Additional file 1, Figure S3e-m). Notably, pS422 immunoreactivity increased as a function of age and 100% of 20-month-old mice had pS422-positive neurons in both l-ENT and TEa (Fig. 5a-h). A one-way ANOVA analysis using Bonferroni's correction showed that the number of pS422 positive neurons was higher in the medial cortex compared to both caudal and rostral l-ENT cortex ($p = 0.0006$ and $p = 0.0048$, respectively; Fig. 5d). In contrast, we found that pS422 immunoreactivity was not

significantly different among the three bregma regions analyzed (Fig. 5h). We also found that there were not positive neurons for pS422 immunostaining in the ECT and v-RSC.

We found a similar pattern in cortical tau phosphorylation with AT8 and AT100 antibodies. Specifically, cortical AT8 immunoreactivity was first detected at 12 months of age in the l-ENT (Additional file 1, Figure S4a-d) but it was not present in all the other three cortical regions analyzed (Additional file 1, Figure S4e-m). At this age, 100% of the mice examined had AT8-positive neurons in the medial l-ENT. Quantitative analyses indicated that within the l-ENT, the number of AT8-positive neurons was significantly higher in the medial l-ENT compared to both caudal and rostral l-ENT (Additional file 1, Figure S4d; $p < 0.0001$ and $p = 0.0061$, respectively). In 20-month-old mice, AT8 immunoreactivity was more prominent in the l-ENT and was present in 100% of the mice in all three regions of the l-ENT (Additional file 1, Figure S5a-d). At this age, AT8 immunoreactivity was very limited and a few AT8-positive neurons were apparent in the caudal and medial TEa (Additional file 1, Figure S5e-h). Quantitative analyses showed that the number of AT8-positive neurons was higher in the medial l-ENT compared to both caudal and rostral l-ENT cortex ($p < 0.0001$; Additional file 1, Figure S5d). In contrast, there were more AT8-positive neurons in the caudal and medial TEa than the TEa of 20-month-old mice ($p < 0.0001$, Additional file 1, Figure S5h). We did not detect any AT8 immunoreactivity in the ECT and v-RSC at this age (Additional file 1, Figure S5i-n). Similarly, in 12-month-old mice a few AT100-positive neurons were detected in the medial and rostral l-ENT but not in the caudal l-ENT (Additional file 1, Figure S6a-d; $p < 0.0001$) or the other cortical regions analyzed (Additional file 1, Figure S6e-m). In 20-month-old mice, we found prominent AT100 immunoreactivity in all three regions of the l-ENT (Additional file 1,

Figure S7a-c). Statistical evaluation revealed that the number of AT100-positive neurons was significantly higher in the medial and rostral l-ENT compared to the caudal l-ENT (Additional file 1, Figure S7d; $p < 0.0001$). We did not detect AT100 immunoreactivity in the other three cortical regions analyzed of 20-month-old mice (Additional file 1, 7e-m). Together these results indicate that tau pathological phosphorylation first appears in the hippocampus of 6-month-old and in the l-ENT of 12-month-old 3xTg-AD mice.

Astrogliosis and microgliosis in 3xTg-AD mice

Inflammation is another hallmark of AD pathogenesis and is considered a sign of neuronal damage [24]. To study the age-dependent inflammatory events in female 3xTg-AD mice, we first assessed astrogliosis in 2-, 6-, 12-, and 20-month-old mice using a GFAP antibody (n = 6/ age group). Compared to age- and sex-matched NonTg mice, GFAP immunoreactivity was significantly increased in 12- and 20-month-old 3xTg-AD mice in the caudal (Fig. 6a-b; $p = 0.0001$ and $p < 0.0001$, respectively) medial (Fig. 6c-d; $p = 0.0054$ and $p = 0.0016$, respectively) and rostral (Fig. 6e-f; $p = 0.0255$, $p = 0.0012$) hippocampus.

To evaluate microglial activation, we co-labeled sections from 2-, 6-, 12-, and 20-month-old 3xTg-AD and NonTg mice with Iba1 and CD68 antibodies (n = 6/age group). The former recognizes total microglia, while the latter is a lysosomal marker. Notably, CD68 levels are lower in quiescent microglia and extensively increased in highly reactive microglia [25]. Therefore, colocalization of CD68 and Iba1 signals indicate the ratio of activated microglia vs total microglia. At 2 months of age, there was no difference in

microglia activation between 3xTg-AD and NonTg mice in the medial hippocampus (Fig. 7a). In contrast, starting at 6 months of age, there was a significant age-dependent increase in microglia activation in the medial hippocampus of 3xTg-AD mice compared to age-matched NonTg mice (Fig. 7a-e; $p < 0.0001$). A similar pattern was evident in the rostral and caudal hippocampus. (Additional file 1, Figure S9a-e, Additional file 1, Figure S8a-e, respectively). An observational analysis of triple labeling with Thioflavin, GFAP and Iba1, showed that astrocytes were present specifically around Aβ plaques while reactive microglia were homogeneously detected along the CA1 of 3xTg-AD mice hippocampi (Fig. 7f). Together, these results indicate microglia activation, which is first detected at 6 months of age, precedes astrogliosis, which was first detected at 12 months of age in female 3xTg-AD mice.

Learning and memory impairment in 3xTg-AD mice

To assess spatial learning and memory, we tested 2-, 6-, 12-, and 20-month-old female 3xTg-AD and NonTg mice on the spatial version of the Morris water maze (2 months, n = 15/genotype; 6 months, n = 15 for 3xTg-AD and n = 10 for NonTg; 12 months, n = 15 for 3xTg-AD and n = 14 for NonTg; and 20 months, n = 15 for 3xTg-AD and n = 11 for NonTg). We gave mice four training trials per day for 5 consecutive days to learn the location of a hidden platform using distal extra-maze cues. The escape latency to find the platform across the training trials is an indication of mouse learning, with less time interpreted as better learning. Using a mixed ANOVA, we found that at 2 months of age there was a significant effect for days ($p < 0.0001$) and no significant effect per genotype

($p = 0.0699$) or genotype × day interaction ($p = 0.681$; Fig. 8a). These results suggest that mice learn the task across days but there is no difference in the pace of learning between the two genotypes. In contrast, we found that at 6 months of age there was a significant effect for days ($p < 0.0001$), genotype ($p < 0.0001$), and a significant genotype × day interaction ($p = 0.0478$; Fig. 8b). Notably, a *post hoc* test with Bonferroni's correction showed that NonTg mice performed significantly better than 3xTg-AD mice on day 2 ($p = 0.0053$), day 3 ($p = 0.0028$), day 4 ($p = 0.0008$) and day 5 ($p <0.0001$). As the mice aged, the difference in learning became more pronounced. To this end, we found that at 12 months of age, there was a significant effect for days ($p < 0.0001$), genotype ($p = 0.0022$) and genotype × day interaction ($p = 0.0003$; Fig. 8c). A *post hoc* test with Bonferroni's correction showed that 3xTg-AD mice were significantly impaired on day 4 and day 5 compared with NonTg mice ($p = 0.0008$; $p = 0.0005$, respectively). Finally, at 20 months of age, there was a significantly different effect for days ($p < 0.0001$), genotype ($p = 0.0022$) and genotype × day interaction ($p = 0.0003$; Fig. 8d) in the escape latency. Notably, *post hoc* analyses with Bonferroni's correction showed that NonTg mice performed better than 3xTg-AD mice on day 3, 4, and 5 ($p = 0.0014$, $p = 0.0018$ and $p = 0.0259$, respectively; Fig. 8d).

Twenty-four hours after the last training trial, we conducted probe trials to measure spatial reference memory. Specifically, we measured the number of platform location crosses during a single 60-second trial. We found that 3xTg-AD mice performed significantly worse when compared with the NonTg at 6, 12, and 20 months of age ($p = 0.0008$, $p = 0.0123$, $p = 0.01400$, respectively; Fig. 8e). We found that the swim speed was not

statistically significant among the two genotypes (Fig. 8g), indicating that the genotype effects on learning and memory were independent of physical performance at all the ages. Together, these findings indicate a clear age-dependent cognitive decline in 3xTg-AD mice.

DISCUSSION

Animal models are invaluable tools to study mechanisms of AD pathogenesis. Most models have been generated using human mutations in the APP or PS1 gene that are associated with familial AD. However, these mice fail to recapitulate the full spectrum of AD pathology, despite developing a high degree of Aβ plaques. In contrast, overexpression of wild type tau does not lead to any phenotype, while expression of a human mutant tau leads to a strong tau pathology, often associated with neurodegeneration. In 2003, we generated the 3xTg-AD mice, which harbor mutations in APP, PS1, and tau, which develop Aβ and tau pathology, as well as neuroinflammation and cognitive deficits. While these mice overexpress mutant tau, which is not associated with AD, they have been invaluable in understanding the interplay between Aβ and tau. Multiple laboratories have consistently reported that in these mice, Aβ pathology contributes to the development of tau. Notably, these findings have been replicated in other models that do not have mutant tau. Further, we previously showed that removing Aβ was sufficient to improve tau pathology. Similar results have been obtained from human clinical trials in which Aβ immunization led to the clearance of tau. Together, these

results highlight how findings in 3xTg-AD mice in regard to Aβ and tau interaction have predicted results in humans.

Our data indicate that at early ages there is a rostral-caudal gradient of Aβ and tau pathology in the hippocampus. Indeed, we found that Aβ plaques and tau phosphorylation were first apparent in the caudal hippocampus of 6-month-old mice; however, as at the same age, none of the mice analyzed had Aβ plaques or evidence of tau phosphorylation in more rostral areas of the hippocampus. Consistent with our observations, MRI studies of 120 participants of the AD Neuroimaging Initiative showed that hippocampal sub-regions undergo differential atrophy in AD [26]. Functionally, the rostral and caudal hippocampus appeared to be involved in different forms of learning and memory. To this end, functional MRI studies have clearly indicated two subnetworks within the medial temporal lobe memory system, one involving the rostral hippocampus and one involving the medial hippocampus [26-28]. The integrity of these networks is differentially regulated during aging and AD [29]. While the significance behind these observations remains to be elucidated, it is tempting to speculate that the rostral hippocampus, at least at earliest ages, might be more resilient to the development of AD-like pathology.

Phosphorylation of tau at Ser422 is considered a disease-specific event and is associated with tau misfolding in AD and other tauopathies [30-32]. We found that Ser422 is one of the earliest tau amino acids to be phosphorylated in 3xTg-AD and that Ser422 immunoreactivity increases as a function of age. Consistent with our observations, tau phosphorylation at Ser422 occurs early in the disease and remains phosphorylated through

the disease progression [33, 34]. As the 3xTg-AD mice age, tau becomes more phosphorylated at other epitopes. Here we show that AT8 and AT100 immunoreactivity occurs at middle and late stages of the disease progression, respectively. These findings are consistent with what has been reported in other transgenic mice expressing mutant human tau [33] and postmortem human AD brains.

CONCLUSIONS

Overall these results indicate that there is a slight temporal delay in the onset of pathology in 3xTg-AD mice with what we and others have reported in the past [35]. Nevertheless, the phenotype of female 3xTg-AD mice is consistent and predictable and shows a close association with that observed in AD patients and other animal models [36-38]. While the presence of the mutant tau gene does not reflect the condition in AD, these mice continue to be an invaluable tool to study the interaction between Aβ and tau. As discussed above, many findings were predictive to what was later observed in human brains. Further, 3xTg-AD mice show a clear interaction between age and development of the phenotype, which makes these mice an excellent tool to study the role of aging in the disease pathogenesis.

Abbreviations

AD: Alzheimer's disease

ANOVA: analysis of variance

APP: amyloid precursor protein

Aβ: amyloid β

CA: cornu ammonis

ECT: ectorhinal cortex

ELISA: enzyme-linked immunosorbent assay

GFAP: Glial fibrillary acidic protein

IL1β: interleukin-1β

IL6: interleukin-6

l-ENT: lateral entorhinal cortex

Mo: month-old

MRI: Magnetic resonance imaging

NonTg: non-transgenic

PS: presenilin

SEM: standard error of the mean

TEa: temporal association area

TNFα: tumor necrosis factor-α

v-RSC: ventral restrosplenial cortex

References

1. Alzheimer's A: **2016 Alzheimer's disease facts and figures.** *Alzheimers Dement* 2016, **12:**459-509.

2. Querfurth HW, LaFerla FM: **Alzheimer's disease.** *N Engl J Med* 2010, **362:**329-344.

3. LaFerla FM, Oddo S: **Alzheimer's disease: Abeta, tau and synaptic dysfunction.** *Trends Mol Med* 2005, **11:**170-176.

4. Medeiros R, Chabrier MA, LaFerla FM: **Elucidating the triggers, progression, and effects of Alzheimer's disease.** *J Alzheimers Dis* 2013, **33 Suppl 1:**S195-210.

5. Heneka MT, Carson MJ, El Khoury J, Landreth GE, Brosseron F, Feinstein DL, Jacobs AH, Wyss-Coray T, Vitorica J, Ransohoff RM, et al: **Neuroinflammation in Alzheimer's disease.** *Lancet Neurol* 2015, **14:**388-405.

6. Mormino EC, Kluth JT, Madison CM, Rabinovici GD, Baker SL, Miller BL, Koeppe RA, Mathis CA, Weiner MW, Jagust WJ, Alzheimer's Disease Neuroimaging I: **Episodic memory loss is related to hippocampal-mediated beta-amyloid deposition in elderly subjects.** *Brain* 2009, **132:**1310-1323.

7. Grontvedt GR, Schroder TN, Sando SB, White L, Brathen G, Doeller CF: **Alzheimer's disease.** *Curr Biol* 2018, **28:**R645-R649.

8. Selkoe DJ: **Alzheimer's disease: genotypes, phenotypes, and treatments.** *Science* 1997, **275:**630-631.

9. Van Cauwenberghe C, Van Broeckhoven C, Sleegers K: **The genetic landscape of Alzheimer disease: clinical implications and perspectives.** *Genet Med* 2016, **18:**421-430.

10. Pluta R: **Unresolved questions concerning etiology of Alzheimer's disease: hypometabolism.** *Nutrition* 2011, **27:**1-2.

11. Zetterberg H, Mattsson N: **Understanding the cause of sporadic Alzheimer's disease.** *Expert Rev Neurother* 2014, **14:**621-630.

12. Lu T, Pan Y, Kao SY, Li C, Kohane I, Chan J, Yankner BA: **Gene regulation and DNA damage in the ageing human brain.** *Nature* 2004, **429:**883-891.

13. Brunden KR, Trojanowski JQ, Smith AB, 3rd, Lee VM, Ballatore C: **Microtubule-stabilizing agents as potential therapeutics for neurodegenerative disease.** *Bioorg Med Chem* 2014, **22:**5040-5049.

14. LaFerla FM, Green KN: **Animal models of Alzheimer disease.** *Cold Spring Harb Perspect Med* 2012, **2**.

15. Puzzo D, Gulisano W, Palmeri A, Arancio O: **Rodent models for Alzheimer's disease drug discovery.** *Expert Opin Drug Discov* 2015, **10:**703-711.

16. Oddo S, Caccamo A, Shepherd JD, Murphy MP, Golde TE, Kayed R, Metherate R, Mattson MP, Akbari Y, LaFerla FM: **Triple-transgenic model of Alzheimer's disease with plaques and tangles: intracellular Abeta and synaptic dysfunction.** *Neuron* 2003, **39:**409-421.

17. Janelsins MC, Mastrangelo MA, Oddo S, LaFerla FM, Federoff HJ, Bowers WJ: **Early correlation of microglial activation with enhanced tumor necrosis factor-alpha and monocyte chemoattractant protein-1 expression specifically within the entorhinal cortex of triple transgenic Alzheimer's disease mice.** *J Neuroinflammation* 2005, **2:**23.

18. Oddo S, Caccamo A, Kitazawa M, Tseng BP, LaFerla FM: **Amyloid deposition precedes tangle formation in a triple transgenic model of Alzheimer's disease.** *Neurobiol Aging* 2003, **24:**1063-1070.

19. Caccamo A, Belfiore R, Oddo S: **Genetically reducing mTOR signaling rescues central insulin dysregulation in a mouse model of Alzheimer's disease.** *Neurobiol Aging* 2018, **68:**59-67.

20. Velazquez R, Shaw DM, Caccamo A, Oddo S: **Pim1 inhibition as a novel therapeutic strategy for Alzheimer's disease.** *Mol Neurodegener* 2016, **11:**52.

21. Caccamo A, Branca C, Piras IS, Ferreira E, Huentelman MJ, Liang WS, Readhead B, Dudley JT, Spangenberg EE, Green KN, et al: **Necroptosis activation in Alzheimer's disease.** *Nat Neurosci* 2017, **20:**1236-1246.

22. Kanaan NM, Cox K, Alvarez VE, Stein TD, Poncil S, McKee AC: **Characterization of Early Pathological Tau Conformations and Phosphorylation in Chronic Traumatic Encephalopathy.** *J Neuropathol Exp Neurol* 2016, **75:**19-34.

23. Simic G, Babic Leko M, Wray S, Harrington C, Delalle I, Jovanov-Milosevic N, Bazadona D, Buee L, de Silva R, Di Giovanni G, et al: **Tau Protein Hyperphosphorylation and Aggregation in Alzheimer's Disease and Other Tauopathies, and Possible Neuroprotective Strategies.** *Biomolecules* 2016, **6:**6.

24. Sudduth TL, Schmitt FA, Nelson PT, Wilcock DM: **Neuroinflammatory phenotype in early Alzheimer's disease.** *Neurobiol Aging* 2013, **34:**1051-1059.

25. Zotova E, Holmes C, Johnston D, Neal JW, Nicoll JA, Boche D: **Microglial alterations in human Alzheimer's disease following Abeta42 immunization.** *Neuropathol Appl Neurobiol* 2011, **37:**513-524.

26. Greene SJ, Killiany RJ, Alzheimer's Disease Neuroimaging I: **Hippocampal subregions are differentially affected in the progression to Alzheimer's disease.** *Anat Rec (Hoboken)* 2012, **295:**132-140.

27. Kahn I, Andrews-Hanna JR, Vincent JL, Snyder AZ, Buckner RL: **Distinct cortical anatomy linked to subregions of the medial temporal lobe revealed by intrinsic functional connectivity.** *J Neurophysiol* 2008, **100:**129-139.

28. Ranganath C, Ritchey M: **Two cortical systems for memory-guided behaviour.** *Nat Rev Neurosci* 2012, **13:**713-726.

29. Dickerson BC, Brickhouse M, McGinnis S, Wolk DA: **Alzheimer's disease: The influence of age on clinical heterogeneity through the human brain connectome.** *Alzheimers Dement (Amst)* 2017, **6:**122-135.

30. Bussiere T, Hof PR, Mailliot C, Brown CD, Caillet-Boudin ML, Perl DP, Buee L, Delacourte A: **Phosphorylated serine422 on tau proteins is a pathological epitope found in several diseases with neurofibrillary degeneration.** *Acta Neuropathol* 1999, **97:**221-230.

31. Guillozet-Bongaarts AL, Cahill ME, Cryns VL, Reynolds MR, Berry RW, Binder LI: **Pseudophosphorylation of tau at serine 422 inhibits caspase cleavage: in vitro evidence and implications for tangle formation in vivo.** *J Neurochem* 2006, **97:**1005-1014.

32. Pennanen L, Gotz J: **Different tau epitopes define Abeta42-mediated tau insolubility.** *Biochem Biophys Res Commun* 2005, **337:**1097-1101.

33. Augustinack JC, Schneider A, Mandelkow EM, Hyman BT: **Specific tau phosphorylation sites correlate with severity of neuronal cytopathology in Alzheimer's disease.** *Acta Neuropathol* 2002, **103:**26-35.

34. Vana L, Kanaan NM, Ugwu IC, Wuu J, Mufson EJ, Binder LI: **Progression of tau pathology in cholinergic Basal forebrain neurons in mild cognitive impairment and Alzheimer's disease.** *Am J Pathol* 2011, **179:**2533-2550.

35. Mastrangelo MA, Bowers WJ: **Detailed immunohistochemical characterization of temporal and spatial progression of Alzheimer's disease-related pathologies in male triple-transgenic mice.** *BMC Neurosci* 2008, **9:**81.

36. Bilkei-Gorzo A: **Genetic mouse models of brain ageing and Alzheimer's disease.** *Pharmacol Ther* 2014, **142:**244-257.

37. Braak H, Alafuzoff I, Arzberger T, Kretzschmar H, Del Tredici K: **Staging of Alzheimer disease-associated neurofibrillary pathology using paraffin sections and immunocytochemistry.** *Acta Neuropathol* 2006, **112:**389-404.

38. Duyckaerts C, Potier MC, Delatour B: **Alzheimer disease models and human neuropathology: similarities and differences.** *Acta Neuropathol* 2008, **115:**5-38.

FIGURES

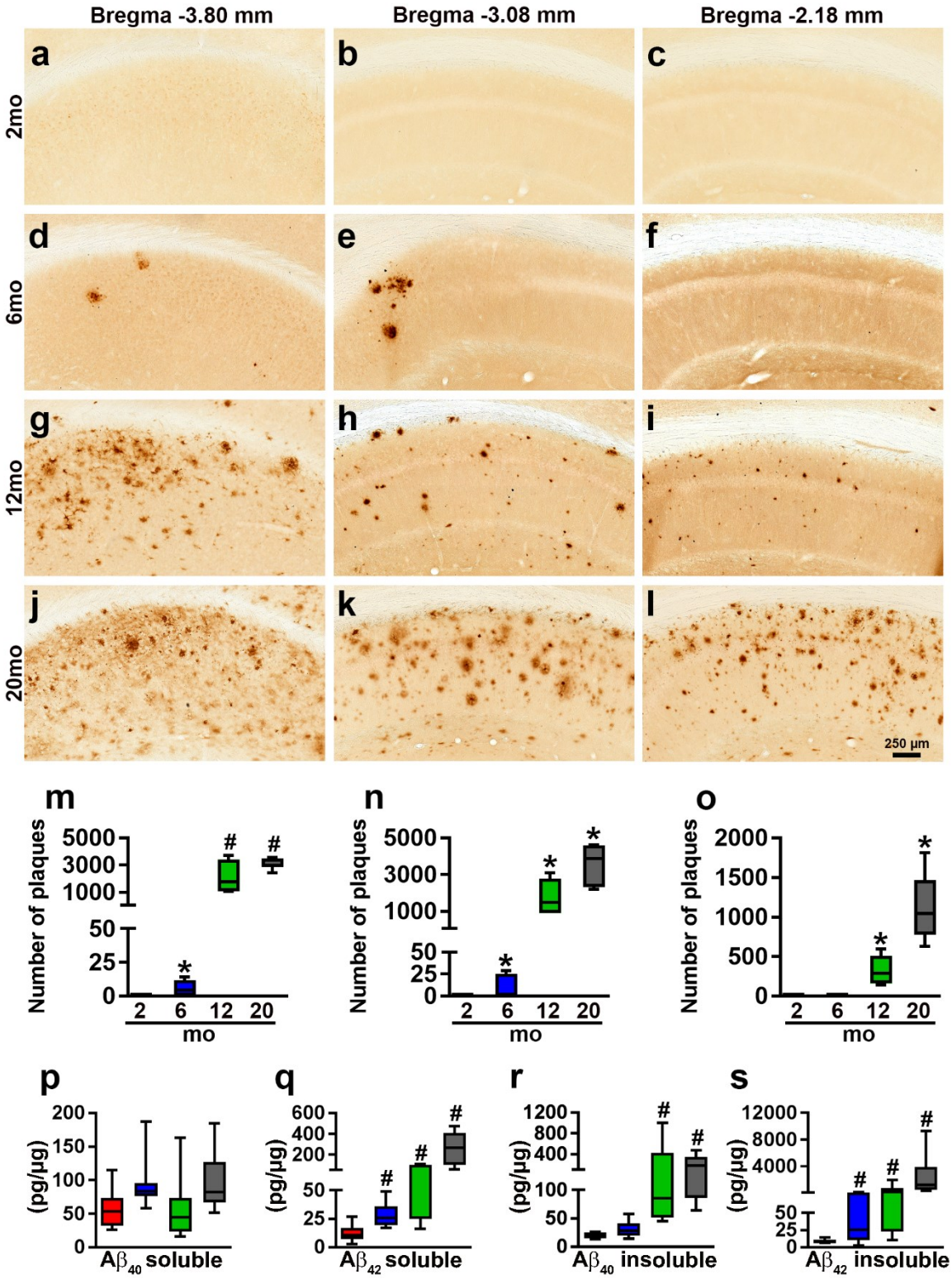
Bregma -3.80 mm
Bregma -3.08 mm
Bregma -2.18 mm
2mo
6mo
12mo
20mo
a
b
c
d
e
f
g
h
i
j
k
l
250 µm
m
n
o
Number of plaques
mo
p
q
r
s
(pg/µg)
Aβ40 soluble
Aβ42 soluble
Aβ40 insoluble
Aβ42 insoluble

Figure 1. Age-dependent Aβ pathology in the hippocampus. ***a–l***, Representative microphotographs of hippocampal sections from 2-, 6-, 12-, and 20-month-old 3xTg-AD mice stained with an anti-$A\beta_{42}$-specific antibody (n = 6/age group). As indicated, brain sections were selected at -3.80 mm, -3.08 mm, and -2.18 mm posterior to bregma. ***m-o***, Quantitative analysis of the anti-$A\beta_{42}$ immunoreactivity from the caudal ($p < 0.0001$, $F_{(3, 20)} = 39.97$), medial ($p < 0.0001$, $F_{(3, 20)} = 32.6$) and rostral ($p < 0.0001$, $F_{(3, 20)} = 26.74$) hippocampus. *Post hoc* analysis indicated that $A\beta_{42}$ immunoreactivity in the caudal hippocampus (m) was significantly increased between 6 and 12 months of age ($p < 0.0001$) but not significantly increased between 12- and 20-month-old mice 3xTg-AD ($p = 0.0764$). In contrast, a quantitative analysis of medial (n) and rostral (o) hippocampus showed significant differences among all the age-groups ($p < 0.001$). ***p-s***, Sandwich ELISA measurements of soluble and insoluble $A\beta_{40}$ and $A\beta_{42}$ levels. The levels of soluble $A\beta_{40}$ did not change as a function of age, whereas soluble $A\beta_{42}$ levels were significantly different among the four age-groups ($p < 0.0001$, $F_{(3, 31)} = 19.74$). Specifically, *post hoc* evaluations showed that the levels of soluble $A\beta_{42}$ were significantly different between all the pairwise comparisons ($p < 0.0001$) except when comparing the 6- and 12-month-old mice. Insoluble $A\beta_{40}$ changed as a function of age ($p = 0.0081$, $F_{(3, 31)} = 4.699$). Post hoc analyses indicated that the 12- and 20-month groups were significantly different than the other two groups ($p < 0.0001$ for both comparisons). Insoluble $A\beta_{42}$ levels also increased as a function of age ($p < 0.0001$, $F_{(3, 30)} = 15.15$). *Post hoc* analyses showed the insoluble Aβ42 levels were significan between all the pairwise comparisons ($p < 0.005$), except when comparing the 6- and 12-month-old mice. Data were analyzed by One-way ANOVA followed by Bonferroni's *post hoc* tests. *Asterisks indicate differences within all the*

groups; hashtags indicate differences with selected groups. Error bars represent mean ± SEM

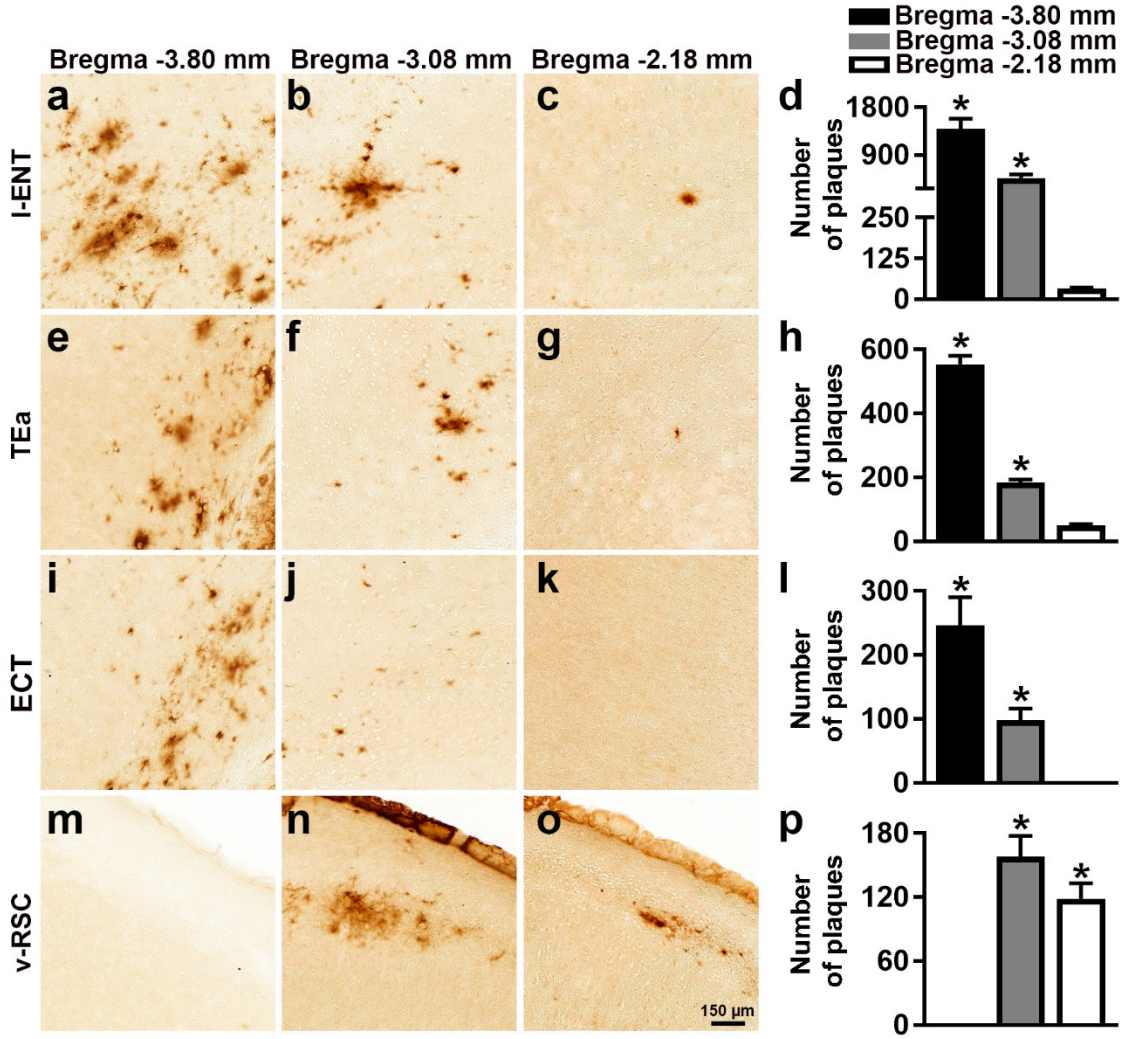

Figure 2. Cortical Aβ plaques deposition in 12-month-old 3xTg-AD mice. Representative microphotographs of brain sections from 12-month-old 3xTg-AD mice (n = 6/age group) stained with a selective $A\beta_{42}$ antibody. Per each brain region, sections were taken at three different rostrocaudal levels. **(a-c)** $A\beta_{42}$ immunoreactivity in the lateral entorhinal cortex (l-ENT). **(d)** Quantitative analyses of the staining indicated that the number of Aβ plaques was higher in the caudal l-ENT compared to the medial and rostral

l-ENT ($p = 0.0013$ and $p < 0.0001$, respectively). Also, there was a statistically significant difference between the medial and the rostral l-ENT cortex ($p = 0.001$). **(e-g)** $A\beta_{42}$ immunoreactivity in the temporal association area (TEa). **(h)** Quantitative analyses of the staining indicated that in the caudal TEa the number of Aβ plaques was higher compared to medial and rostral TEa ($p < 0.0001$ for both comparisons). Further, the number of plaques was higher in the medial TEa compared to rostral TEa ($p = 0.0008$). **(i-k)** $A\beta_{42}$ immunoreactivity in the ectorhinal cortex (ECT). **(l)** Quantitative analyses of the staining indicated that there was a higher number of Aβ plaques in the caudal ECT cortex compared to medial and rostral ECT ($p = 0.0125$ and 0.0004, respectively. **(m-o)** $A\beta_{42}$ immunoreactivity in the ventral retrosplenial cortex (v-RSC). **(p)** Quantitative analyses of the staining indicated that the caudal v-RSC had significantly fewer plaques compared to the medial and rostral v-RSC ($p = 0.003$ and 0.004, respectively). *Data were analyzed by One-way ANOVA followed by Bonferroni's post hoc evaluations. Asterisks indicate differences within all the groups. Error bars represent mean ± SEM*

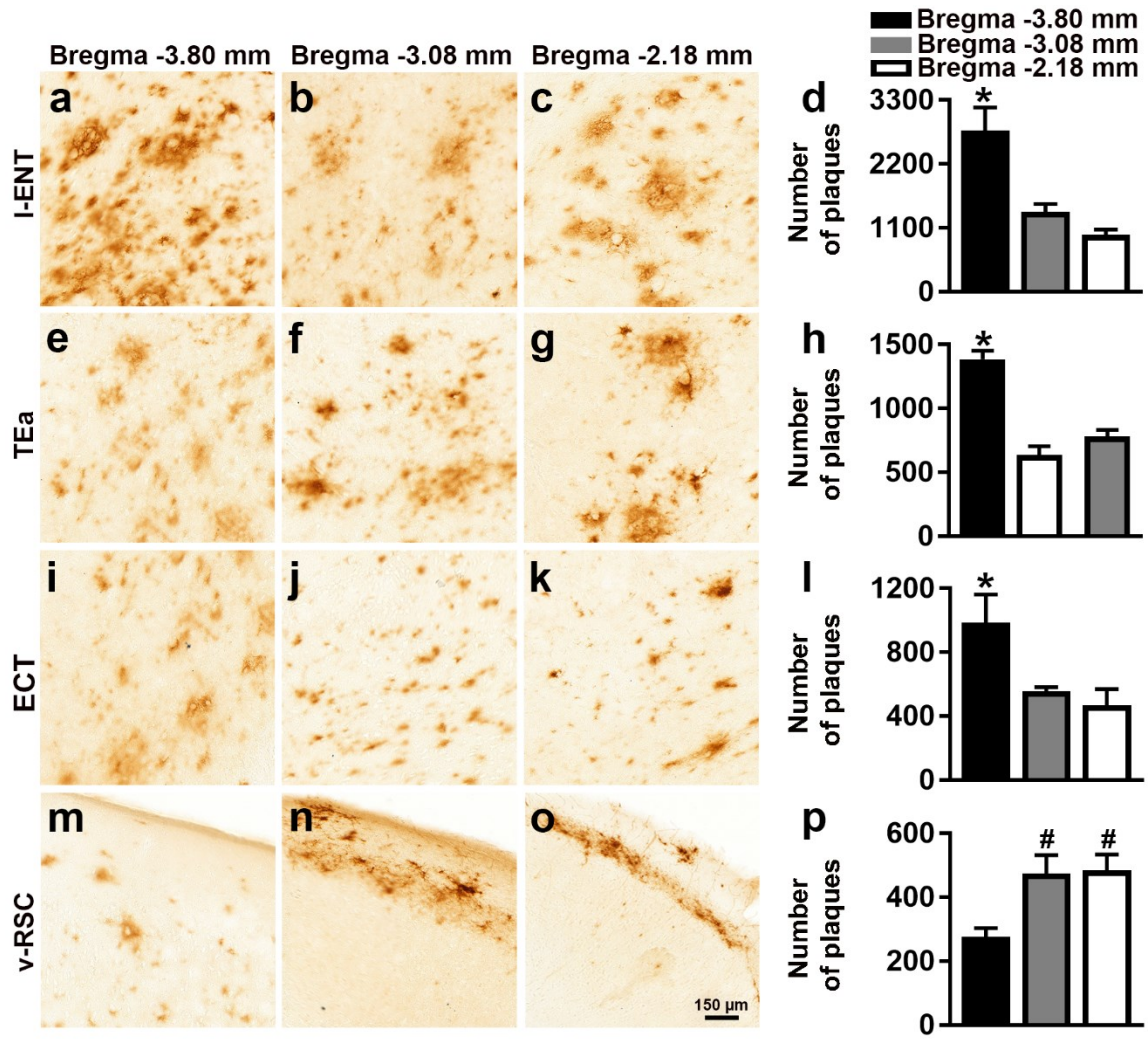

Figure 3. Cortical Aβ pathology in 20-month-old 3xTg-AD mice. Representative microphotographs of brain sections from 20-month-old 3xTg-AD mice (n = 6/age group) stained with a selective $A\beta_{42}$ antibody. Per each brain region, sections were taken at three different rostrocaudal levels. **(a-c)** $A\beta_{42}$ immunoreactivity in the lateral entorhinal cortex (l-ENT). **(d)** Quantitative analyses of the staining indicated that the number of Aβ plaques was higher in the caudal l-ENT compared to the medial and rostral l-ENT ($p = 0.0002$ and $p < 0.0001$, respectively). **(e-g)** $A\beta_{42}$ immunoreactivity in the temporal association area (TEa). **(h)** Quantitative analyses of the staining indicated that in the caudal TEa the

number of Aβ plaques was higher than the medial and rostral TEa ($p = 0.009$ and 0.001, respectively). **(i-k)** $A\beta_{42}$ immunoreactivity in the ectorhinal cortex (ECT). **(l)** Quantitative analyses of the staining indicated that there was a higher number of Aβ plaques in the caudal ECT compared to the medial and rostral ECT ($p = 0.09$ and 0.03, respectively. **(m-o)** $A\beta_{42}$ immunoreactivity in the ventral retrosplenial cortex (v-RSC). **(p)** Quantitative analyses of the staining indicated that the number of plaques was significantly increased in the medial and rostral v-RSC compared to the caudal v-RSC ($p = 0.04$ and 0.03, respectively). *Data were analyzed by One-way ANOVA followed by Bonferroni's post hoc evaluations. Asterisks indicate differences within all the groups; hashtags indicate differences with selected groups. Error bars represent mean ± SEM.*

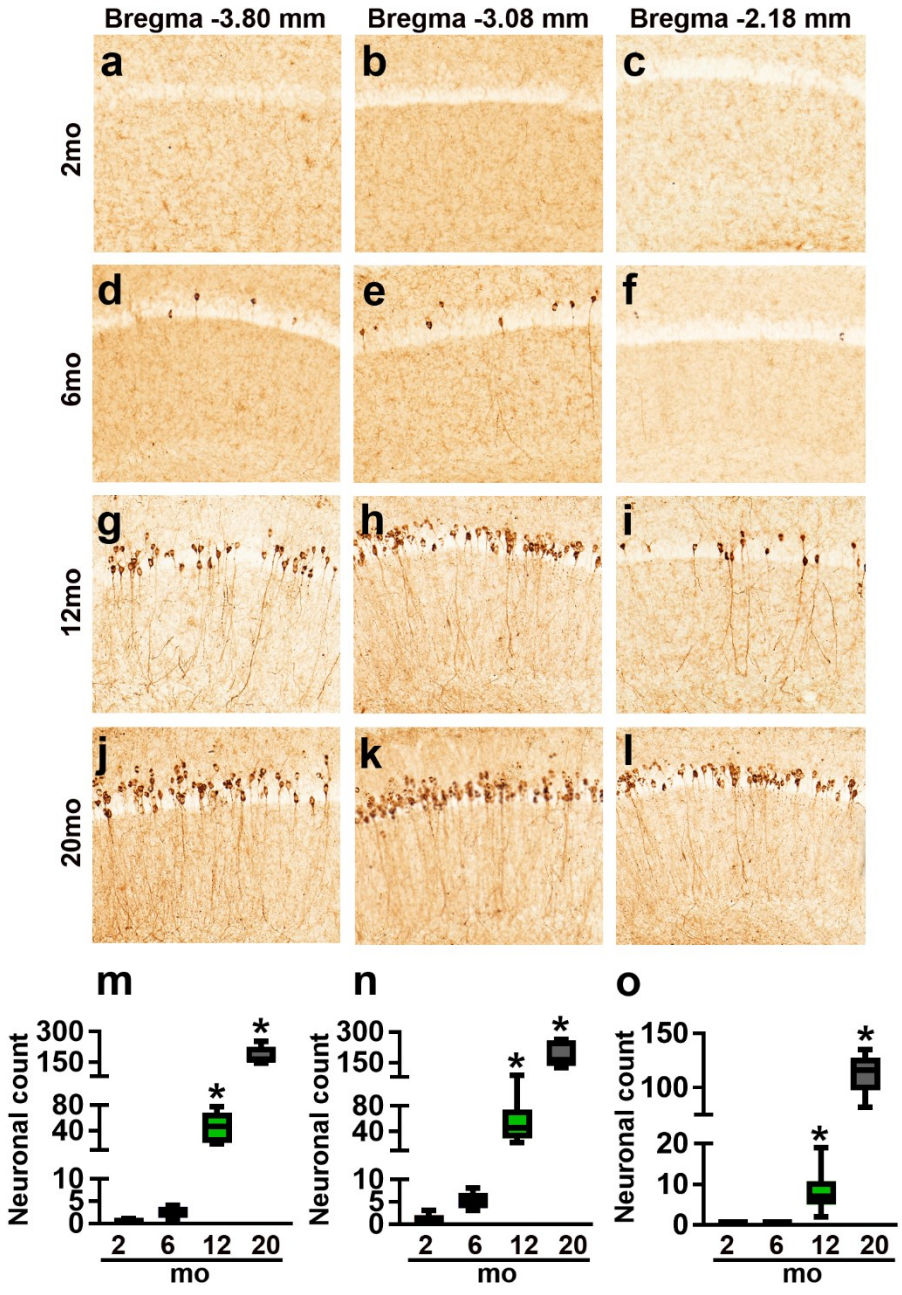

Figure 4. Age-dependent progression of Tau phosphorylation at S422 in hippocampi of 3xTg-AD mice. **a-l**, Representative microphotographs of hippocampal sections from 2-, 6-, 12-, and 20-month-old 3xTg-AD mice stained with an anti-pS422-specific antibody (n = 6/age group). Brain sections were selected at -3.80 mm, -3.08 mm, and -2.18 mm posterior to bregma. **(*m-o*)** Quantitative analysis of the anti-pS422 immunoreactivity by

one-way ANOVA followed by a Bonferroni's multiple-comparison test show statistically significant age-dependent difference in the caudal *(*$p < 0.0001$, $F_{(3, 20)} = 83.1$), medial ($p < 0.0001$, $F_{(3, 20)} = 47.88$) and rostral ($p < 0.0001$, $F_{(3, 20)} = 188.5$) hippocampus. *Post hoc* analysis indicated that pS422 immunoreactivity in all three hippocampal regions was significantly higher in 12-month-old mice compared to the 2- and 6-month groups ($p < 0.005$*)*. Further, the 20-month-old mice have significantly higher pS422 immunoreactivity compared to all the other three age-groups ($p < 0.0001$). *Asterisks indicate differences within all the groups. Error bars represent mean ± SEM.*

S422						
	-3.80 mm		-3.08 mm		-2.18 mm	
Age	positive neurons	% mice	positive neurons	% mice	positive neurons	% mice
2 mo	0.2 ± 0.20	33.3	1 ± 0.5400	50	0	0
6 mo	5.2 ± 0.86	100	2.5 ± 0.64	100	0.3 ± 0.21	33
12 mo	44.6 ± 11.01	100	50.2 ± 11.83	100	8.1 ± 2.33	100
20 mo	182 ± 19.55	100	191 ± 28.85	100	113± 8.66	100
AT8						
	-3.80 mm		-3.08 mm		-2.18 mm	
Age	positive neurons	% mice	positive neurons	% mice	positive neurons	% mice
2 mo	0.3 ± 0.21	33.3	0	0	0	0
6 mo	10 ± 1.59	100	2.2 ± 0.2	100	0.3 ± 0.21	33.3
12 mo	44.6 ± 18.24	100	56.83 ± 11.04	100	21.83 ± 9.96	100
20 mo	182 ± 12.89	100	187 ± 20.61	100	95.17 ± 18.25	100
AT100						
	-3.80 mm		-3.08 mm		-2.18 mm	
Age	positive neurons	% mice	positive neurons	% mice	positive neurons	% mice
2 mo	0	0	0	0	0	0
6 mo	1.5 ± 0.64	50	2.2 ± 0.91	50	0	0
12 mo	21.5 ± 3.83	100	55.6 ± 6.60	100	25.2 ± 12.96	100
20 mo	107.5 ± 6.58	100	252.75 ± 34.6	100	85 ± 11.98	100

Table 1

Age-dependent progression of Tau phosphorylation in of 3xTg-AD mice. The percentage of mice is calculated on n = 6/age group. The neuronal count is represented by mean ± SEM.

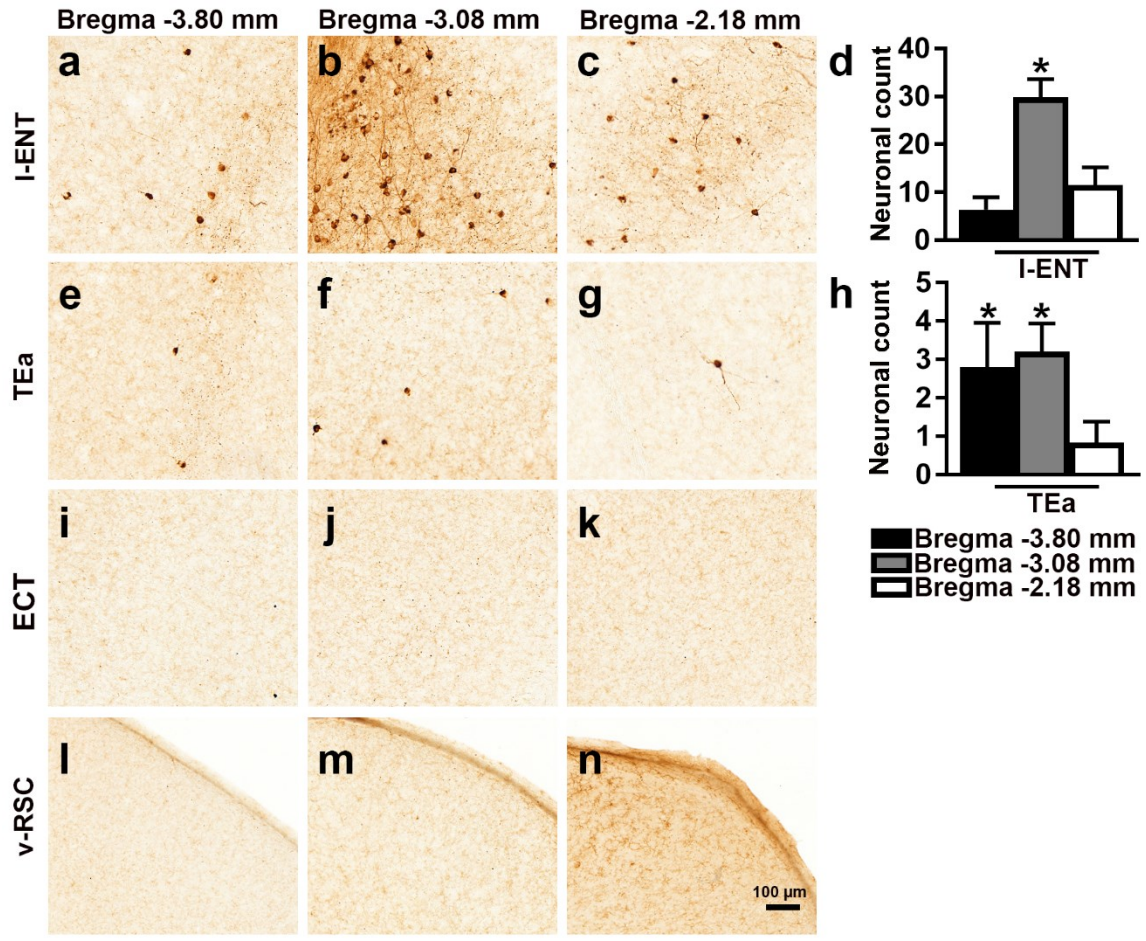

Figure 5. Cortical Tau S422 phosphorylation in 20-month-old 3xTg-AD mice. Representative microphotographs of brain sections from 20-month-old 3xTg-AD mice (n = 6/age group) stained with a selective pS422 tau antibody. Per each brain region, sections were taken at three different rostrocaudal levels. **(a-c)** pS422 immunoreactivity in the l-ENT cortex. **(d)** Quantitative analyses of the staining indicated that the number of pS422-positive neurons was higher in the medial l-ENT cortex compared to the caudal ($p = 0.0006$) and rostral l-ENT cortex ($p = 0.054$). **(e-g)** pS422 immunoreactivity in the TEa cortex. **(h)** Quantitative analyses of the staining indicated that the number of pS422-positive neurons was not significantly different among the three rostrocaudal regions of

the TEa cortex. (**i-k** and **l-n**) Lack of pS422 immunoreactivity in the ECT and v-RSC cortices. *Asterisks indicate differences within all the groups. Error bars represent mean ± SEM.*

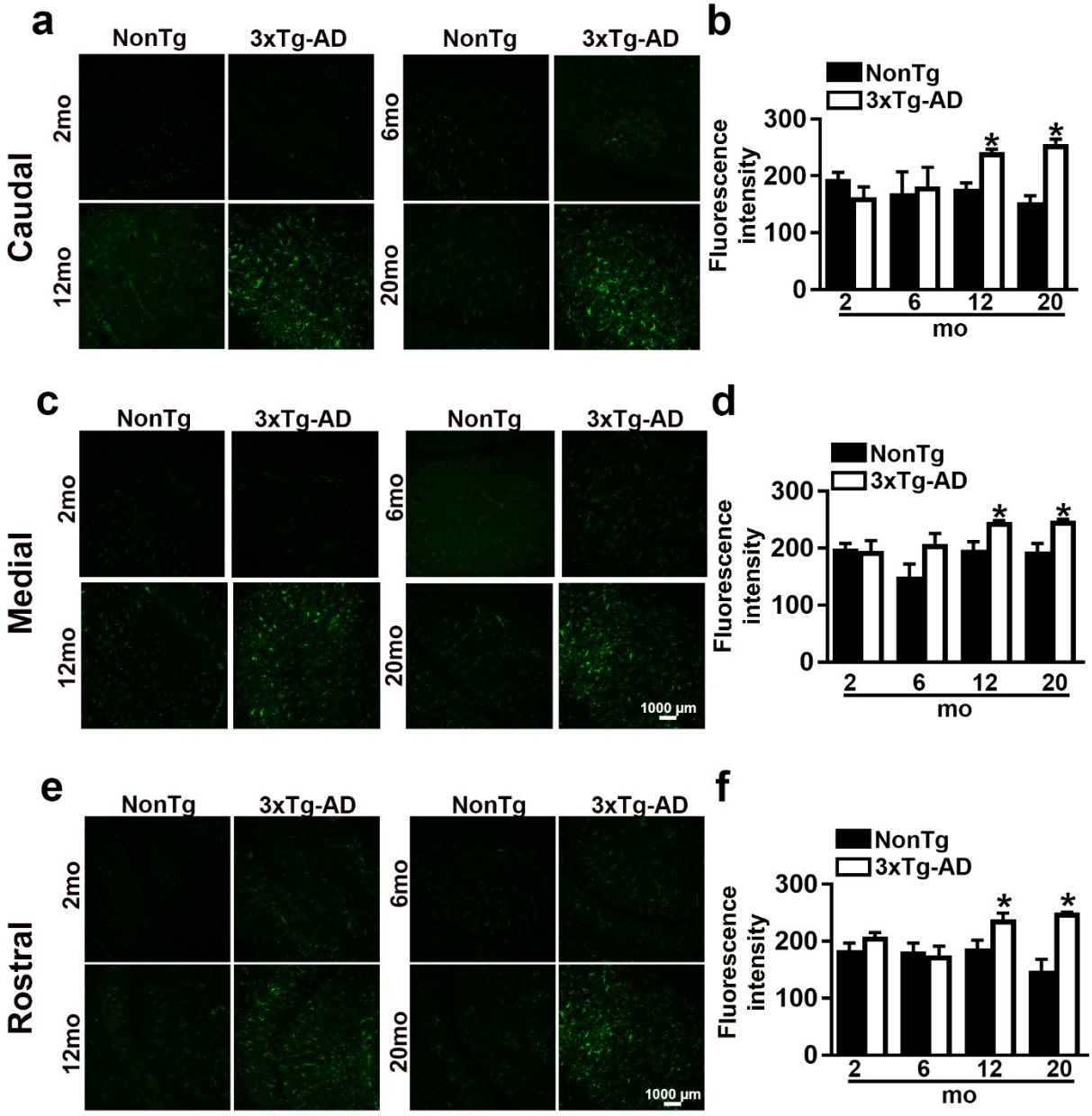

Figure 6. Age-dependent astrogliosis in 3xTg-AD mice. Representative confocal microphotographs of 3xTg-AD and NonTg CA1 sections stained with a GFAP antibody (n = 6/age group). Per each brain region, sections were taken at three different rostrocaudal levels. **(a-b)** GFAP immunoreactivity and quantitative analyses in the caudal hippocampus. GFAP immunoreactivity was higher in 12- and 20-month-old 3xTg-AD mice compared to age-matched NonTg mice ($p = 0.0001$ and $p < 0.0001$, respectively). **(c-d)** GFAP immunoreactivity and quantitative analyses in the medial hippocampus. GFAP immunoreactivity was higher in 12- and 20-month-old 3xTg-AD mice compared to age-matched NonTg mice ($p = 0.0054$ and $p = 0.0016$, respectively). **(e-f)** GFAP immunoreactivity and quantitative analyses in the medial hippocampus. GFAP immunoreactivity was higher in 12- and 20-month-old 3xTg-AD mice compared to age-matched NonTg mice ($p = 0.022$ and $p = 0.0012$, respectively). Data were analyzed by student's *t*-test. *Error bars represent mean ± SEM.*

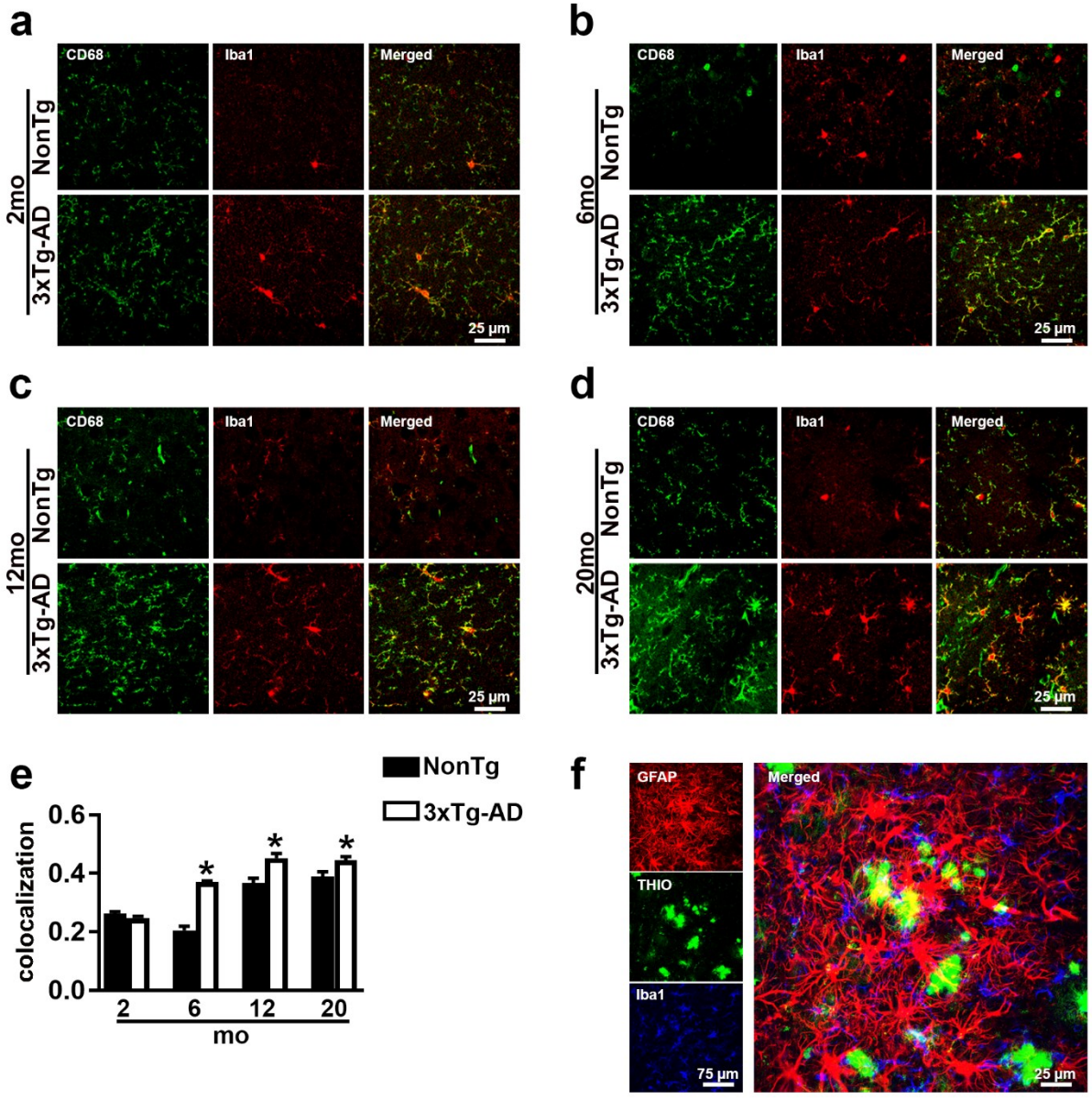

***Figure 7. Age-dependent microglia activation in* 3xTg-AD mice. (a-d)** Representative confocal microphotographs of CA1 sections from the medial hippocampus of NonTg and 3xTg-AD mice (*n* = 6/genotype/age group). Sections were stained with an anti-Iba1 and an anti-CD68 antibodies. **(e)** Quantitative analysis revealed that the number of colocalized pixels was significantly higher in 3xTg-AD mice than NonTg mice at 6 months, 12 months and 20 months ($p < 0.0001$, $p < 0.0001$, $p = 0.0076$ respectively). **(f)** Representative

confocal microphotographs of CA1 section from 20-month-old 3xTg-AD mice stained with Thioflavin, anti-GFAP and anti-Iba1 antibodies. The image shows the different distribution of microglial (homogenously distributed) and reactive astrocytes (surrounding Aβ plaques). Statistical evaluation was obtained by the Pearson's correlation coefficients. Error bars represent mean ± SEM.

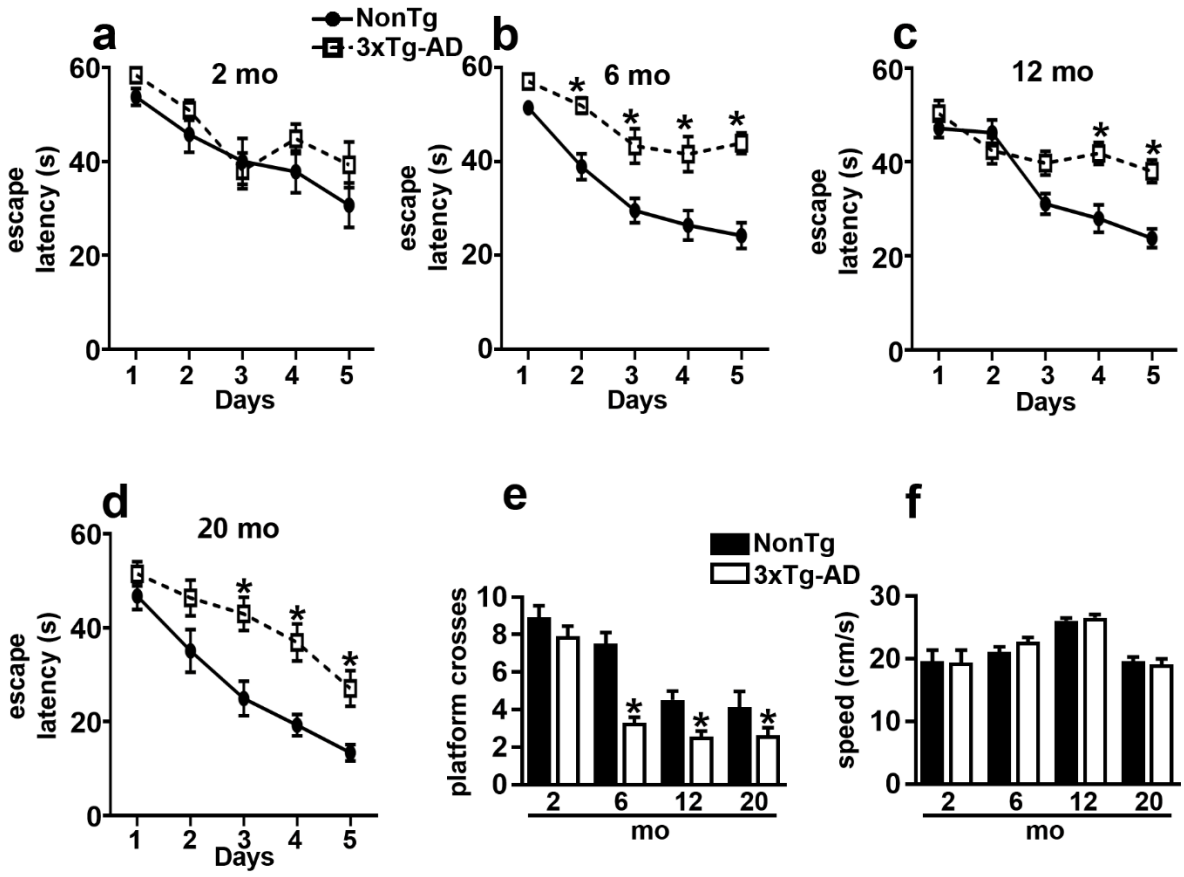

Figure 8. Age-dependent spatial learning and memory deficits. (*a*-d) Learning curves of mice trained in the spatial reference version of the Morris water maze (2 months, n = 15/genotype; 6 months, n = 15 for 3xTg-AD and n = 10 for NonTg; 12 months, n = 15 for

3xTg-AD and n = 14 for NonTg; and 20 months, n = 15 for 3xTg-AD and n = 11 for NonTg). The escape latency to find the hidden platform was plotted against the days of training. The values for each day represent the average of four training trails. At 2 months of age, we found a significant effect for day ($p < 0.0001$, $F_{(4,135)} = 10.90$) but a not a significant effect for genotype ($p = 0.0623$, $F_{(1,135)} = 3.53$). At 6 months of age, we found significant effects for day ($p < 0.0001$, $F_{(4, 92)} = 23.37$) and genotype ($p < 0.0001$, $F_{(1, 23)} = 41.86$). *Post hoc* tests indicated that NonTg mice performed significantly better than 3xTg-AD on day 2 (p = 0.0053), day 3 (p = 0.0028), day 4 (p = 0.0008) and day 5 (p <0.0001). At 12 months of age, there were significant effects for day ($p < 0.0001$, $F_{(4, 108)} = 21.85$) and genotype ($p = 0.0022$, $F_{(1, 27)} = 11.46$). *Post hoc* tests indicated that NonTg mice performed significantly better than 3xTg-AD on day 4 (p = 0.0008) and day 5 (p = 0.0005). At 20 months of age, there was a significant effect for day ($p < 0.0001$, $F_{(4, 92)} = 26.03$) and by genotype ($p < 0.0001$, $F_{(1, 23)} = 22.05$). *Post hoc* tests showed that 3xTg-AD mice performed significantly worse when compared with NonTg mice on day 3 (p = 0.0014), day 4 (p = 0.0018) and day 5 (p = 0.0259). ***(e)*** Number of platform location crosses during a single 60-second probe trial. 3xTg-AD mice performed significantly worse compared to NonTg mice at 6 (p = 0.0008), 12 (p = 0.0123), and 20 months of age (p = 0.01400). ***(f)*** Swim speed was similar between the two different groups at all the ages ($p > 0.05$). Learning data were analyzed by two-way ANOVA; probe trials were analyzed by one-way ANOVA. Bonferroni's was used for *post hoc* tests. Asterisk indicates a significant difference between NonTg and 3xTg-AD mice. Error bars represent mean ± SEM.

ADDITIONAL FILES

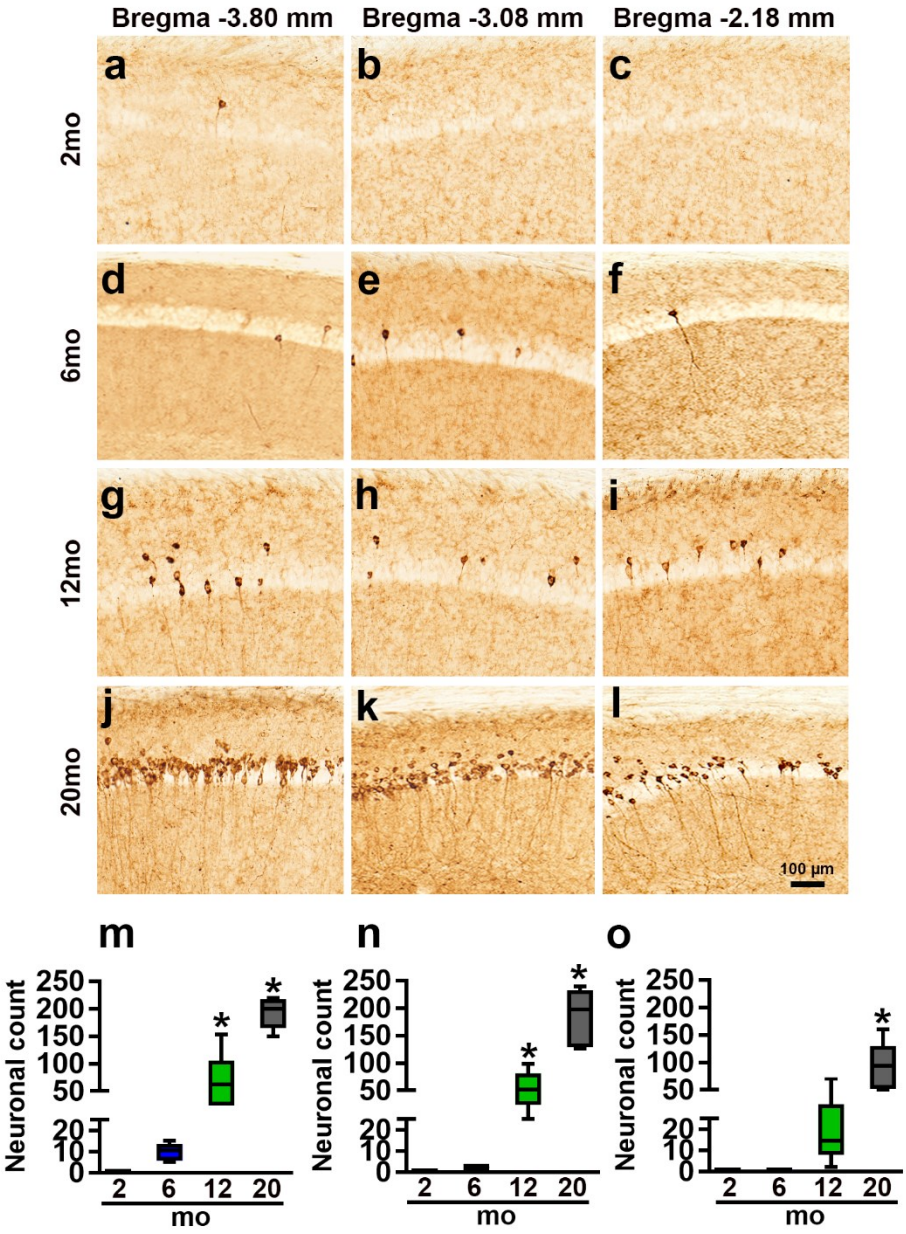

Additional file 1: Figure S1

Age-dependent progression of Tau AT8 phosphorylation in hippocampi of 3xTg-AD mice. (A-L), Representative microphotographs of hippocampal sections from 2-, 6-, 12-, and 20-month-old 3xTg-AD and mice stained with an anti-pS422-specific antibody. Brain

sections were selected at -3.80 mm, -3.08 mm, and -2.18 mm posterior to bregma. (M-O), Quantitative analysis of the anti-AT8 immunoreactivity by one-way ANOVA followed by a Bonferroni's multiple-comparison test (n = 6 mice/genotype; from 2 to 20 month of age $p < 0.0001$, $F (3, 20) = 59.57$). Post hoc analysis indicated that AT8 immunoreactivity in the posterior bregma was significantly increased between 6 and 12 months and between 12- and 20-month-old mice 3xTg-AD (M; $p = 0.003$ and $p < 0.0001$, respectively). Similarly, a quantitative analysis in the medial and rostral bregma showed significant differences in 3xTg-AD mice between 6 and 12 months (N-O; $p = 0.04$ and $p = 0.05$ for medial and rostral respectively) and between 12- and 20-month (N-O, $p = 0.0001$ and $p < 0.0001$ for medial and rostral respectively). Asterisks indicate differences within all the groups; hashtags indicate differences with selected groups. Error bars represent mean ± SEM.

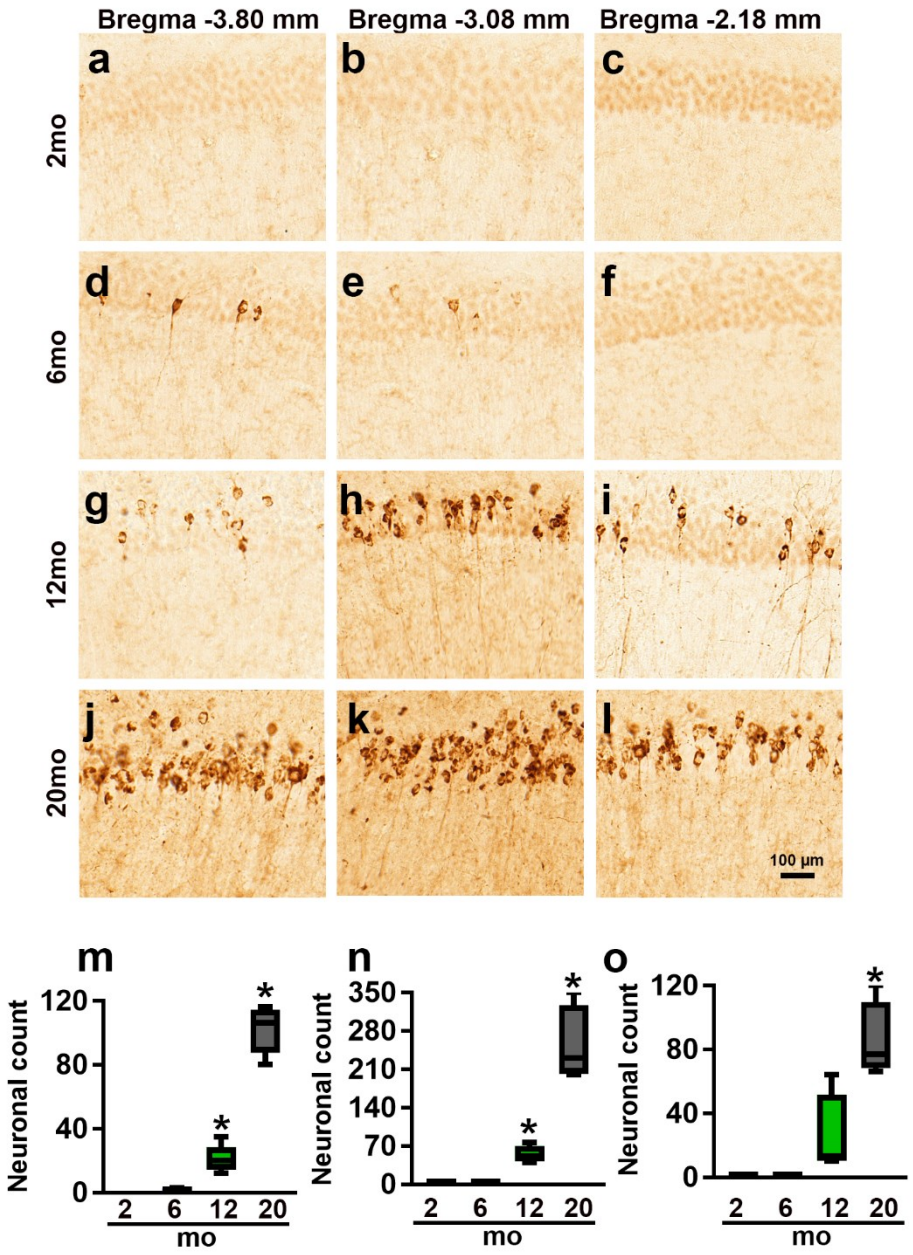

Additional file 1: Figure S2

Age-dependent progression of Tau AT100 phosphorylation in hippocampi of 3xTg-AD mice. (A-L), Representative microphotographs of hippocampal sections from 2-, 6-, 12-, and 20-month-old 3xTg-AD and mice stained with an anti-AT100-specific antibody. Brain sections were selected at -3.80 mm, -3.08 mm, and -2.18 mm posterior to bregma. (M-O),

Quantitative analysis of the anti-AT100 immunoreactivity by one-way ANOVA followed by a Bonferroni's multiple-comparison test (n = 6 mice/genotype; from 2 to 20 month of age $p < 0.0001$, $F(3, 20) = 76.3$). Post hoc analysis indicated that AT100 immunoreactivity in the posterior bregma was significantly increased between 6 and 12 months and between 12- and 20-month-old mice 3xTg-AD (M; $p = 0.023$ and $p < 0.0001$, respectively). Similarly, a quantitative analysis in the medial bregma showed significant differences in 3xTg-AD mice between 6 and 12 months (N-O; $p = 0.002$ and $p = 0.003$, respectively) and between 12- and 20-month (N-O, $p = 0.0002$ and $p < 0.0001$, respectively). Asterisks indicate differences within all the groups; hashtags indicate differences with selected groups. Error bars represent mean ± SEM

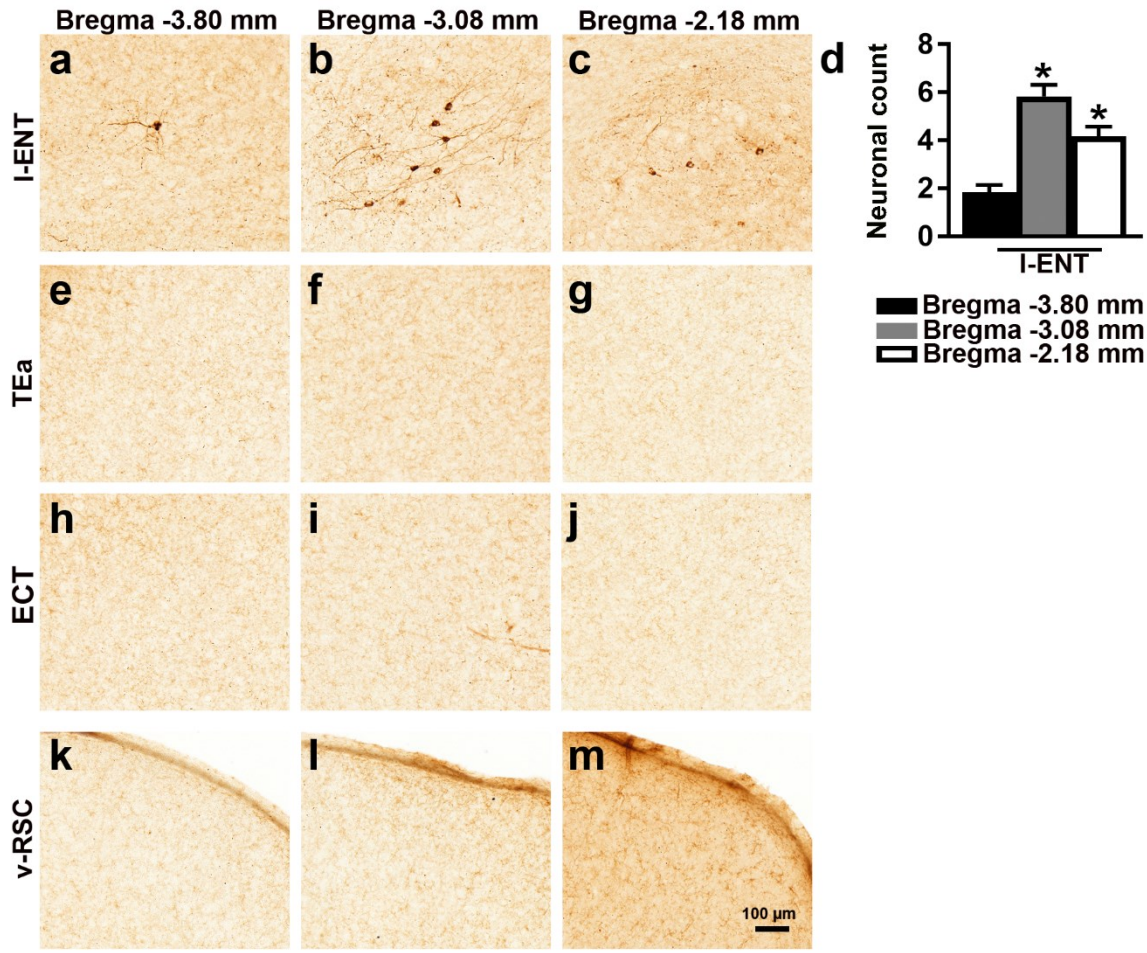

Additional file 1: Figure S3

Cortical Tau S422 phosphorylation in 12-month-old 3xTg-AD mice. Representative microphotographs of lateral entorhinal cortex (A-C, l-ENT), temporal association area (E-G, TEa), ectorhinal cortex (I-K, ECT), and ventral restrosplenial cortex (M-O, v-RSC) from 12-month-old 3xTg-AD mice stained with an anti-p-S422 specific antibody. (D), Quantitative analysis of the p-S422 immunoreactivity by One-way ANOVA analysis of l-ENT. The number of positive neurons was higher in the medial l-ENT compared to both caudal ($p < 0.0001$) and rostral ($p = 0.0006$) l-ENT and in the rostral compared to the caudal l-ENT ($p = 0.0025$). We found no positive neurons for Tau p-S422 immunostaining

in the temporal association area, ectorhinal cortex and ventral restrosplenial cortex of 12-month-old 3xTg-AD mice. Asterisks indicate differences within all the groups; hashtags indicate differences with selected groups. Error bars represent mean ± SEM.

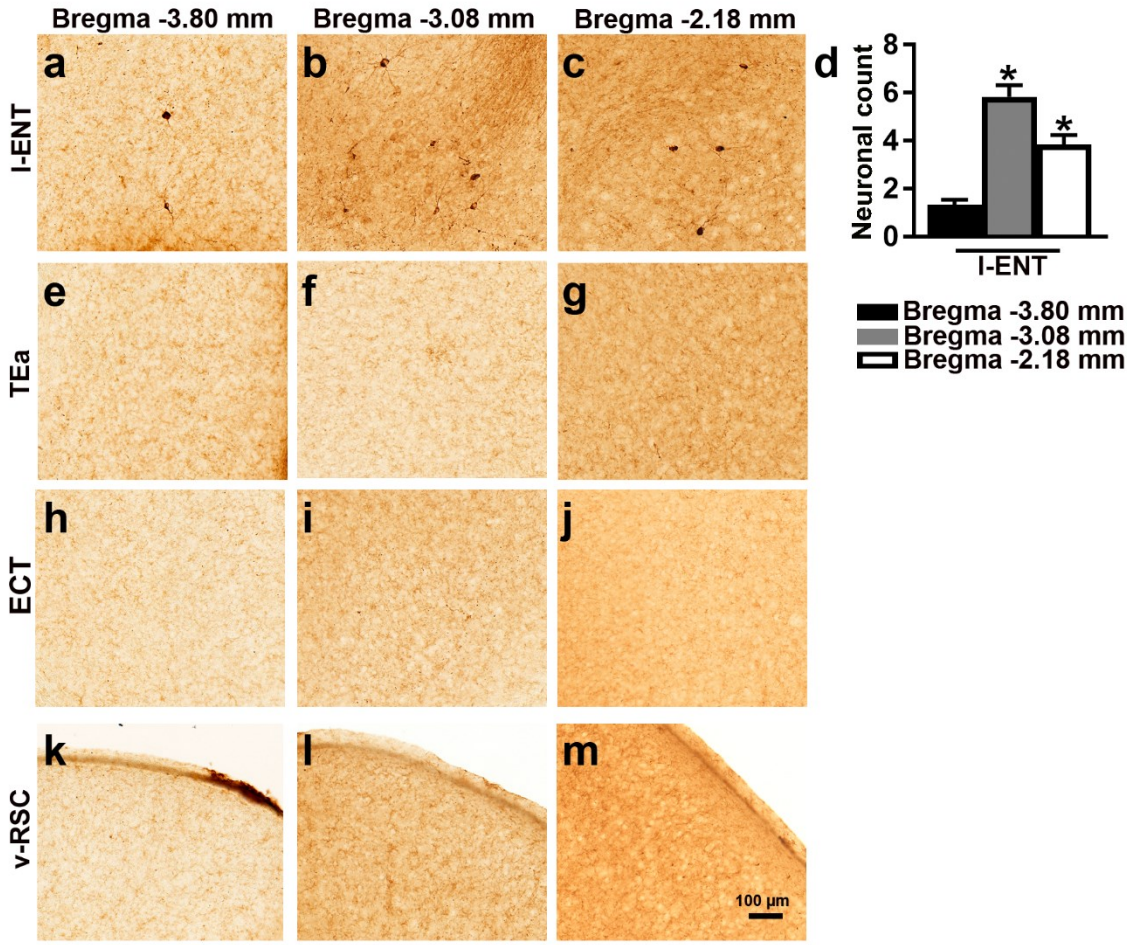

Additional file 1: Figure S4

Cortical Tau AT8 phosphorylation in 12-month-old 3xTg-AD mice. Representative microphotographs of lateral entorhinal cortex (A-C, l-ENT), temporal association area (E-G, TEa), ectorhinal cortex (I-K, ECT), and ventral restrosplenial cortex (M-O, v-RSC) from 12-month-old 3xTg-AD mice stained with an anti-AT8 specific antibody. (D), Quantitative analysis of the AT8 immunoreactivity by One-way ANOVA analysis of l-

ENT. The number of positive neurons was higher in the medial l-ENT compared to both caudal ($p < 0.0001$) and rostral ($p = 0.0061$) l-ENT and in the rostral compared to the caudal l-ENT ($p = 0.0009$). We found no positive neurons for Tau AT8 immunostaining in the temporal association area, ectorhinal cortex and ventral restrosplenial cortex of 12-month-old 3xTg-AD mice. Asterisks indicate differences within all the groups; hashtags indicate differences with selected groups. Error bars represent mean ± SEM.

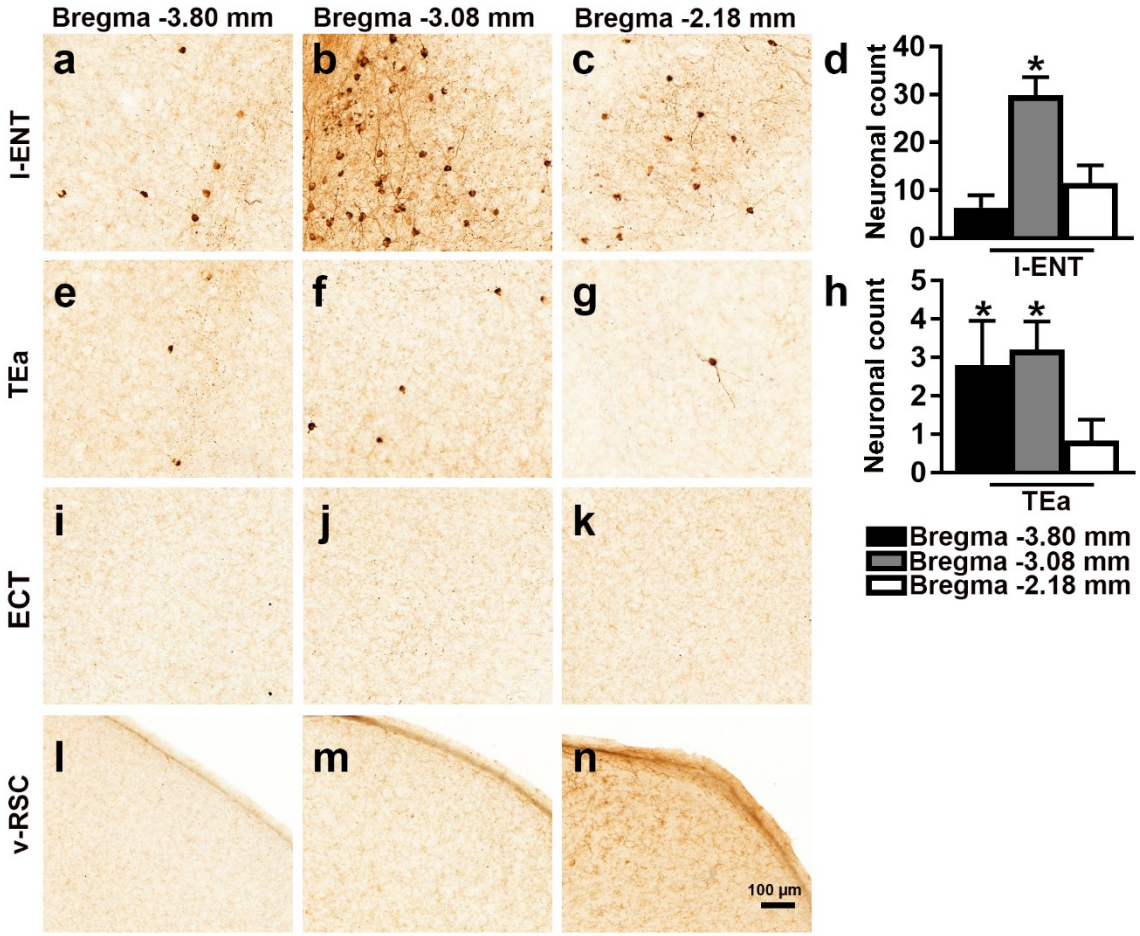

Additional file 1: Figure S5

Cortical Tau AT8 phosphorylation in 20-month-old 3xTg-AD mice. Representative microphotographs of lateral entorhinal cortex (A-C, l-ENT), temporal association area (E-

G, TEa), ectorhinal cortex (I-K, ECT), and ventral restrosplenial cortex (M-O, v-RSC) from 20-month-old 3xTg-AD mice stained with an anti-AT8 specific antibody. (D), Quantitative analysis of the AT8 immunoreactivity by One-way ANOVA analysis of l-ENT. The number of positive neurons was higher in the medial l-ENT compared to both caudal ($p < 0.0001$) and rostral ($p = 0.0436$) l-ENT and in the rostral compared to the caudal l-ENT ($p = 0.0041$). (H), In the TEa the number of positive neurons was significative different higher in the caudal and in the medial compared to the rostral bregma ($p < 0.0001$ and $p = 0.0016$, respectively). We found no positive neurons for Tau AT8 immunostaining in the ectorhinal cortex and ventral restrosplenial cortex of 20-month-old 3xTg-AD mice. Asterisks indicate differences within all the groups; hashtags indicate differences with selected groups. Error bars represent mean ± SEM.

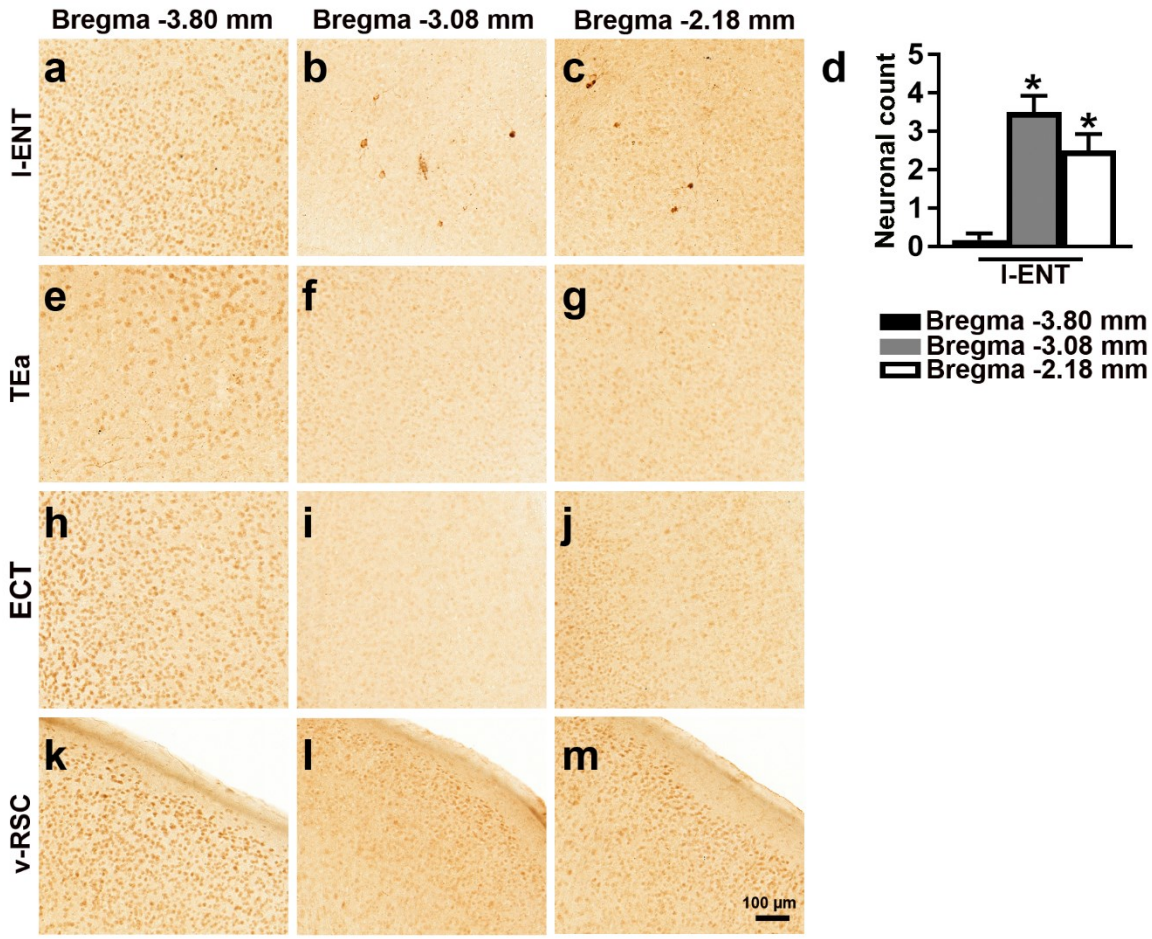

Additional file 1: Figure S6

Cortical Tau AT100 phosphorylation in 12-month-old 3xTg-AD mice. Representative microphotographs of lateral entorhinal cortex (A-C, l-ENT), temporal association area (E-G, TEa), ectorhinal cortex (I-K, ECT), and ventral restrosplenial cortex (M-O, v-RSC) from 12-month-old 3xTg-AD mice stained with an anti-AT100 specific antibody. (D), Quantitative analysis of the AT100 immunoreactivity by One-way ANOVA analysis of l-ENT. The number of positive neurons was higher in the medial l-ENT compared to both caudal ($p < 0.0001$) and rostral ($p = 0.0011$) l-ENT. We found no positive neurons for Tau AT100 immunostaining in the temporal association area, ectorhinal cortex and ventral

restrosplenial cortex of 12-month-old 3xTg-AD mice. Asterisks indicate differences within all the groups; hashtags indicate differences with selected groups. Error bars represent mean ± SEM.

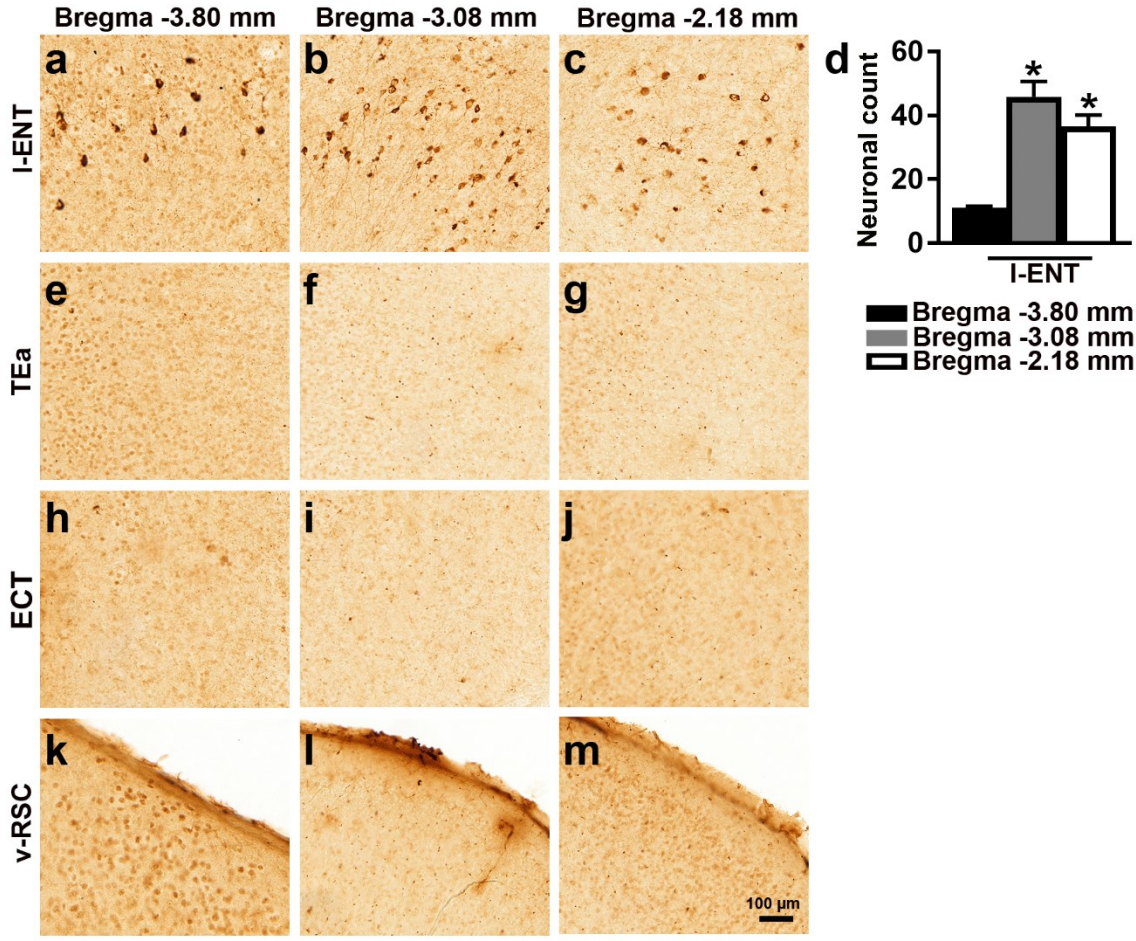

Additional file 1: Figure S7

Cortical Tau AT100 phosphorylation in 20-month-old 3xTg-AD mice. Representative microphotographs of lateral entorhinal cortex (A-C, l-ENT), temporal association area (E-G, TEa), ectorhinal cortex (I-K, ECT), and ventral restrosplenial cortex (M-O, v-RSC) from 20-month-old 3xTg-AD mice stained with an anti-AT100 specific antibody. (D), Quantitative analysis of the AT100 immunoreactivity by One-way ANOVA analysis of l-

ENT. The number of positive neurons was higher in the medial l-ENT compared to both caudal ($p < 0.0001$) and rostral ($p = 0.0004$). We found no positive neurons for Tau AT100 immunostaining in the temporal association area, ectorhinal cortex and ventral restrosplenial cortex of 20-month-old 3xTg-AD mice. Asterisks indicate differences within all the groups; hashtags indicate differences with selected groups. Error bars represent mean ± SEM

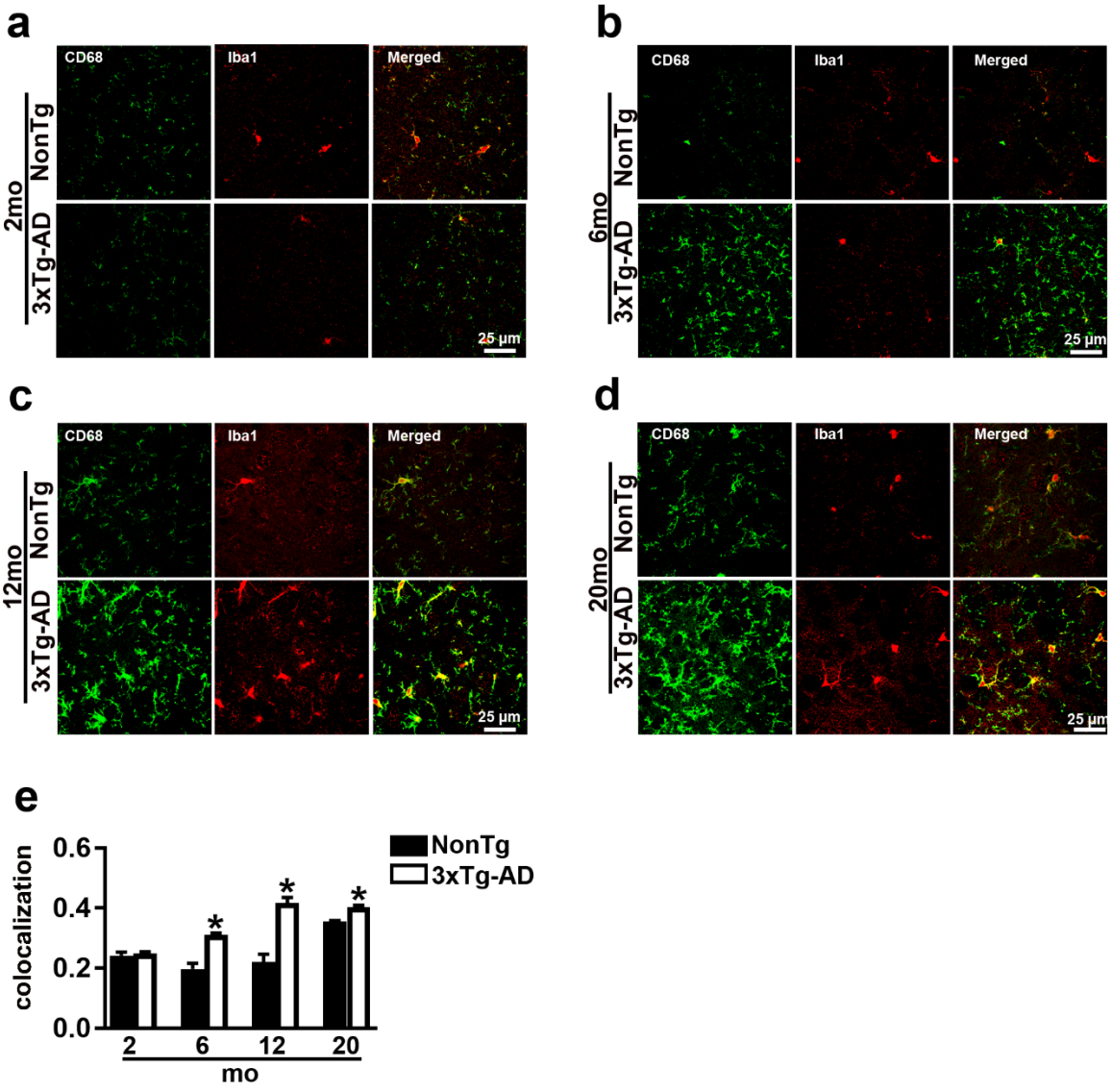

Additional file 1: Figure S8

3xTg-AD mice gliosis activation. Representative confocal microphotographs of CA1 sections from the caudal begma of NonTg (n= 6 mice) and 3xTg-AD (n= 6 mice). (A-D) Sections from 2-, 6-, 12-, and 20-month-old 3xTg-AD and NonTg mice were stained with an anti-Iba1 and anti-CD68 antibody. (E) Quantitative analysis of 10 images per tissue section of CA1 revealed that the number of colocalized pixels was significantly higher in 3xTg-AD mice than NonTg mice at 6 months, 12 months and 20 months ($p < 0.0001$, $p = 0.0006$ and $p < 0.0001$, respectively). Statistical evaluation was obtained by the Pearson's correlation coefficients across the 10 images. Error bars represent mean ± SEM.

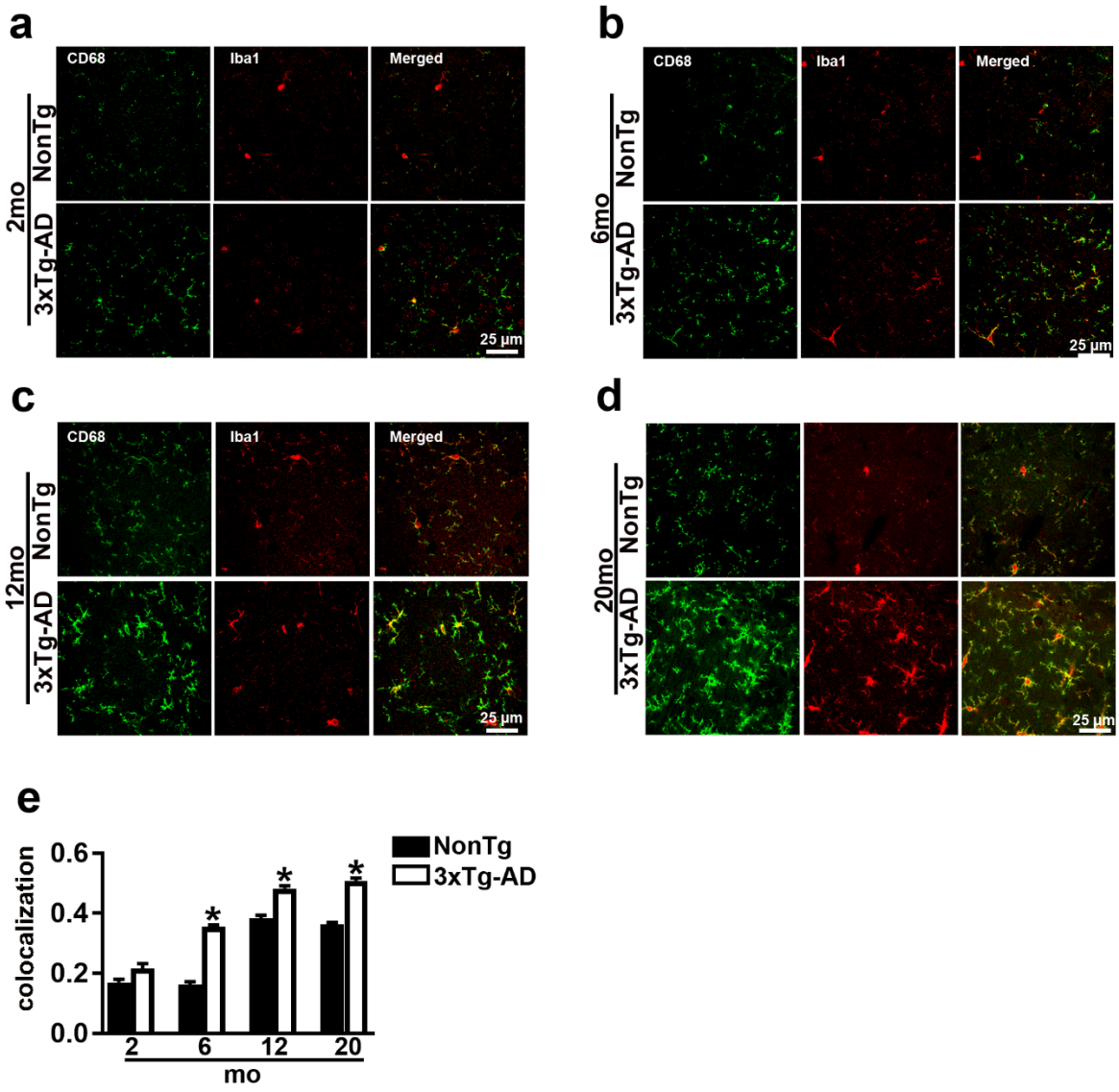

Additional file 1: Figure S9

3xTg-AD mice gliosis activation. Representative confocal microphotographs of CA1 sections from the rostral begma of NonTg (n= 6 mice) and 3xTg-AD (n= 6 mice). (A-D) Sections from 2-, 6-, 12-, and 20-month-old 3xTg-AD and NonTg mice were stained with an anti-Iba1 and anti-CD68 antibody. (E) Quantitative analysis of 10 images per tissue section of CA1 revealed that the number of colocalized pixels was significantly higher in

3xTg-AD mice than NonTg mice at 6 months, 12 months and 20 months ($p < 0.0001$ for all the three ages). Statistical evaluation was obtained by the Pearson's correlation coefficients across the 10 images. Error bars represent mean ± SEM.

GENERAL DISCUSSION AND CONCLUSIONS

Neurodegenerative diseases incidence is worldwide increasing (Feigin et al., 2017). Most of disorders of neurodegeneration as Parkinson's disease, Alzheimer's disease and Amyotrophic Lateral Sclerosis do share a similar pathological pattern that appears as a toxic intracellular and extracellular accumulation of misfolded or mutant proteins (Brettschneider et al., 2015; Soto, 2003). Main consequences of deposition and propagation of toxic misfolded proteins are neuronal death and synaptic disfunction (Lim and Yue, 2015).

At earlier stages of neurodegenerative diseases, many events of neuronal stress develop and increase as the pathology worsen (Vyas et al., 2016). For instance, both Alzheimer disease and ALS develop mitochondrial disfunction, oxidative stress, calcium signaling unbalance and neuroinflammation (Jha et al., 2017; Sayre et al., 2008).

Due to the severity of neurodegenerative diseases, several therapeutic approaches are constantly screened to reduce the morbidity and mortality of those disorders. The most common study approaches on neurodegeneration target different steps among processing, misfolding, transport, and clearance of proteins (Ciechanover and Kwon, 2015a).

In Alzheimer's disease the first targets have been suggested after the discovery of neuronal deposition of Aβ and NFT: originally it was thought that Aβ plaques were the toxic form but lately researchers found that the soluble fibers and oligomeric forms of Aβ represent the actual dangerous structure of aggregation (Reitz, 2012). As mentioned above, those oligomers and soluble fibrillary amyloid can assume different conformation with difference toxicity, so it has been difficult to select peptides to build a molecular

compound (Goure et al., 2014). Despite many doubts surround the reliability of studying human diseases on animal models (Shanks et al., 2009), the use of rats and mice leaded to the most important findings on neurodegenerative disorders in the past decades (Barré-Sinoussi and Montagutelli, 2015). Many researchers refer the importance of transgenic mice models to study molecular mechanism of neuronal death and associate them with behavioral tasks that can mimic the onset and the evolution of protein-diseases: for instance, widely used transgenic models harbor APP and SOD1mutations to investigate on AD and ALS respectively (Balducci and Forloni, 2011; Julien and Kriz, 2006).

Due to an increase of the average age of the world population, the lack of therapeutic approaches on age-dependent disorders represent an urgent global problem. The multifactorial character of neurodegenerative diseases represents one of main adversity on drugs development: for instance, it's extremely hard to build a perfect disease model that reproduce all the conditions and associated risks that the human brain is expose to (i.e., environmental pollution, alimentation, stress, and genetic predisposition) (Nicolò et al., 2014; Sheikh et al., 2013). For all these reasons, the few available clinical drugs are not able to contrast the onset of the disease but only to delay his progression and reduce the aggressivity. According to the most recent reviews on drug discovery and neurodegeneration, a big step forward can be done only with a mechanistic understanding of protein-protein interaction and aggregation: this will be most likely possible thanks to multidisciplinary approaches comprehensive of *in vitro* studies, *in vivo* drug screening on animal models and tridimensional imaging studies on human brains (Ciechanover and Kwon, 2015b; Spires-Jones et al., 2017).

REFERENCES

Aksoy, H., Dean, G., Elian, M., Deng, H.X., Deng, G., Juneja, T., Storey, E., McKinlay Gardner, R.J., Jacob, R.L., Laing, N.G., et al. (2003). A4T mutation in the SOD1 gene causing familial amyotrophic lateral sclerosis. Neuroepidemiology *22*, 235–238.

Alonso, A., Logroscino, G., Jick, S.S., and Hernán, M.A. (2009). Incidence and lifetime risk of motor neuron disease in the United Kingdom: a population-based study. Eur. J. Neurol. *16*, 745–751.

Alonso, A. del C., Li, B., Grundke-Iqbal, I., and Iqbal, K. (2006). Polymerization of hyperphosphorylated tau into filaments eliminates its inhibitory activity. Proc Natl Acad Sci USA *103*, 8864.

Balducci, C., and Forloni, G. (2011). APP transgenic mice: their use and limitations. Neuromolecular Med. *13*, 117–137.

Barral, J.M., Broadley, S.A., Schaffar, G., and Hartl, F.U. (2004). Roles of molecular chaperones in protein misfolding diseases. Seminars in Cell & Developmental Biology *15*, 17–29.

Barré-Sinoussi, F., and Montagutelli, X. (2015). Animal models are essential to biological research: issues and perspectives. Future Sci OA *1*.

Beghi, E., Logroscino, G., Chiò, A., Hardiman, O., Millul, A., Mitchell, D., Swingler, R., and Traynor, B.J. (2010). Amyotrophic lateral sclerosis, physical exercise, trauma and sports: results of a population-based pilot case-control study. Amyotroph Lateral Scler *11*, 289–292.

Bekris, L.M., Yu, C.-E., Bird, T.D., and Tsuang, D.W. (2010). Genetics of Alzheimer Disease. J Geriatr Psychiatry Neurol *23*, 213–227.

Belmont, P., Constant, J.-F., and Demeunynck, M. (2001). Nucleic acid conformation diversity: from structure to function and regulation. Chemical Society Reviews *30*, 70–81.

Bhat, A.H., Dar, K.B., Anees, S., Zargar, M.A., Masood, A., Sofi, M.A., and Ganie, S.A. (2015). Oxidative stress, mitochondrial dysfunction and neurodegenerative diseases; a mechanistic insight. Biomedicine & Pharmacotherapy *74*, 101–110.

Bird, T.D. (2008). Genetic aspects of Alzheimer disease. Genet. Med. *10*, 231–239.

Bliss, T.V.P., and Cooke, S.F. (2011). Long-term potentiation and long-term depression: a clinical perspective. Clinics (Sao Paulo) *66*, 3–17.

Bordo, D., Djinović, K., and Bolognesi, M. (1994). Conserved patterns in the Cu,Zn superoxide dismutase family. J. Mol. Biol. *238*, 366–386.

Bowling, A.C., Schulz, J.B., Brown, R.H., and Beal, M.F. (1993). Superoxide dismutase activity, oxidative damage, and mitochondrial energy metabolism in familial and sporadic amyotrophic lateral sclerosis. J. Neurochem. *61*, 2322–2325.

Branca, C., Sarnico, I., Ruotolo, R., Lanzillotta, A., Viscomi, A.R., Benarese, M., Porrini, V., Lorenzini, L., Calzà, L., Imbimbo, B.P., et al. (2014). Pharmacological targeting of the β-amyloid precursor protein intracellular domain. Sci Rep *4*.

Brettschneider, J., Del Tredici, K., Lee, V.M.-Y., and Trojanowski, J.Q. (2015). Spreading of pathology in neurodegenerative diseases: a focus on human studies. Nat Rev Neurosci *16*, 109–120.

Bucciantini, M., Giannoni, E., Chiti, F., Baroni, F., Formigli, L., Zurdo, J., Taddei, N., Ramponi, G., Dobson, C.M., and Stefani, M. (2002). Inherent toxicity of aggregates implies a common mechanism for protein misfolding diseases. Nature *416*, 507–511.

Camandola, S., and Mattson, M.P. Brain metabolism in health, aging, and neurodegeneration. The EMBO Journal *36*, 1474–1492.

Carrì, M.T., Ferri, A., Battistoni, A., Famhy, L., Gabbianelli, R., Poccia, F., and Rotilio, G. (1997). Expression of a Cu,Zn superoxide dismutase typical of familial amyotrophic lateral sclerosis induces mitochondrial alteration and increase of cytosolic Ca2+ concentration in transfected neuroblastoma SH-SY5Y cells. FEBS Lett. *414*, 365–368.

Cheon, M., Kang, M., and Chang, I. (2016). Polymorphism of fibrillar structures depending on the size of assembled Aβ17-42 peptides. Scientific Reports *6*.

Chiò, A., Benzi, G., Dossena, M., Mutani, R., and Mora, G. (2005). Severely increased risk of amyotrophic lateral sclerosis among Italian professional football players. Brain *128*, 472–476.

Chiò, A., Logroscino, G., Hardiman, O., Swingler, R., Mitchell, D., Beghi, E., Traynor, B.G., and Eurals Consortium (2009). Prognostic factors in ALS: A critical review. Amyotroph Lateral Scler *10*, 310–323.

Chow, V.W., Mattson, M.P., Wong, P.C., and Gleichmann, M. (2010). An Overview of APP Processing Enzymes and Products. Neuromolecular Med *12*, 1–12.

Ciechanover, A., and Kwon, Y.T. (2015a). Degradation of misfolded proteins in neurodegenerative diseases: therapeutic targets and strategies. Exp Mol Med *47*, e147.

Ciechanover, A., and Kwon, Y.T. (2015b). Degradation of misfolded proteins in neurodegenerative diseases: therapeutic targets and strategies. Experimental & Molecular Medicine *47*, e147.

Clayton, K.A., Van Enoo, A.A., and Ikezu, T. (2017). Alzheimer's Disease: The Role of Microglia in Brain Homeostasis and Proteopathy. Front Neurosci *11*.

Condello, C., Lemmin, T., Stöhr, J., Nick, M., Wu, Y., Maxwell, A.M., Watts, J.C., Caro, C.D., Oehler, A., Keene, C.D., et al. (2018). Structural heterogeneity and intersubject variability of Aβ in familial and sporadic Alzheimer's disease. PNAS 201714966.

Corcia, P., Mayeux-Portas, V., Khoris, J., de Toffol, B., Autret, A., Müh, J.-P., Camu, W., Andres, C., and French ALS Research Group. Amyotrophic Lateral Sclerosis (2002). Abnormal SMN1

gene copy number is a susceptibility factor for amyotrophic lateral sclerosis. Ann. Neurol. *51*, 243–246.

Craigen, W.J., and Graham, B.H. (2008). Genetic strategies for dissecting mammalian and Drosophila voltage-dependent anion channel functions. J Bioenerg Biomembr *40*, 207–212.

Cudkowicz, M.E., McKenna-Yasek, D., Sapp, P.E., Chin, W., Geller, B., Hayden, D.L., Schoenfeld, D.A., Hosler, B.A., Horvitz, H.R., and Brown, R.H. (1997). Epidemiology of mutations in superoxide dismutase in amyotrophic lateral sclerosis. Ann. Neurol. *41*, 210–221.

Diekstra, F.P., Saris, C.G.J., van Rheenen, W., Franke, L., Jansen, R.C., van Es, M.A., van Vught, P.W.J., Blauw, H.M., Groen, E.J.N., Horvath, S., et al. (2012). Mapping of gene expression reveals CYP27A1 as a susceptibility gene for sporadic ALS. PLoS ONE *7*, e35333.

Dineley, K.T., Xia, X., Bui, D., Sweatt, J.D., and Zheng, H. (2002). Accelerated Plaque Accumulation, Associative Learning Deficits, and Up-regulation of α7 Nicotinic Receptor Protein in Transgenic Mice Co-expressing Mutant Human Presenilin 1 and Amyloid Precursor Proteins. J. Biol. Chem. *277*, 22768–22780.

Dobson, C.M. (2003). Protein folding and misfolding. Nature *426*, 884.

Dobson, C.M. (2004). Principles of protein folding, misfolding and aggregation. Seminars in Cell & Developmental Biology *15*, 3–16.

Drubin, D.G., and Kirschner, M.W. (1986). Tau protein function in living cells. J Cell Biol *103*, 2739.

Elder, G.A., Gama Sosa, M.A., and De Gasperi, R. (2010). Transgenic Mouse Models of Alzheimer's Disease. Mt Sinai J Med *77*, 69–81.

Ellis, R.J., and Hartl, F.U. (1999). Principles of protein folding in the cellular environment. Current Opinion in Structural Biology *9*, 102–110.

Erkkinen, M.G., Kim, M.-O., and Geschwind, M.D. (2018). Clinical Neurology and Epidemiology of the Major Neurodegenerative Diseases. Cold Spring Harb Perspect Biol *10*, a033118.

Feigin, V.L., Abajobir, A.A., Abate, K.H., Abd-Allah, F., Abdulle, A.M., Abera, S.F., Abyu, G.Y., Ahmed, M.B., Aichour, A.N., Aichour, I., et al. (2017). Global, regional, and national burden of neurological disorders during 1990–2015: a systematic analysis for the Global Burden of Disease Study 2015. The Lancet Neurology *16*, 877–897.

Folz, R.J., and Crapo, J.D. (1994). Extracellular superoxide dismutase (SOD3): tissue-specific expression, genomic characterization, and computer-assisted sequence analysis of the human EC SOD gene. Genomics *22*, 162–171.

Gamblin, T.C., Chen, F., Zambrano, A., Abraha, A., Lagalwar, S., Guillozet, A.L., Lu, M., Fu, Y., Garcia-Sierra, F., LaPointe, N., et al. (2003). Caspase cleavage of tau: Linking amyloid and neurofibrillary tangles in Alzheimer's disease. Proc Natl Acad Sci U S A *100*, 10032–10037.

Goetz, C.G. (2000). Amyotrophic lateral sclerosis: early contributions of Jean-Martin Charcot. Muscle Nerve *23*, 336–343.

Gordon, P.H., Salachas, F., Lacomblez, L., Le Forestier, N., Pradat, P.-F., Bruneteau, G., Elbaz, A., and Meininger, V. (2013). Predicting survival of patients with amyotrophic lateral sclerosis at presentation: a 15-year experience. Neurodegener Dis *12*, 81–90.

Goure, W.F., Krafft, G.A., Jerecic, J., and Hefti, F. (2014). Targeting the proper amyloid-beta neuronal toxins: a path forward for Alzheimer's disease immunotherapeutics. Alzheimer's Research & Therapy *6*, 42.

Grad, L.I., Rouleau, G.A., Ravits, J., and Cashman, N.R. (2017). Clinical Spectrum of Amyotrophic Lateral Sclerosis (ALS). Cold Spring Harb Perspect Med *7*, a024117.

Grolla, A.A., Sim, J.A., Lim, D., Rodriguez, J.J., Genazzani, A.A., and Verkhratsky, A. (2013). Amyloid-*β* and Alzheimer's disease type pathology differentially affects the calcium signalling toolkit in astrocytes from different brain regions. Cell Death & Disease *4*, e623.

Hall, A.M., and Roberson, E.D. (2012). Mouse Models of Alzheimer's Disease. Brain Res Bull *88*, 3–12.

Hebda-Bauer, E.K., Simmons, T.A., Sugg, A., Ural, E., Stewart, J.A., Beals, J.L., Wei, Q., Watson, S.J., and Akil, H. (2013). 3xTg-AD Mice Exhibit an Activated Central Stress Axis during Early-Stage Pathology. J Alzheimers Dis *33*, 407–422.

Heneka, M.T., Sastre, M., Dumitrescu-Ozimek, L., Dewachter, I., Walter, J., Klockgether, T., and Van Leuven, F. (2005). Focal glial activation coincides with increased BACE1 activation and precedes amyloid plaque deposition in APP[V717I] transgenic mice. Journal of Neuroinflammation *2*, 22.

Higgins, C.M.J., Jung, C., Ding, H., and Xu, Z. (2002). Mutant Cu, Zn superoxide dismutase that causes motoneuron degeneration is present in mitochondria in the CNS. J. Neurosci. *22*, RC215.

Holmuhamedov, E., and Lemasters, J.J. (2009). Ethanol exposure decreases mitochondrial outer membrane permeability in cultured rat hepatocytes. Arch Biochem Biophys *481*, 226–233.

Hooper, C., Killick, R., and Lovestone, S. (2008). The GSK3 hypothesis of Alzheimer's disease. J Neurochem *104*, 1433–1439.

Iqbal, K., Liu, F., Gong, C.-X., and Grundke-Iqbal, I. (2010). Tau in Alzheimer Disease and Related Tauopathies. Curr Alzheimer Res *7*, 656–664.

Israelson, A., Arbel, N., Da Cruz, S., Ilieva, H., Yamanaka, K., Shoshan-Barmatz, V., and Cleveland, D.W. (2010). Misfolded mutant SOD1 directly inhibits VDAC1 conductance in a mouse model of inherited ALS. Neuron *67*, 575–587.

Jacobsen, J.S., Wu, C.-C., Redwine, J.M., Comery, T.A., Arias, R., Bowlby, M., Martone, R., Morrison, J.H., Pangalos, M.N., Reinhart, P.H., et al. (2006). Early-onset behavioral and synaptic deficits in a mouse model of Alzheimer's disease. PNAS *103*, 5161–5166.

Jha, S.K., Jha, N.K., Kumar, D., Ambasta, R.K., and Kumar, P. (2017). Linking mitochondrial dysfunction, metabolic syndrome and stress signaling in Neurodegeneration. Biochimica et Biophysica Acta (BBA) - Molecular Basis of Disease *1863*, 1132–1146.

Julien, J.-P., and Kriz, J. (2006). Transgenic mouse models of amyotrophic lateral sclerosis. Biochimica et Biophysica Acta (BBA) - Molecular Basis of Disease *1762*, 1013–1024.

Juneja, T., Pericak-Vance, M.A., Laing, N.G., Dave, S., and Siddique, T. (1997). Prognosis in familial amyotrophic lateral sclerosis: progression and survival in patients with glu100gly and ala4val mutations in Cu,Zn superoxide dismutase. Neurology *48*, 55–57.

Jung, C., Higgins, C.M.J., and Xu, Z. (2002). A quantitative histochemical assay for activities of mitochondrial electron transport chain complexes in mouse spinal cord sections. J. Neurosci. Methods *114*, 165–172.

Kadavath, H., Hofele, R.V., Biernat, J., Kumar, S., Tepper, K., Urlaub, H., Mandelkow, E., and Zweckstetter, M. (2015). Tau stabilizes microtubules by binding at the interface between tubulin heterodimers. PNAS *112*, 7501–7506.

Kanekiyo, T., Xu, H., and Bu, G. (2014). ApoE and Aβ in Alzheimer's disease: accidental encounters or partners? Neuron *81*, 740–754.

Kanouchi, T., Ohkubo, T., and Yokota, T. (2012). Can regional spreading of amyotrophic lateral sclerosis motor symptoms be explained by prion-like propagation? J. Neurol. Neurosurg. Psychiatry *83*, 739–745.

Kawamata, H., and Manfredi, G. (2008). Different regulation of wild-type and mutant Cu,Zn superoxide dismutase localization in mammalian mitochondria. Hum. Mol. Genet. *17*, 3303–3317.

Kempuraj, D., Thangavel, R., Natteru, P., Selvakumar, G., Saeed, D., Zahoor, H., Zaheer, S., Iyer, S., and Zaheer, A. (2016). Neuroinflammation Induces Neurodegeneration. J Neurol Neurosurg Spine *1*.

Kim, N.-H., Kim, H.-J., Kim, M., and Lee, K.-W. (2003). A novel SOD1 gene mutation in a Korean family with amyotrophic lateral sclerosis. J. Neurol. Sci. *206*, 65–69.

Kompoliti, K., Doumbe, J., Mapoure, Y.N., Nyinyikua, T., Ouyang, B., Shah, H., Calvo, S., Fernandez-Sierra, A., and Delgado, M.E.C. (2017). Mortality and morbidity among hospitalized adult patients with neurological diseases in Cameroon. Journal of the Neurological Sciences *381*, 165–168.

Kyritsis, N., Kizil, C., and Brand, M. (2014). Neuroinflammation and central nervous system regeneration in vertebrates. Trends in Cell Biology *24*, 128–135.

Le Verche, V., and Przedborski, S. (2010). Is Amyotrophic Lateral Sclerosis a Mitochondrial Channelopathy? Neuron *67*, 523–524.

Lepeta, K., Lourenco, M.V., Schweitzer, B.C., Martino Adami, P.V., Banerjee, P., Catuara-Solarz, S., de La Fuente Revenga, M., Guillem, A.M., Haidar, M., Ijomone, O.M., et al. (2016). Synaptopathies: synaptic dysfunction in neurological disorders – A review from students to students. J Neurochem *138*, 785–805.

Levenson, R.W., Sturm, V.E., and Haase, C.M. (2014). Emotional and behavioral symptoms in neurodegenerative disease: A model for studying the neural bases of psychopathology. Annu Rev Clin Psychol *10*, 581–606.

Lewis, J., Dickson, D.W., Lin, W.L., Chisholm, L., Corral, A., Jones, G., Yen, S.H., Sahara, N., Skipper, L., Yager, D., et al. (2001). Enhanced neurofibrillary degeneration in transgenic mice expressing mutant tau and APP. Science *293*, 1487–1491.

Li, S., Jin, M., Koeglsperger, T., Shepardson, N., Shankar, G., and Selkoe, D. (2011). Soluble Aβ oligomers inhibit long-term potentiation through a mechanism involving excessive activation of extrasynaptic NR2B-containing NMDA receptors. J Neurosci *31*, 6627–6638.

Liddelow, S.A., and Barres, B.A. (2017). Reactive Astrocytes: Production, Function, and Therapeutic Potential. Immunity *46*, 957–967.

Lim, J., and Yue, Z. (2015). Neuronal aggregates: formation, clearance and spreading. Dev Cell *32*, 491–501.

Liu, F., and Gong, C.-X. (2008). Tau exon 10 alternative splicing and tauopathies. Mol Neurodegener *3*, 8.

Liu, J., Lillo, C., Jonsson, P.A., Velde, C.V., Ward, C.M., Miller, T.M., Subramaniam, J.R., Rothstein, J.D., Marklund, S., Andersen, P.M., et al. (2004). Toxicity of Familial ALS-Linked SOD1 Mutants from Selective Recruitment to Spinal Mitochondria. Neuron *43*, 5–17.

Llorens-Marítin, M., Jurado, J., Hernández, F., and Ávila, J. (2014). GSK-3β, a pivotal kinase in Alzheimer disease. Front Mol Neurosci *7*.

Mandelkow, E.-M., and Mandelkow, E. (2012). Biochemistry and Cell Biology of Tau Protein in Neurofibrillary Degeneration. Cold Spring Harb Perspect Med *2*.

Mannella, C.A. (1997). Minireview: on the structure and gating mechanism of the mitochondrial channel, VDAC. J. Bioenerg. Biomembr. *29*, 525–531.

Martin, L.J. (1999). Neuronal death in amyotrophic lateral sclerosis is apoptosis: possible contribution of a programmed cell death mechanism. J. Neuropathol. Exp. Neurol. *58*, 459–471.

Millecamps, S., Salachas, F., Cazeneuve, C., Gordon, P., Bricka, B., Camuzat, A., Guillot-Noël, L., Russaouen, O., Bruneteau, G., Pradat, P.-F., et al. (2010). SOD1, ANG, VAPB, TARDBP, and

FUS mutations in familial amyotrophic lateral sclerosis: genotype-phenotype correlations. J. Med. Genet. *47*, 554–560.

Montacute, R., Foley, K., Forman, R., Else, K.J., Cruickshank, S.M., and Allan, S.M. (2017). Enhanced susceptibility of triple transgenic Alzheimer's disease (3xTg-AD) mice to acute infection. J Neuroinflammation *14*.

Morita, M., Aoki, M., Abe, K., Hasegawa, T., Sakuma, R., Onodera, Y., Ichikawa, N., Nishizawa, M., and Itoyama, Y. (1996). A novel two-base mutation in the Cu/Zn superoxide dismutase gene associated with familial amyotrophic lateral sclerosis in Japan. Neurosci. Lett. *205*, 79–82.

Mucke, L., Masliah, E., Johnson, W.B., Ruppe, M.D., Alford, M., Rockenstein, E.M., Forss-Petter, S., Pietropaolo, M., Mallory, M., and Abraham, C.R. (1994). Synaptotrophic effects of human amyloid beta protein precursors in the cortex of transgenic mice. Brain Res. *666*, 151–167.

Murphy, M.P., and LeVine, H. (2010). Alzheimer's Disease and the β-Amyloid Peptide. J Alzheimers Dis *19*, 311.

Nelson, L.M., McGuire, V., Longstreth, W.T., and Matkin, C. (2000). Population-based case-control study of amyotrophic lateral sclerosis in western Washington State. I. Cigarette smoking and alcohol consumption. Am. J. Epidemiol. *151*, 156–163.

Nicolò, S.D., Carito, V., Fiore, M., and Laviola, G. (2014). Aberrant Behavioral and Neurobiologic Profiles in Rodents Exposed to Ethanol or Red Wine Early in Development. Curr Dev Disord Rep *1*, 173–180.

Noble, W., Hanger, D.P., Miller, C.C.J., and Lovestone, S. (2013). The Importance of Tau Phosphorylation for Neurodegenerative Diseases. Front Neurol *4*.

O'Brien, R.J., and Wong, P.C. (2011). Amyloid Precursor Protein Processing and Alzheimer's Disease. Annu Rev Neurosci *34*, 185–204.

Oh, K.-J., Perez, S.E., Lagalwar, S., Vana, L., Binder, L., and Mufson, E.J. (2010). Staging of Alzheimer's Pathology in Triple Transgenic Mice: A Light and Electron Microscopic Analysis.

Parge, H.E., Hallewell, R.A., and Tainer, J.A. (1992). Atomic structures of wild-type and thermostable mutant recombinant human Cu,Zn superoxide dismutase. Proc Natl Acad Sci U S A *89*, 6109–6113.

Querfurth, H.W., and LaFerla, F.M. (2010). Alzheimer's Disease. New England Journal of Medicine *362*, 329–344.

Quon, D., Wang, Y., Catalano, R., Scardina, J.M., Murakami, K., and Cordell, B. (1991). Formation of beta-amyloid protein deposits in brains of transgenic mice. Nature *352*, 239–241.

Rajmohan, R., and Reddy, P.H. (2017). Amyloid Beta and Phosphorylated Tau Accumulations Cause Abnormalities at Synapses of Alzheimer's disease Neurons. J Alzheimers Dis *57*, 975–999.

Ramsden, M., Kotilinek, L., Forster, C., Paulson, J., McGowan, E., SantaCruz, K., Guimaraes, A., Yue, M., Lewis, J., Carlson, G., et al. (2005). Age-Dependent Neurofibrillary Tangle Formation, Neuron Loss, and Memory Impairment in a Mouse Model of Human Tauopathy (P301L). J. Neurosci. *25*, 10637–10647.

Rapoport, M., Dawson, H.N., Binder, L.I., Vitek, M.P., and Ferreira, A. (2002). Tau is essential to β-amyloid-induced neurotoxicity. Proc Natl Acad Sci U S A *99*, 6364–6369.

Ravits, J., Appel, S., Baloh, R.H., Barohn, R., Brooks, B.R., Elman, L., Floeter, M.K., Henderson, C., Lomen-Hoerth, C., Macklis, J.D., et al. (2013). Deciphering amyotrophic lateral sclerosis: what phenotype, neuropathology and genetics are telling us about pathogenesis. Amyotroph Lateral Scler Frontotemporal Degener *14 Suppl 1*, 5–18.

Reddy, P.H. (2007). Mitochondrial dysfunction in aging and Alzheimer's disease: strategies to protect neurons. Antioxid. Redox Signal. *9*, 1647–1658.

Reitz, C. (2012). Alzheimer's Disease and the Amyloid Cascade Hypothesis: A Critical Review. Int J Alzheimers Dis *2012*.

Ringholz, G.M., Appel, S.H., Bradshaw, M., Cooke, N.A., Mosnik, D.M., and Schulz, P.E. (2005). Prevalence and patterns of cognitive impairment in sporadic ALS. Neurology *65*, 586–590.

Rowland, L.P., and Shneider, N.A. (2001). Amyotrophic lateral sclerosis. N. Engl. J. Med. *344*, 1688–1700.

Rubio-Perez, J.M., and Morillas-Ruiz, J.M. (2012). A Review: Inflammatory Process in Alzheimer's Disease, Role of Cytokines.

Rutter, G.A., and Rizzuto, R. (2000). Regulation of mitochondrial metabolism by ER Ca2+ release: an intimate connection. Trends Biochem Sci *25*, 215–221.

Ryan, N.S., and Rossor, M.N. (2010). Correlating familial Alzheimer's disease gene mutations with clinical phenotype. Biomark Med *4*, 99–112.

Sampson, M.J., Lovell, R.S., and Craigen, W.J. (1997). The murine voltage-dependent anion channel gene family. Conserved structure and function. J. Biol. Chem. *272*, 18966–18973.

Sampson, M.J., Ross, L., Decker, W.K., and Craigen, W.J. (1998). A novel isoform of the mitochondrial outer membrane protein VDAC3 via alternative splicing of a 3-base exon. Functional characteristics and subcellular localization. J. Biol. Chem. *273*, 30482–30486.

Santovito, G., Cassini, A., and Piccinni, E. (2006). Cu,Zn superoxide dismutase from Trematomus bernacchii: functional conservation and erratic molecular evolution in Antarctic teleosts. Comp. Biochem. Physiol. C Toxicol. Pharmacol. *143*, 444–454.

Sayre, L.M., Perry, G., and Smith, M.A. (2008). Oxidative Stress and Neurotoxicity. Chemical Research in Toxicology *21*, 172–188.

Scarmeas, N., Shih, T., Stern, Y., Ottman, R., and Rowland, L.P. (2002). Premorbid weight, body mass, and varsity athletics in ALS. Neurology *59*, 773–775.

Schaeffer, E.L., Figueiró, M., and Gattaz, W.F. (2011). Insights into Alzheimer disease pathogenesis from studies in transgenic animal models. Clinics (Sao Paulo) *66*, 45–54.

Schein, S.J., Colombini, M., and Finkelstein, A. (1976). Reconstitution in planar lipid bilayers of a voltage-dependent anion-selective channel obtained from paramecium mitochondria. J. Membr. Biol. *30*, 99–120.

Selkoe, D.J. (2001). Alzheimer's disease: genes, proteins, and therapy. Physiol. Rev. *81*, 741–766.

Sengupta, U., Nilson, A.N., and Kayed, R. (2016). The Role of Amyloid-β Oligomers in Toxicity, Propagation, and Immunotherapy. EBioMedicine *6*, 42–49.

Serrano-Pozo, A., Frosch, M.P., Masliah, E., and Hyman, B.T. (2011). Neuropathological Alterations in Alzheimer Disease. Cold Spring Harb Perspect Med *1*.

Shanks, N., Greek, R., and Greek, J. (2009). Are animal models predictive for humans? Philos Ethics Humanit Med *4*, 2.

Sheikh, S., Safia, Haque, E., and Mir, S.S. (2013). Neurodegenerative Diseases: Multifactorial Conformational Diseases and Their Therapeutic Interventions.

Shinde, U., and Inouye, M. (1993). Intramolecular chaperones and protein folding. Trends in Biochemical Sciences *18*, 442–446.

Shoshan-Barmatz, V., De Pinto, V., Zweckstetter, M., Raviv, Z., Keinan, N., and Arbel, N. (2010). VDAC, a multi-functional mitochondrial protein regulating cell life and death. Mol. Aspects Med. *31*, 227–285.

Shoshan-Barmatz, V., N. Maldonado, E., and Krelin, Y. (2017). VDAC1 at the crossroads of cell metabolism, apoptosis and cell stress. Cell Stress *1*, 11–36.

Sochocka, M., Diniz, B.S., and Leszek, J. (2017). Inflammatory Response in the CNS: Friend or Foe? Mol Neurobiol *54*, 8071–8089.

Sofroniew, M.V., and Vinters, H.V. (2010). Astrocytes: biology and pathology. Acta Neuropathol *119*, 7–35.

Sokolowski, J.D., and Mandell, J.W. (2011). Phagocytic Clearance in Neurodegeneration. Am J Pathol *178*, 1416–1428.

Solito, E., and Sastre, M. (2012). Microglia Function in Alzheimer's Disease. Front Pharmacol *3*.

Soto, C. (2003). Unfolding the role of protein misfolding in neurodegenerative diseases. Nature Reviews Neuroscience *4*, 49.

Spires-Jones, T.L., and Hyman, B.T. (2014). The Intersection of Amyloid Beta and Tau at Synapses in Alzheimer's Disease. Neuron *82*, 756–771.

Spires-Jones, T.L., Attems, J., and Thal, D.R. (2017). Interactions of pathological proteins in neurodegenerative diseases. Acta Neuropathol *134*, 187–205.

Sutedja, N.A., Veldink, J.H., Fischer, K., Kromhout, H., Wokke, J.H.J., Huisman, M.H.B., Heederik, D.J.J., and Van den Berg, L.H. (2007). Lifetime occupation, education, smoking, and risk of ALS. Neurology *69*, 1508–1514.

Takashima, A. (2006). GSK-3 is essential in the pathogenesis of Alzheimer's disease. J. Alzheimers Dis. *9*, 309–317.

TAKASHIMA, A., NOGUCHI, K., SATO, K., HOSHINO, Toshimits., and IMAHORI, K. tau protein kinase I is essential for amyloid f8-protein- induced neurotoxicity. 5.

Tarasoff-Conway, J.M., Carare, R.O., Osorio, R.S., Glodzik, L., Butler, T., Fieremans, E., Axel, L., Rusinek, H., Nicholson, C., Zlokovic, B.V., et al. (2015). Clearance systems in the brain—implications for Alzheimer disease. Nat Rev Neurol *11*, 457–470.

Vander Heiden, M.G., Chandel, N.S., Li, X.X., Schumacker, P.T., Colombini, M., and Thompson, C.B. (2000). Outer mitochondrial membrane permeability can regulate coupled respiration and cell survival. Proc. Natl. Acad. Sci. U.S.A. *97*, 4666–4671.

Vassar, R., Bennett, B.D., Babu-Khan, S., Kahn, S., Mendiaz, E.A., Denis, P., Teplow, D.B., Ross, S., Amarante, P., Loeloff, R., et al. (1999). Beta-secretase cleavage of Alzheimer's amyloid precursor protein by the transmembrane aspartic protease BACE. Science *286*, 735–741.

Verkhratsky, A., Matteoli, M., Parpura, V., Mothet, J., and Zorec, R. (2016). Astrocytes as secretory cells of the central nervous system: idiosyncrasies of vesicular secretion. EMBO J *35*, 239–257.

Vyas, S., Rodrigues, A.J., Silva, J.M., Tronche, F., Almeida, O.F.X., Sousa, N., and Sotiropoulos, I. (2016). Chronic Stress and Glucocorticoids: From Neuronal Plasticity to Neurodegeneration.

Welsh, K.A., Butters, N., Hughes, J.P., Mohs, R.C., and Heyman, A. (1992). Detection and Staging of Dementia in Alzheimer's Disease: Use of the Neuropsychological Measures Developed for the Consortium to Establish a Registry for Alzheimer's Disease. Arch Neurol *49*, 448–452.

Westerman, M.A., Cooper-Blacketer, D., Mariash, A., Kotilinek, L., Kawarabayashi, T., Younkin, L.H., Carlson, G.A., Younkin, S.G., and Ashe, K.H. (2002). The relationship between Abeta and memory in the Tg2576 mouse model of Alzheimer's disease. J. Neurosci. *22*, 1858–1867.

Westermarck, J., Ivaska, J., and Corthals, G.L. (2013). Identification of Protein Interactions Involved in Cellular Signaling. Mol Cell Proteomics *12*, 1752–1763.

Wijesekera, L.C., and Leigh, P.N. (2009). Amyotrophic lateral sclerosis. Orphanet J Rare Dis *4*, 3.

Wong, P.C., Pardo, C.A., Borchelt, D.R., Lee, M.K., Copeland, N.G., Jenkins, N.A., Sisodia, S.S., Cleveland, D.W., and Price, D.L. (1995). An adverse property of a familial ALS-linked SOD1 mutation causes motor neuron disease characterized by vacuolar degeneration of mitochondria. Neuron *14*, 1105–1116.

Xia, D., Li, C., and Götz, J. (2015). Pseudophosphorylation of Tau at distinct epitopes or the presence of the P301L mutation targets the microtubule-associated protein Tau to dendritic spines. Biochim. Biophys. Acta *1852*, 913–924.

Yamamoto, T., Yamada, A., Watanabe, M., Yoshimura, Y., Yamazaki, N., Yoshimura, Y., Yamauchi, T., Kataoka, M., Nagata, T., Terada, H., et al. (2006). VDAC1, having a shorter N-terminus than VDAC2 but showing the same migration in an SDS-polyacrylamide gel, is the predominant form expressed in mitochondria of various tissues. J. Proteome Res. *5*, 3336–3344.

Yankner, B.A., Dawes, L.R., Fisher, S., Villa-Komaroff, L., Oster-Granite, M.L., and Neve, R.L. (1989). Neurotoxicity of a fragment of the amyloid precursor associated with Alzheimer's disease. Science *245*, 417–420.

Youn, H.D., Kim, E.J., Roe, J.H., Hah, Y.C., and Kang, S.O. (1996). A novel nickel-containing superoxide dismutase from Streptomyces spp. Biochem J *318*, 889–896.

Zempel, H., Thies, E., Mandelkow, E., and Mandelkow, E.-M. (2010). Aβ Oligomers Cause Localized Ca2+ Elevation, Missorting of Endogenous Tau into Dendrites, Tau Phosphorylation, and Destruction of Microtubules and Spines. J. Neurosci. *30*, 11938–11950.

Zhao, J., O'Connor, T., and Vassar, R. (2011). The contribution of activated astrocytes to Aβ production: Implications for Alzheimer's disease pathogenesis. Journal of Neuroinflammation *8*, 150.

(2016). 2016 Alzheimer's disease facts and figures. Alzheimer's & Dementia *12*, 459–509.

LIST OF PUBLICATIONS

Temporal and regional progression of Alzheimer's disease-like pathology in 3xTg-AD mice. Belfiore R, Rodin A., Ferreira, Velazquez R., Branca C., Caccamo A., Oddo S. Aging Cell. 2018 October

Acute tau knockdown in the hippocampus of adult mice causes learning and memory deficits. Velazquez R, Ferreira E, Tran A, Turner EC, Belfiore R, Branca C, Oddo S. Aging Cell. 2018 May, PMID: 29749079.

Genetically reducing mTOR signaling rescues central insulin dysregulation in a mouse model of Alzheimer's disease. Caccamo A, Belfiore R, Oddo S. Neurobiol Aging. 2018 Aug. PMID: 29729422

Necroptosis activation in Alzheimer's disease. Branca C, Caccamo A, Piras IS, Ferreira E, Huentelman MJ, Liang WS, Readhead B, Dudley JT, Spangenberg EE, Green KN, Belfiore R, Winslow W, Oddo S**.** Nat Neurosci. 2017 Sep. PMID: 28758999

Dyrk1 inhibition improves Alzheimer's disease-like pathology. Branca C, Shaw DM, Belfiore R, Gokhale V, Shaw AY, Foley C, Smith B, Hulme C, Dunckley T, Meechoovet B, Caccamo A, Oddo S. Aging Cell, 2017 Jun. PMID: 28779511

High Resolution Mass Spectrometry Characterization of The Complex Oxidation Pattern of Methionine and Cysteine Residues in Voltage-Dependent Anion Selective Channel 3 (Vdac3). Saletti R, Reina S, Pittalà MG, Belfiore R, Cunsolo V, Messina A, De Pinto V, Foti S. Biochim Biophys Acta. 2017 Mar. PMID: 27989743

Hexokinase I N-terminal based peptide prevents the VDAC1-SOD1 G93A interaction and re-establishes ALS cell viability. Magrì A, Belfiore R, Reina S, Tomasello MF, Di Rosa MC, Guarino F, Leggio L, De Pinto V, Messina A. Sci Rep. 2016 Oct. PMID: 27721436

SCIENTIFIC CONFERENCES

2018 Arizona Alzheimer's Consortium Scientific Conference

FUSION 2018: Biodesign Institute Scientific Retreat

8th Annual ASU-BNI Neuroscience Research Symposium

SFN Nov 2017 Washington, DC

AZBio Awards 2017

2016 Arizona Alzheimer's Consortium Scientific Conference

ACKNOWLEDGEMENTS

I would like to express my sincere gratitude to Dr. Oddo and Dr. Caccamo who provided me the opportunity to join their team and gave me access to their laboratory and research facilities. Their help was crucial for my growth in science and in life.

I would like to acknowledge Prof. De Pinto and Prof. Messina for the immense and continuous support, for their suggestions, motivation, and knowledge.

I’m grateful to Prof. Salomone, who tracked my progresses as former PhD student with great scientific rigor, extreme professionality and punctuality.

I thank my Italian and American lab mates for sustaining me with stimulating discussions and unforgettable experiences.

Last but not least, I would like to thank my family: my parents, my brother and Taylor, for supporting me with their altruism, incredible patience, and love.